

**T.R  
SAKARYA UNIVERSITY  
INSTITUTE OF SCIENCE AND TECHNOLOGY**

**INELASTIC STATIC (PUSHOVER) ANALYSIS FOR  
ESTIMATING SEISMIC DEMANDS OF RC BUILDINGS  
INCLUDING SOIL-STRUCTURE INTERACTION**

**M.Sc. THESIS**

**Mukhtar AHMADI**

**Department : CIVIL ENGINEERING**  
**Field of Science : STRUCTURE**  
**Supervisor : Prof. Dr. Erkan ÇELEBİ**

**January 2020**

SAKARYA UNIVERSITY  
INSTITUTE OF SCIENCE AND TECHNOLOGY

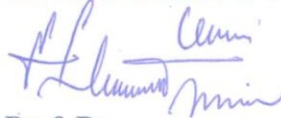
INELASTIC STATIC (PUSHOVER) ANALYSIS FOR  
ESTIMATING SEISMIC DEMANDS OF RC BUILDINGS  
INCLUDING SOIL-STRUCTURE INTERACTION

M.Sc. THESIS

Mukhtar AHMADI

Department : CIVIL ENGINEERING  
Field of Science : STRUCTURE  
Supervisor : Prof. Dr. Erkan ÇELEBİ

This thesis has been accepted unanimously / with majority of votes by the  
examination committee on 24.01.2020



Prof. Dr.  
Erkan ÇELEBİ  
Head of Jury



Asst. Prof.  
Aydın DEMİR  
Jury Member



Asst. Prof.  
Fatih GÖKTEPE  
Jury Member

## **DECLARATION**

I declare that all the data in this thesis was obtained by myself in academic rules, all visual and written information and results were presented in accordance with academic and ethical rules, there is no distortion in the presented data, in case of utilizing other people's works they were refereed properly to scientific norms, the data presented in this thesis has not been used in any other thesis in this university or in any other university.

Mukhtar AHMADI

24.01.2020

## **ACKNOWLEDGMENTS**

I am grateful to all people, who have supported me and encouraged me during my post-graduate study. I would not be able to complete this study without their support and contribution.

First of all, I would like to express my sincere appreciation to my supervisor Prof. Dr. Erkan ÇELEBİ, for his support, guidance, and wisdom that he provided me throughout this study. He constantly advised and encouraged me during my studies, and also patiently worked through difficult problems with me, which has provided a significant and unique contribution which I am greatly indebted for. I also would like to specially thank Asst. Prof. Dr. Aydin DEMİR, for his support and technical contribution provided for part of my thesis. This study would not be completed without their help and advice.

Finally, I would like to express my deepest appreciation to my family, the most precious people in my life, for their financial and spiritual support, love and understanding that they have provided me throughout my education.

## TABLE OF CONTENTS

DECLARATION .....	i
ACKNOWLEDGMENTS .....	i
TABLE OF CONTENTS .....	ii
LIST OF SYMBOLS AND ABBREVIATIONS .....	vi
LIST OF FIGURES.....	ix
LIST OF TABLES.....	xiii
SUMMARY .....	xv
ÖZET.....	xvi
CHAPTER 1.	
INTRODUCTION .....	2
1.1. Problem Statement .....	2
1.2. Literature Review .....	3
1.3. Objective and Scope of the Study .....	10
CHAPTER 2.	
SEISMIC PERFORMANCE CONCEPT .....	14
2.1. Performance Definition According to ATC-40.....	15
2.2. Acceptance Criteria According to ATC-40.....	17
2.2.1. Global acceptance criteria for the buildings .....	17
2.3. Performance Definition According to TEC-2018 .....	18
2.4. Acceptance Criteria According to TEC-2018 .....	19
2.4.1. Acceptance criteria for collapse prevention (GÖ) performance level.....	21
2.4.2. Acceptance criteria for damage control (KH) performance level.....	23

2.4.3. Acceptance criteria for limited damage (SH) performance level.....	23
2.5. Earthquake Ground Shaking Hazard Levels .....	23
2.5.1. Earthquake ground shaking hazard level-1 (DD-1).....	24
2.5.2. Earthquake ground shaking hazard level-2 (DD-2).....	24
2.5.3. Earthquake ground shaking hazard level-3 (DD-3).....	24
2.5.4. Earthquake ground shaking hazard level-4 (DD-4).....	25
2.6. Standard Earthquake Ground Shaking Response Spectra.....	25
2.6.1. Determination of mapped and design spectral acceleration coefficients.....	25
2.6.2. Determination of the local site parameters .....	26
2.6.3. Design elastic response spectra .....	26
 CHAPTER 3.	
FUNDAMENTALS OF SOIL-STRUCTURE INTERACTION ANALYSIS.....	29
3.1. Kinematic Interaction .....	30
3.2. Inertial Interaction .....	31
3.3. Methods of Analysis.....	32
3.3.1. Direct approach.....	32
3.3.2. Substructure approach .....	34
3.4. Implementation of SSI in Displacement-Based Analysis Procedure (Pushover Analysis) in view of the Seismic Building Codes.....	45
3.4.1. Including SSI effects into the displacement-based analysis method .....	46
 CHAPTER 4.	
NONLINEAR STATIC ANALYSIS .....	55
4.1. Evaluation of Pushover Analysis.....	58
4.1.1. Advantages and limitation of pushover analysis .....	59
4.2. Implementation of Pushover Analysis for Determining Seismic Responses of RC Buildings.....	61

4.3. Capacity spectrum method of ATC-40 .....	61
4.4. Nonlinear static procedures based on TEC-2018 .....	66
4.4.1. Non-linear modeling of structural system .....	67
4.4.2. Acceptance criteria for modeling of the RC structures .....	69
4.4.3. Single-mode pushover analysis (SMPA) .....	71
 CHAPTER 5.	
NUMERICAL EXAMPLES AND RESULTS.....	81
5.1. General Description of the Case Study .....	82
5.2. Selection of the Local Soil Properties .....	87
5.3. Modeling of the Case Studies in SAP2000 .....	89
5.3.1. Material models .....	89
5.3.2. Modeling of the superstructure .....	91
5.3.3. Calculation of gravity loads and masses.....	98
5.3.4. Modeling of SSI in SAP2000: Sub-structures approaches .....	100
5.3.5. Assumptions made in modelling .....	103
5.4. Conducting Pushover Analysis in SAP2000 .....	104
5.4.1. Definition of modal load cases .....	104
5.4.2. Definition of gravity load case (vertical loads) .....	105
5.4.3. Pushover Load cases .....	107
5.5. Analysis Results and Discussions .....	109
5.5.1. Effects of SSI on vibration periods.....	109
5.5.2. Effects of SSI on the maximum displacement demand .....	110
5.5.3. Effects of SSI on the capacity curves .....	116
5.5.4. Effects of SSI on the inter-story drift ratios.....	123
5.5.5. Effects of SSI on the damage states of structural elements .....	132
 CHAPTER 6.	
CONCLUSIONS AND RECOMMENDATIONS .....	142
6.1. Conclusion.....	142
6.2. Recommendation for the Future Studies .....	144

REFERENCES.....	145
RESUME .....	149



## LIST OF SYMBOLS AND ABBREVIATIONS

BYS	: Building height range
$d_b$	: Longitudinal bar size
DTS	: Design zone of seismicity
$d_{1,\max}^{(X)}$	: Maximum modal displacement associated with the first mode of vibration in an ( $X$ ) direction of earthquake
$EI$	: Section stiffness of the elements
$(EI)_e$	: Effective section stiffness of the elements
$F_S$	: Local site coefficient for short-period (0.2 second) zone
$F_{S1}$	: Local site coefficient for 1-second period zone
$G_0$	: Maximum soil shear modulus
GÖ	: Collapse prevention
KH	: Damage control performance level
KK	: Fully operational performance level
$K_{x, \text{sur}}$	: Static stiffness of the footing for translation degree of freedom along x-axis
$K_{y, \text{sur}}$	: Static stiffness of the footing for translation degree of freedom along y-axis
$K_{z, \text{sur}}$	: Static stiffness of the footing for translation degree of freedom along z-axis
$K_{xx, \text{sur}}$	: Static stiffness of the footing for rocking degree of freedom about x-axis
$K_{yy, \text{sur}}$	: Static stiffness of the footing for rocking degree of freedom about y-axis

$K_{zz, sur}$	: Static stiffness of the footing for rocking degree of freedom about z-axis
LD	: Limited damage performance region
$L_p$	: Plastic hinge length
MD	: Moderate damage performance region
MMPA	: Multi-mode pushover analysis
SD	: Severe damage performance region
SH	: Limited damage performance level
SMPA	: Single-mode pushover analysis
SSI	: Soil-structure interaction
$S_1$	: Dimensionless response acceleration coefficient at one second
$S_{DS}$	: Design response acceleration coefficients at short period
$S_{D1}$	: Design response acceleration coefficients at one second period
$S_{ae}(T)$	: Horizontal design elastic spectral acceleration
$S_{de}(T)$	: Horizontal design elastic spectral displacement
$S_{de}(T_1)$	: elastic spectral displacement corresponding to the first mode of vibration
$S_{di}(T_1)$	: Inelastic spectral displacement corresponding to the first mode of vibration
$S_S$	: Dimensionless short-period (0.2 second) response acceleration coefficient
$T$	: Building natural vibration period
$T_1$	: Fundamental mode (first mode) of vibration of the building
$T_A$	: Corner period for horizontal elastic design acceleration spectrum
$T_B$	: Corner period for horizontal elastic design acceleration spectrum
$T_L$	: Transition period for horizontal elastic design acceleration spectrum
$u_{Nx1}^{(X)}$	: Total displacement demand at the roof level for the x-direction associated with the first mode of vibration

$V_S$	: Soil shear wave velocity
$\varepsilon_c$	: Concrete compressive strain
$\varepsilon_s$	: Tensile strain of steel
$\theta_p$	: Plastic rotation
$\nu$	: Poison ratio of the soil
$\phi_u$	: Total curvature
$\phi_y$	: Yield curvature
$\Phi_{Nx1}^{(1)}$	: Amplitude of the first mode shape at the roof level, in x-direction
$\rho_S$	: Soil mass density
$\Gamma_1^{(X,1)}$	: Modal participation factor for the first mode (fundamental mode)

## LIST OF FIGURES

Figure 1.1. Modeling strategies for including SSI effects in nonlinear analysis procedures .....	7
Figure 2.1. Structural element damage levels and regions.....	20
Figure 2.2. Turkish earthquake hazard map.....	24
Figure 2.3. Horizontal design elastic acceleration response spectrum curve.....	28
Figure 2.4. Horizontal design elastic displacement response spectrum curve.....	28
Figure 3.1. Kinematic interaction due to base-slab averaging.....	31
Figure 3.2. Modelling SSI using the direct method .....	33
Figure 3.3. Soil-structure interaction analysis using the direct method.....	33
Figure 3.4. Soil structure interaction analysis using substructure approach.....	35
Figure 3.5. Substructure approach for analyzing the SSI problem .....	37
Figure 3.6. Schematic representation of soil by springs and dashpots.....	38
Figure 3.7. Foundation stiffness and damping factors for elastic and viscoelastic halfspace, for Poisson ratios, $\nu = 0.4$ .....	40
Figure 3.8. Schematic demonstration of foundation .....	42
Figure 3.9. Application of static lateral loads to a flexible base model.....	47
Figure 3.10. General representation of soil-foundation stiffness by equivalent springs .....	48
Figure 3.11. Relationship between foundation damping and period lengthening .....	54
Figure 4.1. Schematic demonstration of nonlinear analysis procedure .....	56
Figure 4.2. Static analysis procedure for performance evaluation of the buildings... ..	57
Figure 4.3. Pushover curve of the building .....	58
Figure 4.4. Graphical demonstration of the capacity spectrum method .....	62
Figure 4.5. Derivation of damping for spectrum reduction .....	64
Figure 4.6. Generalized force-deformation curve (backbone curve) for concrete elements.....	68

Figure 4.7. Schematic representation of structural capacity in the direction of the x-axis .....	74
Figure 4.8. Design elastic spectrum diagram .....	75
Figure 4.9. Demand diagram (transformation of design elastic spectrum in ADRS format).....	76
Figure 4.10. Illustration of the modal capacity curve and demand diagram in ADRS format .....	77
Figure 4.11. Estimation of inelastic spectral displacement through the iterative process.....	80
Figure 5.1. Plan view of the reference structures.....	83
Figure 5.2. 3D view of the case studies .....	84
Figure 5.3. Location of ground investigation for different points at the central part of the Adapazari region .....	88
Figure 5.4. Material model for concrete C25 developed in XTRACT program.....	90
Figure 5.5. Steel Model for S420 steel type developed in the XTRACT program....	91
Figure 5.6. A generalized monotonic force-deformation curve representing plastic hinge behavior .....	93
Figure 5.7. Backbone curve purposed by TEC-2018.....	94
Figure 5.8. Normal force moment interaction surface (P-M3) for the columns .....	95
Figure 5.9. Idealized moment rotation (P-M2-M3) diagram (backbone curve) for columns .....	96
Figure 5.10. Pure bending moment hinge definition for beam in SAP2000.....	97
Figure 5.11. Effective Cross-Section stiffness coefficient assigned in SAP2000 .....	98
Figure 5.12. Schematic distribution of gravity loads .....	99
Figure 5.13. Definition of mass source in SAP2000.....	100
Figure 4.13. Front view of the 4-story model .....	101
Figure 5.14. Definition of modal load case in SAP2000 .....	105
Figure 5.15. Definition of gravity load case in SAP2000 .....	106
Figure 5.16. Definition of nonlinear static pushover load case in SAP2000 .....	108
Figure 5.17. Transformation of pushover curve into modal capacity curve for 4-story model with the fixed base condition .....	112

Figure 5.18. Elastic response spectrum diagram representing the design earthquake (DD-2), for soil type ZD .....	113
Figure 5.19. Seismic demand diagram for the design earthquake (DD-2), for soil type ZD.....	113
Figure 5.20. Determination of modal displacement demand for 4-story model .....	113
Figure 5.21. Pushover curves of the 2-Story model in the x-direction; comparison between FB and SSI conditions for different soil classes .....	117
Figure 5.22. Pushover curves of the 4-Story model in the x-direction; comparison between FB and SSI conditions for different soil classes .....	118
Figure 5.23. Pushover curves of the 8-Story model; comparison between FB and SSI conditions for different soil classes.....	119
Figure 5.24. Pushover curves of the 2-Story models; comparison between FB and SSI conditions for different soil classes.....	120
Figure 5.25. Pushover curves of the 2-Story models; comparison between FB and SSI conditions for different soil classes.....	121
Figure 5.26. Pushover curves of the 8-Story models in the x-direction; comparison between FB and SSI conditions for different soil classes .....	122
Figure 5.27. Inter-story drift ratios for the 2-Story models; comparison between FB and SSI conditions for different soil classes .....	125
Figure 5.28. Inter-story drift ratios for the 4-Story models; comparison between FB and SSI conditions for different soil classes .....	126
Figure 5.29. Inter-story drift ratios for the 8-Story models; comparison between FB and SSI conditions for different soil classes .....	127
Figure 5.30. Inter-story drift ratios for the 2-Story models; comparison between FB and SSI conditions for different soil classes .....	129
Figure 5.31. Inter-story drift ratios for the 4-Story models; comparison between FB and SSI conditions for different soil classes .....	130
Figure 5.32. Inter-story drift ratios for the 8-Story models; comparison between FB and SSI conditions for different soil classes .....	131
Figure 5.33. Selected columns in the ground floor for performance investigation..	132
Figure 5.34. Comparison of plastic hinge formations for 2, 4 and 8 story models in the x-direction .....	140

Figure 5.35. Comparison of plastic hinge formations for 2, 4 and 8 story models in the y-direction ..... 141

## LIST OF TABLES

Table 2.1. Global lateral deformation limits .....	18
Table 2.2. Values of $F_s$ , defined in TEC-2018 for different soil types.....	26
Table 2.3. Values of $F_1$ , defined in TEC-2018 for different soil types.....	26
Table 3.1. Expressions for calculating the static stiffness of rigid rectangular footings .....	44
Table 3.2. Expressions for calculating the static stiffness of rigid rectangular footings .....	44
Table 5.1. Details of structural members and reinforcement ratios .....	85
Table 5.2. General requirements and assumption of the project.....	86
Table 5.3. Design seismicity zone classification (TEC-2018).....	87
Table 5.4. Mechanical properties of selected soils .....	88
Table 5.4. Effective stiffness coefficient proposed by TEC-2018.....	98
Table 5.5. Footing dimensions and equivalent spring stiffness for different soil types used in this study .....	102
Table 5.6. Total masses and mass participation ratios of the models associated with the fundamental modes of vibration ( $T_1$ ) in the direction of x-axis.....	107
Table 5.7. Total masses and mass participation ratios of the models associated with the fundamental modes of vibration ( $T_1$ ) in the direction of y-axis.....	107
Table 5.8. Variation in vibration period due to the SSI effects in the x-direction...	110
Table 5.9. Variation in vibration period due to the SSI effects in the y-direction...	110
Table 5.10. Determination of modal capacity curve for the 4-story model in the x- direction.....	111
Table 5.11. Parameters for constructing elastic spectrum for DD-2 and selected site conditions .....	112
Table 5.12. Estimation of seismic displacement demands for the studied buildings in the x-direction .....	115



Table 5.13. Estimation of seismic displacement demands for the studied buildings in the y-direction .....	115
Table 5.14. The changes in plastic rotation demands obtained from SAP2000 for the 2-story model.....	133
Table 5.15. The changes in plastic rotation demands obtained from SAP2000 for the 4-story model.....	133
Table 5.16. The changes in plastic rotation demands obtained from SAP2000 for the 8-story model.....	134
Table 5.17. Column plastic rotation limits, calculated based on TEC-2018.....	135
Table 5.18. Selected columns damage levels for the 2-story model.....	136
Table 5.19. Selected columns damage levels for the 4-story model.....	136
Table 5.20. Selected columns damage levels for the 8-story model.....	136
Table 5.21. The variation in plastic rotation demands, obtained from SAP2000 for the 2-story model.....	137
Table 5.22. The variation in plastic rotation demands, obtained from SAP2000 for the 4-story model.....	137
Table 5.23. The variation in plastic rotation demands, obtained from SAP2000 for the 8-story model.....	138
Table 5.24. Damage levels of the reference columns in the y-direction for the 2-story model.....	138
Table 5.25. Damage levels of the reference columns in the y-direction for the 4-story model.....	139
Table 5.26. Damage levels of the reference columns in the y-direction for the 8-story model.....	139

## SUMMARY

Keywords: Pushover Analysis, Soil-Structure interaction (SSI), Seismic Responses, Impedance Functions, TEC-2018

The earthquakes that occurred in the past have revealed the destructive impacts of soil-structure interaction (SSI) on the seismic responses of the buildings. For example, during an earthquake that occurred in Turkey (Gediz, 1970), a factory in a city located 135 km from the epicenter was destroyed, whereas the other buildings were undamaged in the town. After the investigation, it was observed that the resonance effect, where the dominant period of the building was almost equal to the vibration of the sub-soil, led to the destruction of the building. The earthquake occurred in the Adapazari region (Kocaeli, 1999), which is the other example, revealed the destructive effects of SSI. During this earthquake, numerous foundations have been failed, resulted from either uplifting in the foundation or exceedance in the soil bearing capacity.

In view of the above-mentioned information, this study intends to investigate how to effect the geotechnical conditions of foundation medium on the seismic performance of 3D reinforced concrete (RC) moment-resisting frame (MRFs) buildings. For this purpose, 2, 4 and 8-story RC buildings are considered as case studies and the analyses are performed by means of a single-mode pushover analysis method in view of the latest version of Turkish Earthquake Code (TEC-2018). The reference structures are considered to perform against the design earthquake level (DD-2). The seismic evaluation of the studied buildings is accomplished as a result of parametric investigations in which the soil properties, the base condition and the height of the structures vary. Two different support cases are considered as (1) fixed base and (2) flexible base conditions. In order to observe how the seismic responses of the compliant and fixed base models differ from each other, a simplified SSI model suitable for pushover analysis was used. For what concern the soil layer under the foundation different soil properties for Adapazari regions is considered and the effects of soil-foundation interaction was modeled by means of equivalent elastic springs. The stiffness characteristics of the deformable soil under the rigid foundation corresponding to the rotational and translational degree of freedoms are formulized by impedance functions within the sub-structure method specified according to the seismic evaluation and retrofit of concrete buildings report (ATC-40). The mechanical characteristics of soil layers considered for Adapazari region are taken into account with respect to TEC-2018 local soil classification. Single-mode- pushover analyses and performance considerations are performed by SAP2000 computer package. The obtained numerical results are evaluated comparatively in terms of roof displacement-base shear force relationships, vibration periods, inter-story drifts and ground story column damage levels. The study shows that the effects of SSI on seismic demand of the structures founded on softer soil (soil type ZD and ZE) is higher, while it has negligible effects when the structures are founded on stiff soil (soil type ZA and ZB). It can be deduced from the capacity curves that when including geotechnical parameters of the flexible soil, non-conservative results of the structural response for weak ground conditions would be obtained in the SSI analysis.

# ÇERÇEVE TİPİ BETONARME YAPILARIN SİSMİK DAVRANIŞIN YAPI-ZEMİN ETKİLEŞİMİNİN ETKİSİNİ DİKKATE ALINARAK DOĞRUSAL OLMAYAN STATİK ÇÖZÜMLEME İLE İRDELENMESİ

## ÖZET

Anahtar kelimeler: Statik itme analizi, yapı-zemin etkileşimi, yapıların sismik davranışı, empedans fonksiyonları, TBDY-2018

Geçmişte meydana gelen depremler, yapı-zemin etkileşiminin, binaların sismik tepkileri üzerindeki yıkıcı etkilerini ortaya çıkarmıştır. Örneğin, Türkiye'deki Gediz depremi (1970) sırasında, merkez üssünden 135 km uzaklıktaki bir kasabada bulunan bir fabrika tahrip ederken, kasabada bulunan diğer binalar herhangi bir hasar görmemişti. Daha sonraki araştırmalar, fabrikanın temel titreşim periyodunun, alttaki toprağınkine yaklaşık olarak eşit olduğunu ortaya koymuştur. Bu uyum bir rezonans etkisi sağladığını ve yapının çökmesine neden olduğunu göstermiştir. Adapazarı bölgesinde yer alan bir başka çarpıcı örnekte, 1999 Kocaeli depreminde, temellerin sallanması (foundation uplifting) ya da temel zeminin taşıma kapasitesinin aşılması nedeniyle birçok temelin çökmesi, dolayısıyla, yapının hasar aldığı gözlemlenmiştir.

Yukarıda belirtilen konular ışığında, bu çalışmada, temel altındaki zeminin geoteknik koşullarının, 3-boyutlu çerçeve tipi betonarme yapıların sismik performansına etkisi incelenmiştir. Bu amaçla 2, 4 ve 8 katlı betonarme bina modelleri referans olarak seçilmiştir ve deplasman bazlı analiz yöntemlerinden biri olan tek modlu itme analizi yeni Türkiye Bina Deprem Yönetmeliğine (TBDY-2018) uygun olarak uygulanmıştır. Bu binaların sismik performans değerlendirmeleri, zemin tipleri, temel bağlantı şekilleri ve binaların yüksekliği farklı ele alınarak parametrik araştırma sonuçlarına göre yapılmıştır. Rijit temel ve yapı-zemin etkileşimi dikkate alındığı iki farklı temel bağlantı şekli varsayılmıştır. Yapı-zemin etkileşimi alt sistem yaklaşımı kullanılarak modellenmiştir. Bu yaklaşım kapsamında rijit temel ve zemin arasındaki etkileşim, elastik yaylar ile temsil edilmiştir. Dönme, yatay ve düşey serbestlik derecelerine tekabül eden yayların rijitlikleri, sismik değerlendirme ve betonarme yapıların güçlendirmesi olan standart (ATC-40) tarafından önerilen empedans fonksiyonları kullanılarak elde edilmiştir. Bu çalışmada, Adapazarı bölgesindeki zemin koşulları, TBDY-2018 yönetmeliğinin yerel zemin sınıflandırmasına, göre dikkate alınmıştır. Tek modlu itme analizi ve yapıların performans durumları SAP2000 paket programı yardımı ile gerçekleştirilmiştir. Analiz sonuçları, tepe yer değiştirme-taban kesme kuvveti ilişkisi, görelî kat ötelemesi, titreşim periyodu ve zemin katındaki kolonların hasar seviyeleri karşılaştırmalı olarak incelenmiştir. Çalışma sonuçları, yapı-zemin ortak davranışının yumuşak zeminlere (zemin sınıfı ZD ve ZE) oturan yapıların deprem performanslarını daha çok etkilediğini, sert zemine inşa edilen (zemin sınıfı ZA ve ZB) yapılarda bu etkileşim etkilerinin azaldığını göstermektedir. Esnek zeminin geoteknik özelliklerinin dikkate alınarak elde edilen sismik kapasite eğrilerinden, yapı-zemin etkileşim analizi zayıf zemin koşulları için yapısal davranışı önemli derecede değiştirdiği anlaşılmaktadır

# **CHAPTER 1. INTRODUCTION**

## **1.1. Problem Statement**

A large number of the buildings constructed worldwide, including in seismic zones, are reinforced concrete structures since it is easy to build and requires less construction time. However, this kind of buildings have been endured significant damages or collapsed during the recent earthquakes that occurred in many countries, including Turkey which is located in a very high seismic zone. For example, the latest earthquakes including Kocaeli-1999, Duzce-1999 and Van 2011 that struck turkey caused serious damages to these types of buildings. Based on the latest building inventory census of Turkey, almost half of the buildings (48%) constructed in this country have been built as reinforced concrete (RC) systems, where 98 percent of them (RC buildings) consist of moment-resisting frames [1].

Reinforced concrete structures show a very complex behavior, especially when it is exposed to severe earthquake excitation. It is impossible to understand this behavior using conventional linear analysis methods (i.e. force-based analysis approaches) which is the subject of current seismic codes. These methods can only provide information about the elastic behavior of the buildings and predict the occurrence of the first yielding but fail to provide information about the failure mechanism of the structures. Therefore, since in reality the buildings experience large deformations and demonstrate inelastic behavior, non-linear analysis tools are required.

Recently, researches have been concentrated on non-linear (i.e. displacement-based) analysis approaches which include non-linear static and dynamic methods.

Generally, these methods are used for seismic design and retrofitting of existing buildings, also can be used to design the new buildings. In addition, the foremost need for the inelastic analysis methods is to get an insight into the expected behavior of the buildings and realize how they will perform against the anticipated earthquake that will occur during their lifetime. Based on past studies, among the non-linear analysis methods, time history analysis is believed as the most reliable and accurate analysis technique and is generally used to examine the accuracy of the other methods [1]. However, like any other analysis procedure, this method also has some disadvantages including its complexity, requirements for long run-time and convergence problems that occur frequently, therefore, this method is rarely used in practice. On the other hand, non-linear static procedure (i.e. pushover analyses) is widely used in practice and preferred as a simpler assessment tool for performance evaluation of the buildings. This method is also recommended by many seismic codes (e.g. ATC-40, FEMA-356, FEMA-440, TEC-2007, and TEC-2018) for seismic investigations.

Furthermore, typically in practice, the seismic investigation is performed by assuming a fixed-base structure. This assumption can only be reliable and realistic when the ground environment is very rigid compared to the superstructure. Whereas mostly this is not the case and the superstructure and the underlying soil layer both behave together against static and dynamic external loads as a deformable systems. Therefore, in order to estimate the real behavior, the ground region should be defined as a part of the structural system and analyzed together with the superstructure. Accordingly, what is needed to be considered in analysis and design of the buildings is the effects of the soil medium against the superstructure and vice versa. In other words, the interaction between the structure and the sub-soil should be considered. Here, the soil-structure interaction describes a phenomenon that expresses the mutual effects of the structure and the ground that form the two parts of the common system [2].

In addition, when a building is exposed to the earthquake excitation its behavior is closely related to the superstructure, earthquake source, soil conditions and the properties of the foundation. The mutual interaction of structure and soil affects the dynamic features of the superstructure and local soil. Conceptually, soil-structure

interaction affects the distribution of mass and stiffness in the structure, causing changes in frequency (or period) and mode patterns throughout the system [3].

Moreover, seismic reactions like inter-story drifts and lateral deformations of the buildings considerably increases, especially when they are founded on relatively soft soil profile, due to the SSI effects. The frame buildings, particularly, are more vulnerable to the effects of SSI, such that it may significantly change the performance levels of these types of buildings and consequently, endanger their safety and integrity [4].

## **1.2. Literature Review**

In recent years, simplified elastic and inelastic static analysis methods based on pushover analysis are widely utilized to assess the seismic performance of structures. The former method is limited to the elastic behavior, while the latter method break this limit and goes further to examine the inelastic behavior of the structures.

Simplified elastic analysis methods, assumes the structures exhibit elastic behavior against earthquake motions, which provide good results for predicting the elastic capacity of the structures and where the first yielding will occur, this method cannot forecast the real failure mechanism of the structures and misinterpret actual performance of the buildings. In reality, the buildings show inelastic behavior against large earthquakes, which dissipate energy through large deformations and undergo severe damages. In this case, the simplified nonlinear techniques or nonlinear dynamic procedures are able to estimate the real behavior of the structures more precisely [5]. Surveying the literature since 2010, many researchers have utilized nonlinear analysis methods specially pushover analysis to assess the nonlinear behavior and seismic performance of Reinforced Concrete (RC) buildings. Kavita and Golghate [6], have studied the seismic behavior of a 4-story RC frame structure by conducting a pushover analysis with the help of the SAP2000 software package. The studied building was designed as per Indian seismic code. The non-linearity of the building was modeled by means of plastic hinges, assigned to the columns and beams. The performance level of the building was determined based on the criteria specified in ATC-40 and

FEMA-356. As a result, they concluded that pushover analysis provides reasonable results than elastic analysis methods, and gives insight into the actual behavior of the buildings. Similarly, Hakim et.al. [7], have studied the seismic performance of a 4-story RC framed building, which was designed only under gravity loads. The building was placed at low to moderate seismic zones and nonlinear static analysis was conducted based on the capacity spectrum method of ATC-40. The seismic demands of the building were obtained by subjecting it to the different seismic zone. Based on their results, the building has been survived in low to medium seismic zone, while failed in the moderate seismic zone.

In addition, plenty of researches has been devoted in order to investigate the seismic behavior of the RC structures considering the effects of various parameters such as modeling strategies, analysis methods, ground conditions, and material properties. Some of them are summarized in the following;

Panyakapo [8], used the cyclic pushover analysis method to investigate the seismic behavior of a 9-story RC frame building. Unlike the conventional pushover analysis in which a uniform lateral load distribution is used, this method considers different types of loading distribution. To test the effects of different load patterns, the analysis was performed assuming various loading protocols. Seismic responses such as peak lateral displacements and the max inter-story drift ratios were investigated. To verify the proficiency of the method, the outcomes were compared with those of the non-linear time history analysis. Consequently, a good agreement amongst the outcomes of the two analysis methods was observed. Furthermore, it was indicated that the cyclic pushover analysis provides better and reasonable results than those with monotonic loading assumptions.

Çollaku [9], investigated the effects of reinforcement percentage, contained in structural elements, on the seismic capacity of RC buildings. For this purpose, an existing residential RC frame building located in Albania was considered as a case study and pushover analysis was performed using SAP2000 software package. The studied building was designed according to the Albanian standard (KTP-1989) and

was consist of 5-bay and seven-story. Based on the minimum and maximum reinforcement percentage in the structural members, different plastic hinge types and various combinations of steel and concrete strength were considered. It was shown that the overall capacity of the structure considerably increases as the steel percentage increases. Furthermore, it was observed that a combination of the concrete with low strength and steel with high strength provides higher structural capacity than the high concrete strength and low steel strength combination.

Karaşin and Işık [10], studied the influence of various soil conditions and building importance factors on the seismic performance of RC buildings. For this purpose, the seismic responses of a 3-story existing school type building, collapsed in the Bingöl earthquake in 2003, located in Çeltiksuyu (a city in Turkey) was investigated. In order to improve their investigation, eight numerical analysis was performed, considering the different combinations of soil types with building importance factors. The soil types (Z1, Z2, Z3, and Z4) and building importance factors (R4 and R8) were selected based on the Turkish earthquake code (TEC-2007). The pushover analysis was conducted with the help of the SeismoStruct software package and the seismic responses of the models were investigated in terms of base shear force and roof displacement (i.e. capacity curve). It was indicated that the soil condition has substantial effects on the seismic performance of the structure, particularly as the soil properties changes from hard to softer soil, accordingly the seismic displacement demand increases and base shear force decreases due to reduction in stiffness.

The researches, summarized above are based on the supposition that buildings are fixed at their bases; ignoring the impacts of SSI. Whereas in reality, the soil beneath the foundation is not rigid, and the seismic responses of the buildings are affected by the response of the three interconnected systems namely superstructure, foundation, and underlying soil profile. Whereas mostly this is not the case and the superstructure and the underlying soil layer both behave together against static and dynamic loads as a deformable systems. Therefore, in order to estimate the real behavior, the ground region should be defined as a part of the structural system and analyzed together with the superstructure [4].



Surveying the literature, the two main approaches used for the idealization of the soil region in the SSI problems are the direct approach and the sub-structure approaches. In general, these two methods are widely used to study the ground condition effects on the seismic actions of the RC buildings and the results are compared with the fixed base conditions or those of the experimental studies. Some of the past studies concerning the SSI problems are summarized in the following paragraphs.

Kraus and Džakić [11], have evaluated the effect of SSI on the behavior of reinforced concrete frames using linear elastic Time History analysis. The analysis was conducted based on European regulations by considering 3, 7 and 10 story 3-bay RC frame structures resting on soft soil profile. Three different soil modeling techniques were employed: fixed base, Winkler springs model (sub-structure approach), and structure on half-space (direct approach), to show the sensibility of results and to give some rough recommendations in the framework of seismic design codes. They indicated that SSI does not always have beneficial effects, which including SSI to the model increases inter-story drift significantly comparing to a fixed base condition especially when the soil is modeled using Winkler springs. In addition, it was shown that including SSI elongates the fundamental period and also increases base shear forces, contrary to the general agreement that it decreases the base shear forces.

Demir et al. [12], studied the seismic performance of different 2D RC moment-resisting frames, taking in to account the SSI effects. The buildings were analyzed by means of pushover analysis, using SAP2000 program package. The foundation was assumed as strip foundation and soil properties of Adapazari (Turkey), with different soil shear velocities, which were considered for flexible base conditions. The SSI was modeled by representing the foundation and soil by a series of linear and nonlinear springs, springs stiffness was calculated by the formula proposed by [13] and later modified for strip foundation by [14]. The seismic responses such as inter-story drift ratios, capacity curve, and plastic hinge rotations of the first-floor columns were estimated and were compared with the results obtained from the fixed base condition. Based on their founding, significant changes were observed in the seismic responses

of the structures due to the SSI effects in both linear and nonlinear soil conditions. However, the variations were shown higher in the case of nonlinear soil model, compared to the fixed base state. In addition, they have recommended that SSI needs to be considered for performance evaluation of RC buildings, founded on unfavorable ground conditions.

Storie and Pender [15], studied the effects of soil foundation structure interaction (SFSI) on seismic responses of a 10-story RC building resting on a mat foundation. The building was modeled and designed in SAP2000 software package, and then it was transformed into a single degree of freedom system. The model was then subjected to the Christchurch Earthquake (22 February 2011), and seismic responses were evaluated by means of time history analysis. They used uniform spring and FEMA spring modeling techniques (Figure 1.1.) to account for SFSI and evaluated the accuracy of them.

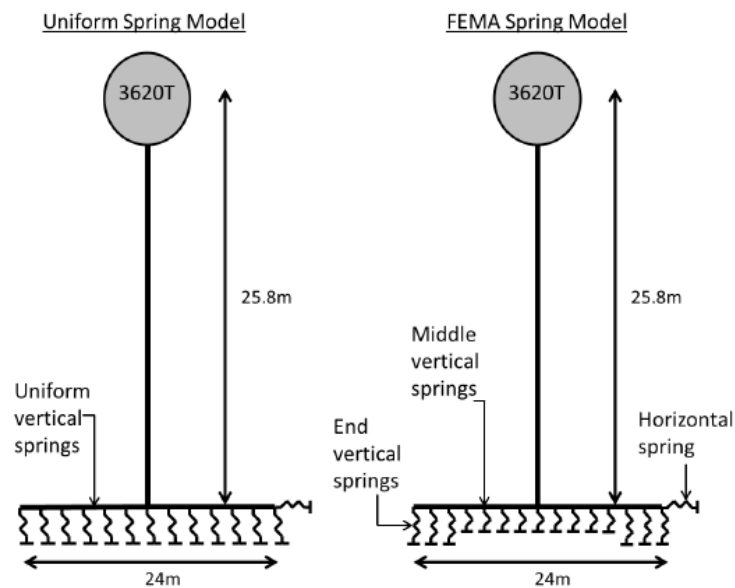


Figure 1.1. Modeling strategies for including SSI effects in nonlinear analysis procedures [15]

Based on their obtained results, in both kinds of modeling techniques, the SFSI effects were shown significant. For example, it was shown that small rotation in the foundation will cause extent uplift in the foundation which affects overall seismic responses of the structure. In addition, SFSI elongates the period and lateral displacement of the structures comparing to the fixed base condition. Finally, it was

recommended that the effects of SFSI should not be neglected for performance evaluation of the structure during large ground motion.

Kalyanshetti et al. [16], investigated the effects of SSI on seismic responses of low to high rise RC buildings. The building was modeled and analyzed in the SAP2000 software package by means of pushover analysis. Soil-foundation interaction surface was simulated in two different ways, once using equivalent springs to represent the soil and the foundation which is also known as the Winkler model, and once the elastic continuum model (direct method), was used for modeling the SSI system. Consequently, the results of the two modeling approaches were studied comparatively. It was indicated that structural responses such as lateral displacement, vibration period, bending moments of beams and shear forces increase due to SSI effects. Furthermore, it was concluded that the continuum modeling technique better represents the SSI effects than the equivalent spring model.

Roopa et al. [17], performed a parametric study to understand how the SSI effects on seismic responses of tall buildings. For this purpose, the responses of a 13 story existing RC building was examined, considering clayey soil under the mat foundation. Nonlinear static pushover analysis and modeling of the structure were performed using SAP2000 software package. SSI was modeled using Winkler modeling technique, representing soil-foundation interaction by equivalent springs. The results were discussed comparatively in terms of base shear, natural period, lateral displacement and inter-story drift. According to the obtained outcomes, all of the seismic responses were increased due to the inclusion of SSI effects, except the base shear, when comparing them to the responses obtained from the fixed base assumption. In addition, they concluded that the significant increase in the seismic responses of tall buildings, caused by the SSI, is due to the flexibility induced to the base by the softness of clayey soil.

Behnamfar and Banizadeh [18], studied the seismic vulnerability of RC buildings considering the SSI effects. For this propose 5 different RC buildings being 3, 5, 6, 8 and 9 stories were analyzed. Two different ground conditions, soft and very soft soil

profile and two kinds of structural systems, moment-resisting frames, and shear walls were assumed. To account for SSI, the foundation was modeled using beam elements (beam on nonlinear Winkler technique) and the soil beneath the foundation was represented by linear and nonlinear springs. Nonlinear dynamic analysis was conducted with the help of OpenSees software by subjecting the models to different earthquake motions. Seismic responses such as maximum base shear, story-drifts, and plastic hinges rotations were estimated for the SSI system and were compared to the results of the fixed base condition. As a result, they have concluded that SSI negatively affects the performance level of structural members specially those in the lower stories.

Tomoe et al. [19], used nonlinear dynamic analysis to find out how the SSI affects the seismic performance of the RC buildings. For this purpose different 2D reinforced concrete frames, being 4 and 8 stories were considered. The buildings under examination were designed once only under gravity loads and once with the high level of seismic details according to the Italian seismic code. The soil beneath the foundation was assumed to be soft soil (medium and soft clays) because of their higher effects on the seismic responses. Two different modeling strategies, sub-structure method (beam on nonlinear Winkler foundation model) and direct approach (complete finite element model), were used to include the SSI effects. The analysis was performed with the help of the OpenSees software package and the results were compared with respect to the fixed base model in terms of max base shear and max inter-story drift ratios. They find out that considering SSI reduces the seismic demands (max base shear and max inter-story drift ratios) with respect to the fixed-base model for both modeling strategies. According to them, this happens since some amount of earthquake energies are consumed by the soil. The reduction in seismic demands was shown higher in a direct approach and lower in case of the sub-structure modeling technique, so they concluded that the sub-structure approach might underestimate the seismic demands of the buildings.

M.Ghandil and F.Behnamfar [20], investigated the SSI effects on the ductility demand and dynamic responses of a 10 story moment-resisting RC frame structure using nonlinear dynamic time history analysis. The direct approach was selected for

modelling of the SSI system, and the soil beneath the foundation was assumed as soft soil, soil type D according to ASCE7 (American Society of Civil Engineering). The results were interpreted comparatively in terms of ductility demand, drift ratio, fundamental period, base shear and lateral displacement. They have shown that SSI increases inter-story drifts and ductility demand, especially in the lower stories, while it decreases the base and story shear forces compared to fixed base condition.

Anwarsamarin et al. [21], have evaluated the effects of SSI on the seismic collapse capacity of the RC structure by means of Incremental Dynamic Analysis (IDA). For this propose seismic responses of 6, 12 and 18 storied RC moment-resisting frame was studied, the foundation was assumed as a rigid rectangular shallow foundation, and the soil beneath the foundation was assumed as soft soil, with soil wave velocity ranging from 180m/s to 360m/s. The numerical modeling and IDA were performed using OpenSees software, taking in to account 23 far fault earthquake records. The SSI was simulated using the Cone model (monkey-tail model). The collapse performance was estimated by relating intensity measure and collapse probability, it was shown that the collapse probability of structures increases in case of the flexible base with respect to the fixed base conditions in all kinds of seismic intensities. In addition, they have shown that SSI increases the fundamental period of the structure, especially in the case of softer soil.

### **1.3. Objective and Scope of the Study**

This study intends to investigate the effects of the geotechnical conditions of foundation medium on the seismic behavior of reinforced concrete (RC) moment-resisting frame (MRFs) buildings. As well as, it is aimed to put additional light on the importance of including SSI in numerical analyses of structures, especially displacement-based analysis procedures (i.e. Pushover analysis). In order to achieve this goal, first, the non-linear analysis procedures including capacity spectrum method of ATC-40 and single-mode pushover analysis contained in the latest Turkish Earthquake Code (TEC-2018) are discussed and their merits and shortcomings are outlined. In addition, the performance levels and acceptance criteria purposed by these

standards for seismic investigation of RC buildings are explained. Furthermore, the theoretical aspects of different approaches for incorporating the impacts of SSI to the numerical modeling of RC buildings are investigated. Among the two main approaches, sub-structure and direct methods, which are available in the literature for solving the SSI problems, sub-structure method is utilized. Afterward, based on the selected modeling and analysis methods the effects of soil-structure interaction on seismic responses of 2, 4 and 8 story RC buildings founded on different soil-profiles are examined. For what concerns the geological condition of the site, five different ground conditions for the Adapazari region are considered, where the mechanical properties of the selected ground conditions correspond to ZA, ZB, ZC, ZD and ZE soil types of TEC-2018 provisions. The non-linear behavior of the super-structure is modeled based on the requirements of TEC-2018, while the substructure (soil-foundation interaction) is modeled by means of the impedance functions. The analysis is performed with the help of SAP2000 software package by means of single-mode pushover analysis and the studied buildings are considered to perform against the design earthquake level (DD-2). Finally, the SSI effects on the seismic responses such as base shear force-roof displacement relationship (i.e. pushover curve), vibration period, displacement demand, damage states of the ground floor columns and inter-story drift ratios are studied. The obtained results from the SSI systems are compared with the results of the same model when fixed at their bases.

This thesis consists of six chapters which are summarized in the following;

Chapter 1 provides general information about the RC moment-resisting built structures and their vulnerability against the severe earthquake motions is mentioned. This is followed by introducing the general analysis approaches for the design and performance evaluation of these kinds of buildings. In addition, the importance and needs of incorporating the SSI effects on the seismic investigation of RC buildings are pointed out. Finally, some studies on the subject are summarized and the purpose and scope of the research are explained.

Chapter 2 evaluates the basic concept of seismic performance analysis. In this regard, the performance definition in view of the available seismic codes, related to performance assessment of reinforced concrete structures (RC) is described. As an example, the performance levels along with the acceptance criteria contained in ATC-40, FEMA-356, and TEC-2018 are reported. In addition, at the end of this chapter, the hazard levels and the design elastic spectrum which is a representative of ground motions are reviewed based on the TEC-2018 provision.

Chapter 3 intends to first review the fundamentals of soil-structure interaction (SSI) including kinematic interaction and inertial interaction effects. After that, the analysis methods, direct and substructure approaches that are widely used for solving the SSI problem are explained. In addition, since the main object of this study is to include SSI effects into nonlinear static (pushover) analysis of RC structures, this chapter is concentrated on simplified procedure based on the substructure method. Finally, a review of including the SSI effects for evaluating seismic responses of structures in seismic code is reported.

Chapter 4 highlights the reliability and the accuracy of the simplified nonlinear static analysis approaches (pushover), as well as the merits and shortcomings of this method, are outlined, the implementation of pushover analysis for determining the performance of the RC building is explained. As an example, the capacity spectrum method given in ATC-40 is briefly described and finally, a step by step description of the single-mode pushover analysis for performance evaluation of the RC buildings proposed by TEC-2018 is reported, which is used later on in this thesis.

Chapter 5 present a numerical example, based on the theoretical concepts described in the former chapters. In this numerical example, it is intended to investigate the effects of soil-structure interaction on the seismic performance of the 3D reinforced concrete (RC) moment-resisting frames (MRFs) buildings. The analytical model includes buildings of 2, 4 and 8 stories that were designed based on the minimum requirement of the Turkish Earthquake Code (TEC-2018). The seismic evaluations of the studied buildings are performed as a result of parametric investigations in which the soil

properties, the base condition and the height of the structures vary. Two different support cases are considered as (1) fixed base and (2) flexible base conditions.

The analysis is performed with the help of SAP2000 software package by means of single-mode pushover analysis and the studied buildings are considered to perform against the design earthquake level (DD-2). Finally, the SSI effects on the seismic responses such as base shear force-roof displacement relationship, vibration period, displacement demand, damage states of the ground floor columns and inter-story drift ratios are evaluated. The obtained results from the SSI systems are compared with the results of the same model while fixed at their bases.

Chapter 6 summarize the findings obtained as a result of the parametric research. In addition, the main outcomes are outlined and comparative evaluations are performed as well as recommendations for future studies have been made.



## **CHAPTER 2. SEISMIC PERFORMANCE CONCEPT**

Earthquake is one of the natural disasters that take many lives every year and causes massive economic losses around the world. In fact, it is impossible to prevent natural disasters like ground motions from occurring and also it is difficult at the time being to predict exactly when and where it will happen. However, it is possible to prevent the loss of life and minimize the financial cost by designing the structures to resist the anticipated forces induced by seismic motions. For this purpose, many researchers and analysts have devoted their efforts to develop a reliable design philosophy in the past decades in order to at least minimize the social and economic damages. Accordingly, the performance-based seismic design has emerged and is accepted as the most efficient and reliable design method at the time being that has the ability to reduce the possible damages which will result from an earthquake. In addition, it is included in recent seismic design codes.

The performance-based seismic design concept, particularly widely discussed and used in the recent few decades, provides a realistic and reliable basis for understanding and predicting the risk of living as well as the economic losses that may result from a future earthquake. This concept is basically developed to determine and assess the various type of losses that a building might experience when exposed to different earthquake intensities. This provides the building owner or officials an insight into the risk that their buildings could experience during the possible earthquakes which accordingly they can decide which performance level (performance objective) to choose [22].

Performance objectives express the behavior of buildings against a possible earthquake which define the seismic performance of the buildings. Seismic performance has been defined as the coupling of expected performance levels with the

anticipated hazard levels [23]. The selection of performance objectives is an important factor in the performance-based seismic design process, and the designer is obliged to explicitly demonstrate that the desired performance objective is obtained. The primary goal in selecting a performance objective is to control or limit the anticipated risk or damage a building is expected to experience when subjected to one or more earthquake effects.

Several uncertain factors affect the seismic performance of the structures, they include the intensity, duration and spectral shape of the ground shaking, building response, the usage purpose and importance of the buildings, as well as post-earthquake actions taken by building officials, owners, design professionals, and contractors. Therefore, it is difficult to exactly estimate the performance of a building in a given earthquake. However, seismic provisions and standards have defined different performance levels based on the damages endured by the buildings during the past earthquakes, where the maximum damages under certain levels of ground motions, occurred in the specific sites, are taken as a reference to measure the performance levels. Based on this concept, current seismic codes including Turkish earthquake code (TEC-2018), FEMA-356 and ATC-40 have defined different performance levels in order to measure the damage levels that a building would experience when exposed to possible earthquake hazard.

The main purpose of this chapter is to evaluate the performance definition in view of the available seismic codes, related to performance assessment of reinforced concrete structures (RC). For this purpose, the performance levels along with the acceptance criteria contained in ATC-40, FEMA-356 and TEC-2018 are reported. In addition, at the end of this chapter, the hazard levels and the design elastic spectrum which is a representative of ground motions are reviewed based on the TEC-2018 provision.

### **2.1. Performance Definition According to ATC-40**

In ATC-40, the damage states of the buildings are identified by considering both structural and non-structural performance levels and the combination of them is used to describe the complete performance (damage state) of the structures, but in this study,

only structural performance is accounted for. The desired performance level is then combined by a given earthquake motion to form the building performance objective.

According to ATC-40 provision, structural damage states (i.e. performance levels) are characterized using five different limits and ranges, where the three of them are discrete limits and the other two are defined as the intermediate-range between the two discrete performance limits. Each of them is explained in the following paragraphs;

- a) Immediate Occupancy (IO): is a discrete damage limit in which the structural damages are negligible after the earthquake and the building maintains its pre-earthquake stability and functionality. Almost there is no risk to endanger life due to structural failure.
- b) Life Safety (LS): This discrete damage limit indicates that the post-earthquake structural damage is significant, but the building still can resist against the total collapse. There may not be a risk to endanger life safety but serious injuries are possible during the earthquake. The damage endured by the structure might be repairable for reoccupation but it would be expensive economically.
- c) Structural Stability (SS): This is the third discrete performance level in which the structural system has suffered severe damage and the building is expected to collapse partially or totally. The life safety might be significantly in danger due to the collapse of the structure and it would be almost impossible to repair it for reoccupation after the earthquake both technically and economically.

As mentioned earlier, the two intermediate performance ranges defined by ATC-40 include Damage Control Range and Limited Safety Range which extends between IO-LS and LS-SS, respectively. The structural performance ranges are defined in order to simplify the selection of building performance objectives to the users.

## **2.2. Acceptance Criteria According to ATC-40**

In ATC-40 provision, each of the damage states or performance levels (Section 2.1.) is quantified using the corresponding response limits, obtained using pushover analysis (Chapter 4.). The ATC-40 document, provide both global acceptance limits and component-based acceptance criteria. Global performance limits are defined in terms of response limits such as gravity load capacity, lateral load resistance and lateral deformation capacities of the structural system. Whereas, component acceptability requirements (minimum damage limits) are described by means of plastic hinge rotations developed in each individual structural element. In this study, only global response limits contained in ATC-40 are reported in the following subsection.

### **2.2.1.Global acceptance criteria for the buildings**

As mentioned earlier the global performance of the structures are quantified in terms of vertical load capacity, lateral load resistance and lateral drifts which are summarized in the following paragraphs;

- a) Gravity load capacities: Based on the damages caused to the buildings during the strong ground motion in the past, the failure of columns and the location and joints where this element was connected to the other elements such as beams and slabs has been identified as the main cause for the collapse of the buildings. Since these damages were caused due to the exceedance in the vertical load capacity of the columns and its connection with the other elements, therefore, ATC-40 emphasizes that the vertical load capacity of the buildings has to remain intact no matter what performance level is considered.
- b) Lateral loads resistance acceptability: When the structure is exposed to multiple cyclic loading, resulting from strong ground motions, some of the components may degrade. If a large amount of the elements degrades, the overall lateral load resistance of the structures may be affected. Therefore, ATC-40 specified an upper bound regarding the degrading amount of the

lateral load resistance components and state that “the lateral load resistance of the building system, including resistance to the effects of gravity loads acting through lateral displacements, should not degrade by more than 20 percent of the max resistance of the structure”.

- c) Lateral deformations (drift) limits: Global lateral deformation limits, corresponding to the performance point, are specified by ATC-40 document for different performance levels which is summarized in Table 2.1. Based on this standard, the total maximum drift ratio is defined as the sum of elastic and inelastic drifts, corresponding to the performance point.

Table 2.1. Global lateral deformation limits

Inter-story drift limits	Performance Level			
	IO	DC	LS	SS
Maximum total drifts (%)	1	1-2	2	$33*V_i/P_i$
Maximum inelastic drifts (%)	0.5	0.5-1.5	no limits	no limits

Where, in Table 2.1.  $V_i$  is the total shear force calculated at the  $i$ 'th story and  $P_i$  is the vertical loads at the same story. However, a 4 percent upper bound for SS performance limit is considered in this study to measure the drift ratios (based on FEMA-356).

### 2.3. Performance Definition According to TEC-2018

According to the TEC-2018 provision, the seismic evaluation can be performed either using force-based or displacement-based analysis approaches, depending on the type of the structure and desired performance objective. However, the force-based method is not covered in this study and the displacement-based method is described in Chapter 4.

Based on TEC-2018, four performance levels have been defined, in order to specify the damage states, for the structural system under the effects of earthquake ground

motions. The performance levels considered in this document include fully operational (KK), limited damage (SH), damage control (KH) and collapse prevention (GÖ) performance levels (see Figure 2.1.). Each of them is summarized in the following paragraphs;

- a) Fully operational (KK) performance level: this performance level describe the condition where no damage has occurred in load-bearing members of the building or the damages are negligible.
- b) Limited damage (SH) performance level: this performance level states that only very little or limited damage has occurred to the structural member, in other words, the inelastic behavior remains limited.
- c) Damage control (KH) performance level: in this performance level life safety is essentially protected, load-bearing member of the buildings undergoes moderate damage and often repairable to ensure safety.
- d) Collapse prevention (GÖ) performance level: corresponds to the pre-collapse state where severe damage has occurred to the building load-bearing members. However, the partial or complete collapse of the building is prevented.

#### **2.4. Acceptance Criteria According to TEC-2018**

According to the TEC-2018 standard, member's performance level, for ductile members, are quantified for three discrete damage states (Section 2.3.). These are limited damage (SH), damage control (KH) and collapse prevention (GÖ) performance levels as is illustrated in Figure 2.1. Furthermore, depending on non-linear modeling strategies, whether distributed plasticity model or concentrated plasticity model (see Chapter 4.), the acceptability requirements are described by means of strain limits at the outmost portion of the critical section (where the most severe damage has occurred) and plastic rotation limits. Strain limits are used as measurement quantity for

distributed plasticity models, while for concentrate plasticity models, plastic rotations at each element are accepted as measurement tools.

In TEC-2018 there is not given information about global acceptance criteria (response limits for story drifts) as it is provided by ATC-40 and FEMA-356. However, the overall performance of the building is determined by considering the distribution of member damage over the structure.

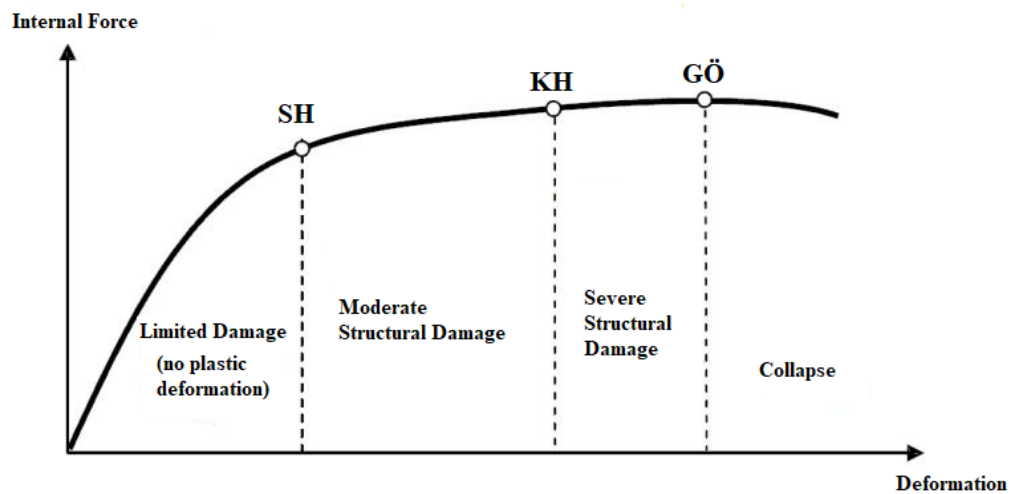


Figure 2.1. Structural element damage levels and regions [24]

The section damage regions are also shown in Figure 2.1. As it is apparent from Figure 2.1, four damage regions are defined. These are limited damage region (LD) in which very little damage has occurred and does not exceed limited damage performance level (SH), moderate damage region (MD) in which element damages extends between limited damage (SH) and damage control performance level (KH), severe damage region (SD) where structural elements undergo higher inelastic deformation and extends between control damage performance level and collapse prevention performance level (GÖ) and finally the collapse damage region where significant plastic deformation has occurred and may not be repairable, this range extends beyond collapse prevention performance level.

For performance evaluation of new reinforced concrete buildings, the response limits of structural members are defined for three discrete performance levels. Both strain

limits (for distributed plasticity model) and plastic rotation limits (for concentrated plasticity model), corresponding to each performance level, are given in the following sub-sections.

#### 2.4.1. Acceptance criteria for collapse prevention (GÖ) performance level

The concrete strain limit at the outmost fiber of critical cross-section (rectangular sections) corresponding to the collapse performance level is described by the following equation;

$$\varepsilon_c^{(G\ddot{O})} = 0.0035 + 0.04\sqrt{\omega_{we}} \leq 0.018 \quad (2.1)$$

Where the first term in equation (2.1) is the unconfined concrete compressive strain and  $\omega_{we}$  is the effective lateral confining stress, which can be computed using the relationship below;

$$\omega_{we} = \alpha_{se} \rho_{sh, \min} \frac{f_{ywe}}{f_{ce}} \quad (2.2)$$

Where  $\alpha_{se}$  is the confinement effectiveness coefficient,  $\rho_{sh, \min}$  is the ratio of the volume of the transverse steel to the volume of the confinement concrete core for rectangular sections in x or y-direction whichever is smaller,  $f_{ywe}$  is the expected yield strength of the transverse reinforcement and  $f_{ce}$  is the expected compression strength of the confinement concrete.

The confinement effectiveness coefficient,  $\alpha_{se}$  and volumetric transverse steel ratio,  $\rho_{sh}$ , are given by equation (2.3) and (2.4), respectively:

$$\alpha_{se} = \left(1 - \frac{\sum a_i^2}{6b_0h_0}\right) \left(1 - \frac{S}{2b_0}\right) \left(1 - \frac{S}{2h_0}\right) \quad (2.3)$$



$$\rho_{sh} = \frac{A_{sh}}{b_k S} \quad (2.4)$$

Where in Equations (2.3) and (2.4),  $A_{sh}$  and  $\rho_{sh}$  are the area of transverse reinforcement bar and volumetric transverse steel ratio, respectively. The letter  $b_k$  represents the core dimension in the perpendicular direction (the distance between the centerline of the outermost transverse bars),  $S$  is the center to center spacing of the transverse bars,  $b_0$  and  $h_0$  is the core dimension to centerline of transverse bars in x and y direction, respectively. The letter  $a_i$  is the  $i$ 'th clear distance between the centerline of adjacent longitudinal bars.

Similarly, the tensile strain limits of steel corresponding to the collapse perversion performance level is given as:

$$\varepsilon_s^{(G\ddot{O})} = 0.4\varepsilon_{su} \quad (2.5)$$

Where  $\varepsilon_{su}$  is the ultimate tensile strain of the reinforcement bar.

In the case of modeling non-linearity of structural members using concentrated hinge model, plastic rotation limits corresponding to the collapse prevention performance level is computed as follow:

$$\theta_p^{(G\ddot{O})} = \frac{2}{3} \left[ (\phi_u - \phi_y) L_p \left( 1 - 0.5 \frac{L_p}{L_s} \right) + 4.5 \phi_u d_b \right] \quad (2.6)$$

Where  $\phi_u$  is the total curvature of the elements corresponding to the concrete and steel strain limits given by Equation (2.1) and Equation (2.5), respectively. The symbol  $\phi_y$  is the yield curvature,  $L_p$  is plastic hinge length,  $L_s$  is the shear span (can be taken as half of the element length) and  $d_b$  is the longitudinal bar size in units of m.

### 2.4.2. Acceptance criteria for damage control (KH) performance level

The total concrete and steel strain limits, as well as the total plastic rotation limits specified for this performance level, is calculated in terms of the strain and plastic rotation limits identified for collapse perversion performance level as:

$$\varepsilon_c^{(KH)} = 0.75 \varepsilon_c^{(G\ddot{O})} \quad ; \quad \varepsilon_s^{(KH)} = 0.75 \varepsilon_s^{(G\ddot{O})} \quad (2.7)$$

$$\theta_p^{(KH)} = 0.75 \theta_p^{(G\ddot{O})} \quad (2.8)$$

### 2.4.3. Acceptance criteria for limited damage (SH) performance level

The total concrete and steel strain limits and the total plastic rotation limits defining this performance level described by the following relationships;

$$\varepsilon_c^{(SH)} = 0.0025 \quad ; \quad \varepsilon_s^{(SH)} = 0.0075 \quad (2.9)$$

$$\theta_p^{(SH)} = 0 \quad (2.10)$$

## 2.5. Earthquake Ground Shaking Hazard Levels

In performance-based seismic design, it is necessary to determine under which earthquake the selected building performance level is to be achieved. In the TEC-2018 document, four different earthquake ground shaking hazard levels have been defined depending on its probability of exceedance and magnitude. These are earthquake hazard level-1(DD-1), earthquake hazard level-2 (DD-2), earthquake hazard level-3 (DD-3) and earthquake hazard level-4 (DD-4). The data for the defined earthquake hazard levels can be obtained from the Turkish earthquake hazard map through <https://tdth.afad.gov.tr/> web address. The Turkish earthquake hazard map is shown in Figure 2.2.

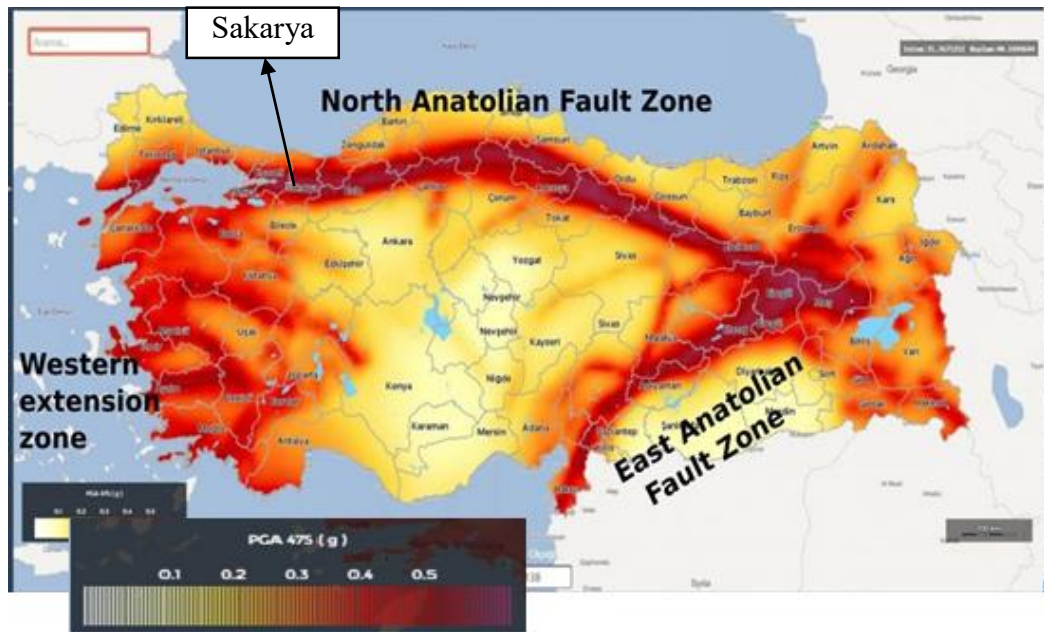


Figure 2.2. Turkish earthquake hazard map (TEC-2018)

### 2.5.1. Earthquake ground shaking hazard level-1 (DD-1)

This level of ground motion describes the hazard level (never experienced in reality) where there is 2% chance that its spectral magnitudes exceed in 50 years and has a repetition period of 2475 years. This level of hazard is also called the largest earthquake ground motion that might ever occur.

### 2.5.2. Earthquake ground shaking hazard level-2 (DD-2)

This level of ground motion characterizes the hazard level that occurs rarely, where there is 10% chance that its spectral magnitudes exceed in 50 years and the corresponding repetition period is 475 years. This level of hazard is also called the standard design earthquake ground motion.

### 2.5.3. Earthquake ground shaking hazard level-3 (DD-3)

This level of ground motion refers to a frequent hazard level (experienced frequently), where there is 50% chance that its spectral magnitudes exceed in 50 years and its corresponding repetition period is 72 years.

#### 2.5.4. Earthquake ground shaking hazard level-4 (DD-4)

This level of hazard motion describes a very frequent earthquake ground motion, where the probability of its spectral magnitudes being exceeded in 50 years is 68% (50% chance of being exceeded in 30 years) and the corresponding repetition period is 43 years. This earthquake ground motion is also called service earthquake ground motion.

### 2.6. Standard Earthquake Ground Shaking Response Spectra

According to TEC-2018, response spectra for any given level of earthquake hazard can be developed for a 5% damping ratio based on the following two procedures: (1) depending on mapped response acceleration coefficient and local site parameters in a standard format, and (2) by implementing site-specific seismic hazard analysis as is described in TEC-2018. In this section, the first procedure will be explained briefly in the following sub-sections.

#### 2.6.1. Determination of mapped and design spectral acceleration coefficients

In TEC-2018, dimensionless mapped spectral acceleration coefficients are given as short-period (0.2 seconds) response acceleration coefficient,  $S_S$ , and long-period (1 second) response acceleration coefficient,  $S_1$ , for four different earthquake ground shaking hazard levels (Section 2.5.). The values of the mapped spectral acceleration coefficient can be obtained in a dimensionless form directly from the Turkish earthquake hazard map by selecting a point, where the building is to be built for any considered earthquake hazard level. After determining mapped values of  $S_S$  and  $S_1$ , the design response acceleration coefficients  $S_{DS}$  and  $S_{D1}$  can be determined as follow:

$$S_{DS} = S_S F_S \quad ; \quad S_{D1} = S_1 F_1 \quad (2.11)$$

Where  $F_S$  and  $F_{S1}$  are the local site coefficients

### 2.6.2. Determination of the local site parameters

The values of the local site parameters  $F_S$  and  $F_{S1}$  defined for different soil classes in TEC-2018 are presented in Tables 2.3 and 2.4 respectively. These parameters are defined based on the site classes and the values of the mapped response acceleration parameters  $S_s$  and  $S_1$  for a selected hazard level. For intermediate values of the mapped spectral acceleration coefficient, straight-line interpolation can be used.

Table 2.2. Values of  $F_S$ , defined in TEC-2018 for different soil types

Site Class	Mapped spectral acceleration at short periods, $S_s$					
	$S_s \leq 0.25$	$S_s = 0.50$	$S_s = 0.75$	$S_s = 1.00$	$S_s = 1.25$	$S_s \geq 1.50$
A	0.8	0.8	0.8	0.8	0.8	0.8
B	0.9	0.9	0.9	0.9	0.9	0.9
C	1.3	1.3	1.2	1.2	1.2	1.2
D	1.6	1.4	1.2	1.1	1	1
E	2.4	1.7	1.3	1.1	0.9	0.8
F	Site-specific geotechnical investigation is required					

Table 2.3. Values of  $F_1$ , defined in TEC-2018 for different soil types

Site Class	Mapped spectral acceleration at one-second periods, $S_1$					
	$S_1 \leq 0.10$	$S_1 = 0.20$	$S_1 = 0.30$	$S_1 = 0.40$	$S_1 = 0.50$	$S_1 \geq 0.60$
A	0.8	0.8	0.8	0.8	0.8	0.8
B	0.8	0.8	0.8	0.8	0.8	0.8
C	1.5	1.5	1.5	1.5	1.5	1.4
D	2.4	2.2	2	1.9	1.8	1.7
E	4.2	3.3	2.8	2.4	2.2	2
F	Site-specific geotechnical investigation is required					

### 2.6.3. Design elastic response spectra

To ensure consistency with a given performance level, displacement consistent with seismic demand across the capacity curve should be determined. For the practical seismic design of structures, simplified response spectra that represent the hazard of a site are used. These spectra represent the average values from a number of possible earthquakes scenarios that could affect the site under consideration [25]. Design elastic

response spectra in many building codes are represented by a plot of acceleration versus building period for a given damping ratio (generally 5% damping ratio is recommended). In this section, the horizontal design elastic spectrum proposed for seismic design of new building or retrofit of the existing building by TEC-2018 seismic code will be explained briefly. Vertical design elastic spectrum is also given in this document, but, since it is beyond the scope of this study will not be discussed.

Depending on the design spectral acceleration coefficient (Section 2.6.1.), for a given earthquake hazard level the design elastic acceleration response spectrum diagram, where its ordinates are represented by horizontal design elastic spectral acceleration,  $S_{ae}(T)$ , and the natural vibration period of the building,  $T$ , can be determined using the following relationships:

$$\begin{aligned}
 S_{ae}(T) &= \left( 0.4 + 0.6 \frac{T}{T_A} \right) S_{DS} & (0 \leq T \leq T_A) \\
 S_{ae}(T) &= S_{DS} & (T_A \leq T \leq T_B) \\
 S_{ae}(T) &= \frac{S_{D1}}{T} & (T_B \leq T \leq T_L) \\
 S_{ae}(T) &= \frac{S_{D1} T_L}{T^2} & (T_L \leq T)
 \end{aligned} \tag{2.12}$$

In which  $S_{DS}$  and  $S_{D1}$  are the design response acceleration coefficient for a short period and 1-second period, respectively, which is defined in Section 2.6.1. The letter  $T$  is the natural vibration period of the building. The symbol  $T_A$  and  $T_B$  are the corner period and are given depending on  $S_{DS}$  and  $S_{D1}$  by Equation (2.13).

$$T_A = 0.2 \frac{S_{D1}}{S_{DS}} ; \quad T_B = \frac{S_{D1}}{S_{DS}} \tag{2.13}$$

And finally  $T_L$  is the transition period with a constant value of 6 seconds.

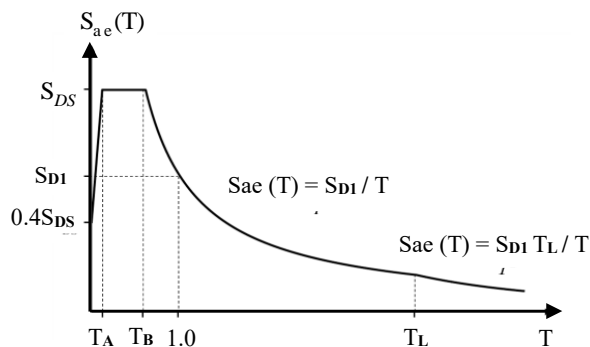


Figure 2.3. Horizontal design elastic acceleration response spectrum curve (TEC-2018)

Similarly, the horizontal design elastic displacement response spectrum is also defined based on the natural period of the building,  $T$ , and the horizontal design elastic spectral acceleration,  $S_{ae}(T)$ , for a given earthquake hazard level. The ordinates of design elastic displacement response spectrums are represented by horizontal design elastic spectral displacement,  $S_{de}(T)$ , which can be obtained as follow in units of m.

$$S_{de}(T) = \frac{T^2}{4\pi^2} g S_{ae}(T) \quad (2.14)$$

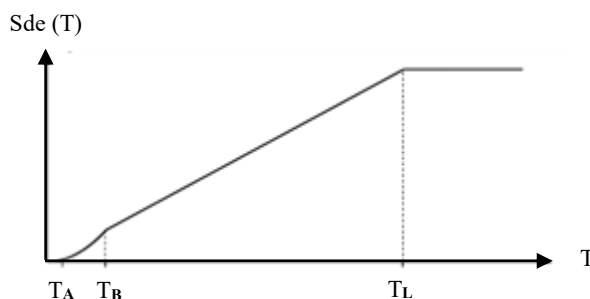


Figure 2.4. Horizontal design elastic displacement response spectrum curve (TEC-2018)

## **CHAPTER 3. FUNDAMENTALS OF SOIL-STRUCTURE INTERACTION ANALYSIS**

Typically in practice, the seismic investigation is performed by assuming the structures to be fixed on their basis. This assumption can only be reliable and realistic when the ground environment is very rigid compared to the superstructure. Whereas mostly this is not the case and the superstructure and the underlying soil layer both behave together against static and dynamic external loads as a deformable systems. Therefore, in order to account for the real behavior, the ground region should be defined as a part of the structural system and analyzed together with the superstructure.

Furthermore, the interaction between the subsoil and the superstructure plays an important role in seismic design, especially for structures that are built on less favorable geotechnical conditions and in high seismic regions. This may change the seismic responses of the structures to a considerable extent [4]. In reality, when a building is subjected to ground shaking its responses are affected by the mutual interaction of the subsoil and the superstructure itself [25]. Accordingly, the soil-structure analysis evaluates the collective behavior of this interacting system.

The interaction between supporting soil, foundation, and structure simultaneously integrates two primary physical phenomena [26]. The first one is denoted as kinematic interaction that is the ability to filter the ground motions transmitted to the structure. The second one is known as inertial interaction, resulting from the building self-vibration, induced to the structure by the earthquake, which, in turn, generates base shear and moment. These two components of soil-structure interaction are further explained in this chapter.



The main purpose of this chapter is to first introduce the soil-structure interaction (SSI) effects (kinematic and inertial effects) briefly, then the analysis method (direct and substructure approaches) that can be used to evaluate the SSI effects is discussed. Since the main object of this study is to include soil-structure interaction into nonlinear static (pushover) analysis of RC structures, this chapter is concentrated on simplified procedure based on substructure method. Finally, a review of including the SSI effects for evaluating seismic responses of structures in seismic code is reported.

### **3.1. Kinematic Interaction**

Kinematic interaction expresses the refraction and reflection of the earthquake waves that are traveling to the surface of the ground when they are encountered to a very rigid foundation located either on the surface or embedded within the soil stratum. The kinematic interaction results from the contribution of the following three mechanisms [26]:

- 1) Base-slab averaging: occur when the foundations are unable to follow the free-field motion. This happens when the earthquake waves, which are variable originally, are encountered with a very rigid foundation causing an averaging effect under its footprint area. This effect reduces the foundation motion with respect to the free-field. In other words, the foundation motion is less than the case that would happen in the free-field. Kinematic interaction due to base-slab averaging is illustrated in Figure 3.1.
- 2) Embedment effects: The effects of ground motion reduce as the depth increases, meaning that by increasing the foundation depth the embedment effects become more important.
- 3) Wave scattering: The seismic waves that hit the foundation is normally scattered from it, especially it happens at the corner of the columns.

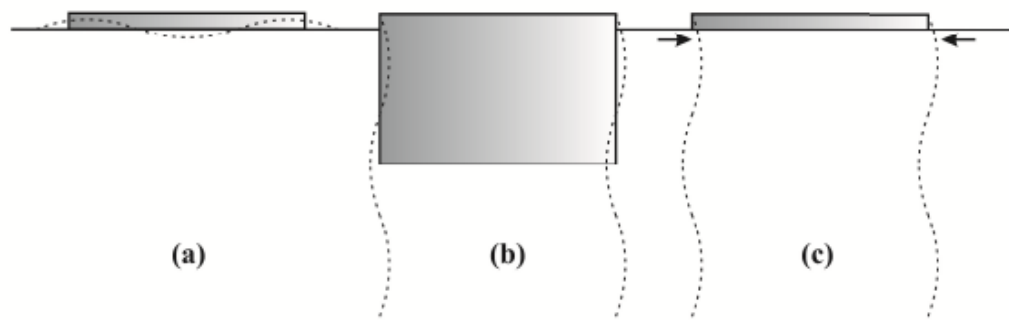


Figure 3.1. Kinematic interaction due to base-slab averaging [2]

The effects of kinematic interaction can be expressed by a complex-valued transfer function relating to free-field and foundation motion [26]. In addition, transfer function depends on the damping characteristic of the soil-medium, which in case of infinitely stiff soil assumption the amplitude and phase of the transfer function is unity and zero, respectively. In other words, there is too much similarity between the foundation and free field motion, which cannot be differentiated.

### 3.2. Inertial Interaction

Structural responses such as base shear, moment and torsional excitation rise in a vibrating structure due to inertia developed in it. Consequently, displacements and rotations are developed in the foundation with respect to the free field, resulted from the induced base shear forces and moments, respectively. However, these relative motions in the foundation only rise when the soil-foundation system is deformable and may cause considerable changes in the overall flexibility of the structural system in some particular cases. In addition, the relative movements of foundation with respect to the free field also causes the development of radiation and hysteretic damping in the soil, which dissipates and spread the earthquake-induced energies into the ground. Accordingly, the damping configuration of the whole soil-structure system may considerably be influenced by this energy propagation. The concept described above is then called inertial interaction effects [3]. In order to incorporate the inertial interaction effects in the seismic design, the soil foundation system is generally represented by a series of equivalent springs, the stiffness and damping parameters of

this equivalent springs are then calculated by means of impedance functions (Section 3.3.2.1.).

### **3.3. Methods of Analysis**

In order to numerically solve soil-structure interaction problems, an interaction surface that divides the supporting soil and structure is generally taken into consideration, and the purpose of introducing this interacting surface is to simplify numerical modeling and analysis. The main problem here is how to optimize the geotechnical condition of the supporting soil, and soil-structure interface. Two main analyzing approaches, direct and sub-structure approaches are generally used to solve soil-structure interaction problems. In this section, first, the direct method is explained briefly and afterward sub-structure method is discussed in more detail which is used later in this study.

#### **3.3.1. Direct approach**

This method can be preferred for solving the SSI problem when the geometry of the structure is simple and also when the consideration of non-linear behavior of the soil-medium is important. In addition, the direct method provides the possibility to model the SSI system together and solve it in a single step. The modeling concept of this method is based on finite elements. Accordingly, a large portion of the soil-layer under the foundation is cut down by a boundary called “transmitting boundary” and is represented by a solid finite element. On the other hand, the structure is generally represented by a finite beam element and an interface between the foundation and the sub-soil is considered to provide the response transition between the soil and the structure (Figure 3.2.).

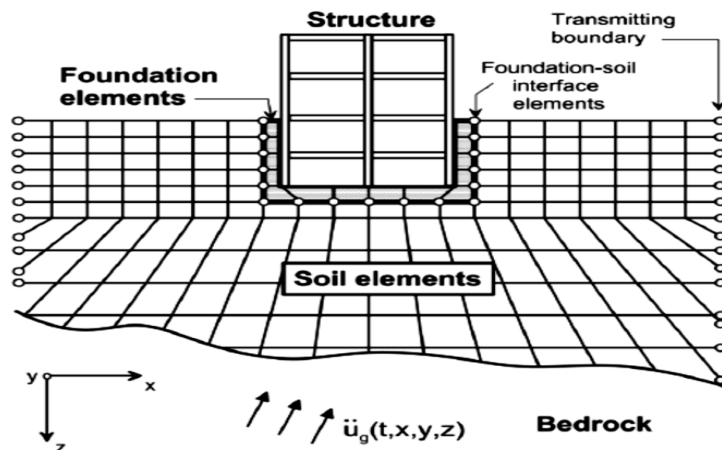


Figure 3.2. Modelling SSI using the direct method [27]

The transmitting boundaries represent the stiffness of the soil up to infinity and prevent the wave propagation that is moving outward from the soil boundaries. In other words, this boundary allows the waves to be reflected inward and absorbed. The seismic excitation is applied along the artificial boundaries of the system. Typically, the seismic free-field input motion  $\{\ddot{u}_{FF}\}$  is utilized as seismic excitation and the seismic displacement response  $\{u\}$  of the soil-structure interaction system is computed using the equation of motion which is defined as follow:

$$[M^*]\{\ddot{u}\} + [C^*]\{\dot{u}\} + [K^*]\{u\} = -[M^*]\{\ddot{u}_{FF}\} \quad (3.1)$$

In which  $[C^*]$ ,  $[K^*]$  and  $[M^*]$  are damping, stiffness and mass matrices, respectively.

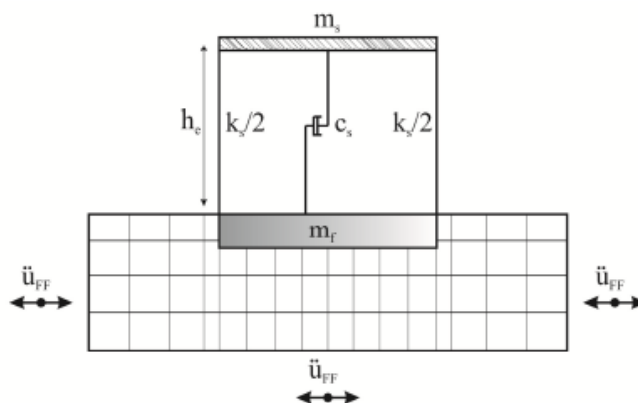


Figure 3.3. Soil-structure interaction analysis using the direct method [2]

In the direct method, a system with complex geometry can be divided into finite elements of known geometry and material behavior can be defined more appropriately. However, the biggest disadvantage of this method is the use of too many elements in the solution of large systems such as soil-structure interaction analysis. Writing the equilibrium equations for the whole system with the help of shape functions for each element requires too many efforts and thus, very long run-time. Therefore, it is rarely used in practice [14].

### **3.3.2. Substructure approach**

The second method to solve complex soil-structure interaction (SSI) problems is referred to as substructure method. Unlike the direct method in which the whole SSI problem is included in the same mathematical model and analyzed in a single step, this method broke down the SSI system into different substructures and each substructure is then modeled and analyzed independently. These independent models are combined by applying equal and opposite interaction forces to each substructure model. Superposition concept is then applied to combine all of the substructure seismic responses to compute the final seismic response of the SSI system. Therefore, since each step is independent of the other the analyst can focus on the most important part. And this is the main advantage of this approach.

In the substructure approach, the displacement response of the SSI system is defined as the sum of displacement responses due to kinematic and inertial responses. In this approach displacements responses on the nodes of the soil-structure interface is related to the interaction forces of unbounded soil by dynamic stiffness matrix based on the boundary element method [28]. In addition, a review of computing displacement responses due to kinematic and inertial interaction, and combining them to formulate the final responses of the SSI system is made by [2] which is summarized here in the following paragraphs.

As it is illustrated in Figure 3.4, in a sub-structure method, the SSI problem is broken down into its basic kinematic and inertial components.

The displacement responses of the SSI problem are calculated as follow;

$$\{u\} = \{u_{KI}\} + \{u_{II}\} \quad (3.2)$$

Where  $\{u_{KI}\}$  is kinematic interaction displacement and  $\{u_{II}\}$  is the inertial interaction displacement.

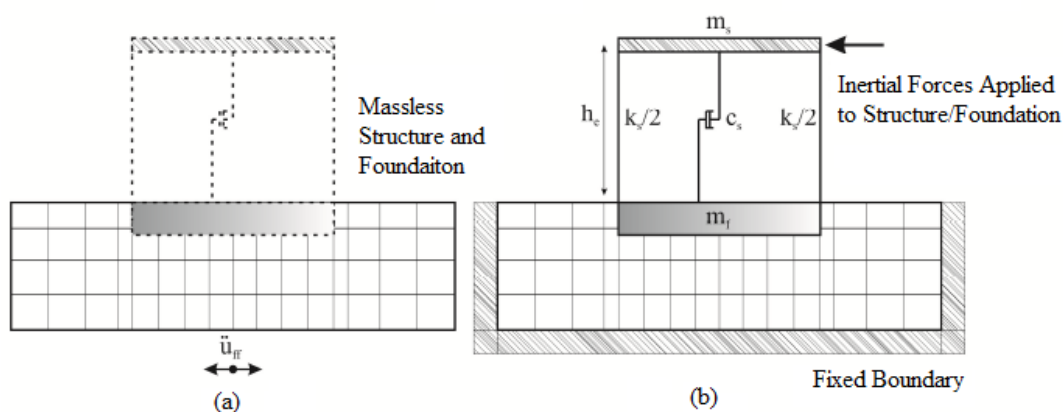


Figure 3.4. Soil structure interaction analysis using substructure approach: (a) kinematic; (b) inertial interaction [2]

Assuming a massless structure and foundation, kinematic interaction displacement is calculated by subjecting the soil-structure interaction system to the free field motion and is expressed by the Equation of motion as follow;

$$[M_{soil}]\{\ddot{u}_{KI}\} + [C^*]\{\dot{u}_{KI}\} + [K^*]\{u_{KI}\} = - [M_{soil}]\{\ddot{u}_{FF}\} \quad (3.3)$$

Where  $[M_{soil}]$  is the mass matrix of the SSI system with assuming massless foundation and structure.

After solving Equation (3.3) the resulting  $[u_{KI}]$  is then used to define inertial loading,  $- [M_{structure}]\{\ddot{u}_{KI} + \ddot{u}_{FF}\}$ , which is required to account for inertial interaction in the analysis. Accordingly, the inertial interaction is expressed by the equation of motion as follow;

$$[M^*]\{\ddot{u}_H\} + [C^*]\{\dot{u}_H\} + [K^*]\{u_H\} = - [M_{structure}]\{\ddot{u}_{KI} + \ddot{u}_{FF}\} \quad (3.4)$$

Where  $[M_{structure}]$  is the mass matrix representing the mass of structure and foundation. It is worth to mention that the inertial loading should be applied to the structure only.

Two kinds of solution is available for solving Equation (3.4); the first one is to model the soil medium using finite elements and the second one is to represent the soil properties including damping and stiffness with the “condensed stiffness matrix”, where each degree of freedom of the soil medium is concentrated into the degrees of freedom in the interacting surface.

Furthermore, the following steps can be tracked for solving the SSI problem within the sub-structure approach [26]:

- 1) Evaluate the foundation input motion by assuming a massless foundation and structure. By making this assumption, inertial effects are neglected and only kinematic interaction, which depends on the geometry and stiffness of the foundation and soil, is accounted for.
- 2) Develop the compliant base model by calculating the stiffness and damping parameters of the soil-foundation system by means of impedance functions. These parameters are required to define the equivalent spring properties (stiffness and damping).
- 3) Subject the structure with the deformable base (Step 2) to earthquake excitation or foundation input motion (Step 1), then compute its dynamic responses.

The process of analyzing the SSI problem considering the above-mentioned steps are schematically demonstrated in Figure 3.5.

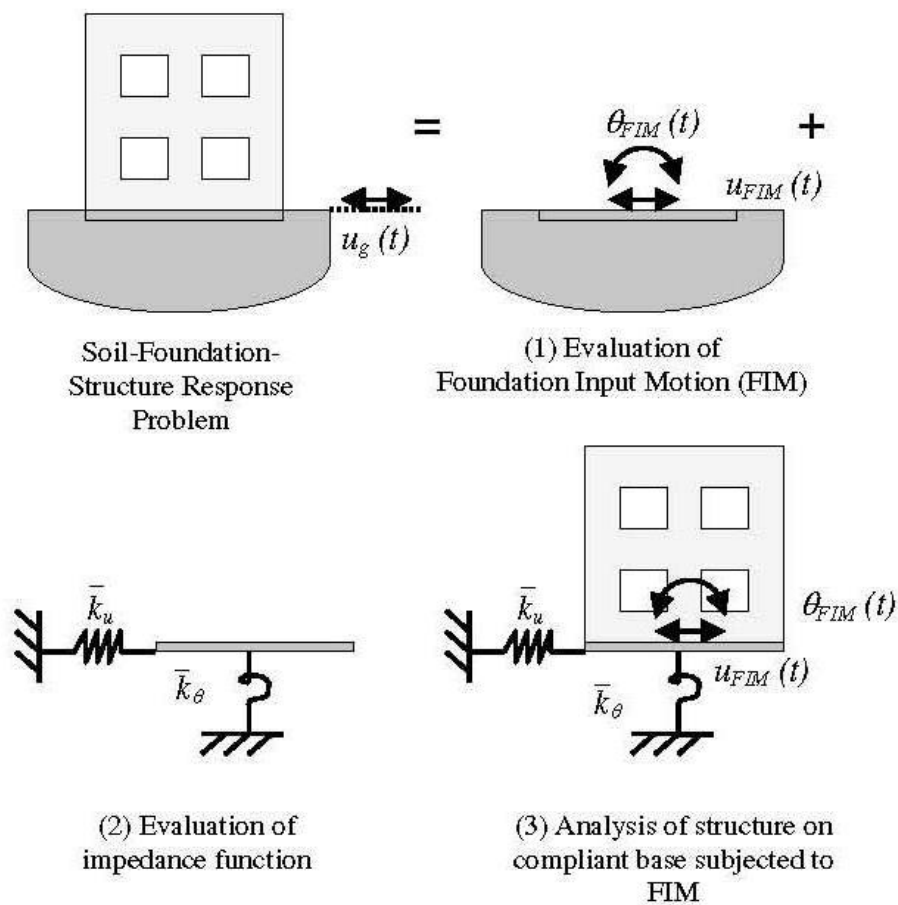


Figure 3.5. Substructure approach for analyzing the SSI problem [26]

### 3.3.2.1. Impedance functions

In order to solve the SSI problem, using substructure method, determination of the impedance function which represents the stiffness and damping features of the soil-foundation interaction is an important step. As mentioned before, the inertial interaction effects can be represented by means of impedance function. The impedance function is defined mathematically by a matrix that relates the forces generated at the base of the structure to the displacement responses (translation and rotation) of the foundation relative to the free field. Typically, in order to define the impedance function, six degrees of freedom are required at each grid point of the soil-foundation interface. However, in the case of assuming a rigid foundation the degrees of freedom reduces to six in total. These degrees of freedom, in turn, coincide with six modes of foundation vibration. The vibration mode for a rigid foundation can be outlined as



three displacements along three major axes namely x, y and z-axis and three rotations around these axis.

Generally, in a substructure method, the soil is represented by a series of springs with stiffness coefficient  $K$  and dashpots with damping coefficient  $C$ . The impedance function associated with each mode of vibration then can be computed by determining the values of these coefficients. As it is schematically illustrated in Figure 3.6, the soil is represented by springs and dashpots.

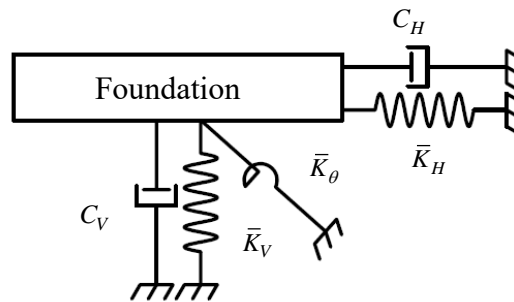


Figure 3.6. Schematic representation of soil by springs and dashpots

In order to compute the impedance function, several analytical procedures have been developed by different researchers. Among them, the most widely used solution is the one developed for a rigid circular foundation located on the surface of visco-elastic half-space (Veletsos and Verbic, [29]; Stewart. et. al, [26]). Accordingly, the complex-valued impedance function can be expressed as:

$$\bar{K}_j = k_j(a_0, \nu) + i\omega c_j(a_0, \nu) \quad (3.5)$$

Equation (3.5) shows the terms in the impedance function, for impedance analysis assuming a rigid disk located on half-space. In which subscript  $j$  indicates which mode should be considered (translational or rotational modes),  $\omega$  stands for the angular frequency in terms of rad/sec. Similarly,  $a_0$  is a dimensionless frequency given by  $a_0 = \omega r / V_s$ , in which  $r$  shows foundation radius,  $V_s$  denotes the shear wave velocity of the sub-soil, and  $\nu$  symbolize soil Poisson ratio. Since the impedance functions for translational modes are calculated depending on the contact area of the foundation,

$A_f$ , and for rotational modes depending on its moment of inertia,  $I_f$ , the values of  $r$  is computed separately for each of them as follow;

$$r_1 = \sqrt{\frac{A_f}{\pi}} \quad r_2 = \sqrt[4]{\frac{4I_f}{\pi}} \quad (3.6)$$

Based on this assumption (circular rigid foundation on the surface of soil halfspace) the actual damping and stiffness coefficient corresponding to rotational and translational springs can be stated as follow:

$$k_u = \alpha_u K_u ; c_u = \beta_u \frac{K_u r_1}{V_S} ; k_\theta = \alpha_\theta K_\theta ; c_\theta = \beta_\theta \frac{K_\theta r_2}{V_S} \quad (3.7)$$

Where  $\alpha_u$ ,  $\beta_u$ ,  $\alpha_\theta$  and  $\beta_\theta$  are dimensionless parameters which indicate the frequency dependence of the results.  $K_u$  and  $K_\theta$  shows the static stiffness of the disk on a halfspace and can be determined using Equation (3.8).

$$K_u = \frac{8}{2-\nu} Gr_1 \quad K_\theta = \frac{8}{3(1-\nu)} Gr_2^3 \quad (3.8)$$

Where  $G$  is the soil shear modulus and can be obtained appropriately with the in situ shear strain. The values of  $\alpha_u$ ,  $\beta_u$ ,  $\alpha_\theta$  and  $\beta_\theta$  can be determined for soil poisson ratio  $\nu = 0.4$  graphically from the charts presented in Figure 3.7.

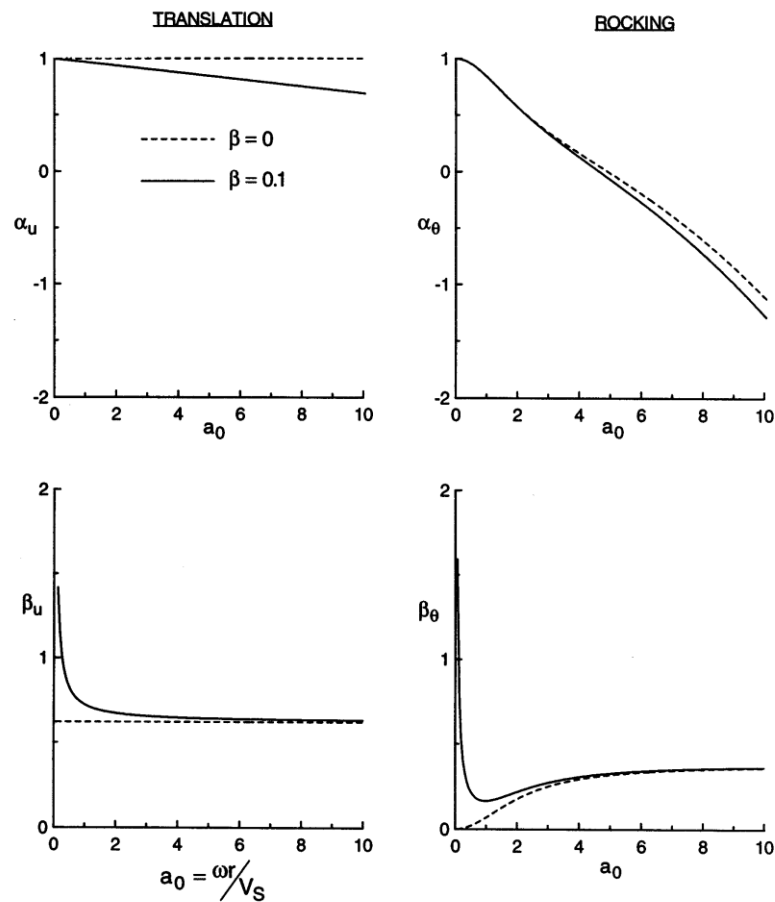


Figure 3.7. Foundation stiffness and damping factors for elastic and viscoelastic halfspace, for Poisson ratios,  $\nu = 0.4$  [29]

The method described above, as mentioned before, is based on the assumption that a rigid circular disk located on the soil half-space, however, in reality, most of the foundation does not have circular geometry. To apply this approach for other types of the foundation a series of assumptions and modifications are needed which makes it less accurate. In addition, this procedure is basically developed for dynamic analysis, and might not be appropriate for nonlinear static analysis which is the object of this study.

Furthermore, many other simplified impedance solutions are available for any arbitrary shaped rigid foundation located on the surface or embedded within the soil-medium. For example Pais and Causel [30], Gazetas [13] and Mylonakis et al. [31] have reviewed the literature for impedance solutions and presented equations for computing the stiffness and damping characteristics of springs and dashpots for

rectangular foundation resting on the surface or embedded within, a uniform, elastic or viscoelastic half-space with shear wave velocity,  $V_S$ .

Based on this solution, the stiffness and damping characteristics of springs and dashpots can be calculated for six degrees of freedom, three translational along x, y and z-axis and three rotations around these axis. The stiffness and damping characteristics of equivalent springs are defined depending on the soil properties (Poisson's ratio,  $\nu_S$ , soil shear wave velocity,  $V_S$  and soil shear modulus,  $G_S$ ), dimensions of the foundation, dynamic stiffness modifiers,  $\alpha_j$  and embedment modifiers,  $\eta_j$ ;

$$k_j = K_j \times \alpha_j \times \eta_j \quad (3.9)$$

Where  $j$  denotes either translational or rotational mode,  $K_j$  is the static stiffness of foundation at zero frequency for mode  $j$  and can be computed depending on soil properties and foundation dimension using Equation (3.10a), dynamic stiffness modifiers,  $\alpha_j$ , is defined as a function of foundation dimensions and dimensionless frequency factor,  $a_0$ , which is expressed by Equation (3.10b) and embedment modifiers,  $\eta_j$ , is defined based on foundation dimensions and foundation depth and is given by Equation (3.10c).

$$K_j = GB^m f(B/L, \nu) \quad (3.10a)$$

$$\alpha_j = f(B/L, a_0) \quad (3.10b)$$

$$\eta_j = f(B/L, D/B, d_w/B, A_w/BL) \quad (3.10c)$$

Where in Equation (3.10)  $m = 1$  for translation and  $m = 3$  for rotation modes,  $B$  and  $L$  are the short and the long dimensions of the rectangular foundation, respectively.  $d_w$  and  $A_w$  are the height of effective side wall contact and side wall-solid contact area,

respectively. The dimension properties of rigid rectangular foundation located at the surface of or embedded within the half-space are schematically demonstrated in Figure 3.8.

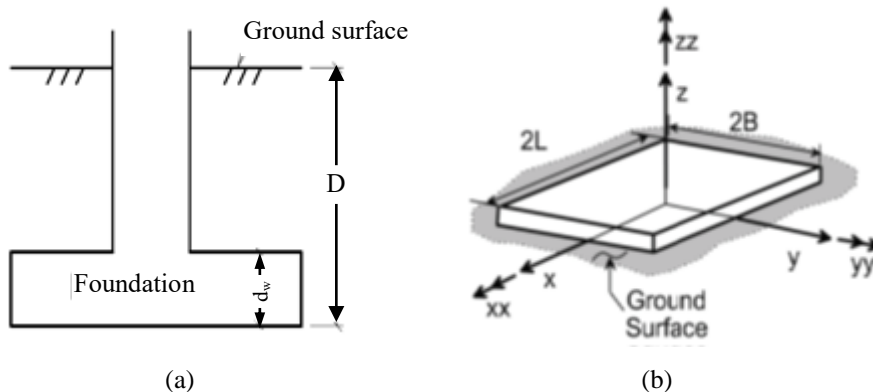


Figure 3.8. Schematic demonstration of foundation: (a) rigid foundation embedded within the half-space, (b) rigid foundation at the surface of the ground (half-space)

The dynamic stiffness modifier,  $\alpha_j$ , is related to the dimensionless frequency factor,  $a_0$  as:

$$a_0 = \omega B / V_S \quad (3.11)$$

Where  $\omega$  denotes the angular frequency.

Equation (3.9) shows the general solution of foundation impedance for any arbitrary rigid foundation shape, embedded into the half-space or located at the surface of the ground. However, in case of rigid foundation located at the surface of the ground the embedment modifiers,  $\eta_j=1$ , this happens when the foundation depth,  $D$  is less than 3m (10 feet) or there is no basement considered [25]. For other cases, when the foundation depth,  $D \geq 3m$  or when the structure consists of a basement and other floors the embedment modifiers,  $\eta_j \neq 1$ , and can be computed using the equation provided by [13] or [30].

For dynamic analysis, first the static stiffness,  $K_j$ , should be calculated by the equation given in Table 3.1 or Table 3.2, then it should be justified by multiplying them with dynamic stiffness modifier  $\alpha_j$ . The values of  $\alpha_j$  and radiation damping ratio,  $\beta_j$  which includes soil hysteretic damping,  $\beta_s$  can also be computed using equation developed by Pais and Causel or Gazetas.

On the other hand, in order to include soil-structure interaction into a displacement-based analysis procedure also known as pushover analysis, dynamic effects are neglected ( $\alpha_j = 1$ ), and the following three steps can be followed:

- 1) Calculate static spring stiffness,  $K_j$ , using either equations given in Table 3.1 or Table 3.2.
- 2) Kinematic interaction can be considered by reducing the free-field response spectrum. The ratios of response spectra among the free-field and foundation motions are used to represent the kinematic interaction effects. Ratios of response spectra depending on base-slab averaging and embedment are formulized as a function of time, which can be computed using the formula given by FEMA-440 standard.
- 3) Use the damping ratio of flexible base system,  $\beta_0$ , which generally is bigger than the damping ratio of the fixed base,  $\beta_f$ , and reduce the response spectrum.

The above three steps can be used to include soil-structure interaction into displacement-based analysis procedure, further explanation is given in the next Section.

Table 3.1. and 3.2. lists expressions for static foundation stiffness,  $K_j$ , which can be used to develop a flexible base model for building resting on a shallow rigid rectangular foundation.

Table 3.1. Expressions for calculating the static stiffness of rigid rectangular footings [27]

<i>Degrees of Freedom</i>	<i>Gazetas (1991); Mylonakis et al. (2006)</i>
Translation along z-axis	$K_{z, \text{sur}} = 2GL/(1-\nu) \left[ 0.73 + 1.54(B/L)^{0.75} \right]$
Translation along y-axis	$K_{y, \text{sur}} = 2GL/(2-\nu) \left[ 2 + 2.5(B/L)^{0.85} \right]$
Translation along x-axis	$K_{x, \text{sur}} = K_{y, \text{sur}} - 0.2/(0.75-\nu)GL(1-B/L)$
Rocking about y-axis	$K_{yy, \text{sur}} = G/(1-\nu)(I_y)^{0.75} \left[ 3(L/B)^{0.15} \right]$
Rocking about x-axis	$K_{xx, \text{sur}} = G/(1-\nu)(I_x)^{0.75} (L/B)^{0.25} \left[ 2.4 + 0.5(B/L) \right]$
Rocking about z-axis	$K_{zz, \text{sur}} = GJ_t^{0.75} \left[ 4 + 11(1-B/L)^{10} \right]$

Notes (also can be applied for Table 3.2):

- Make sure that  $L \geq B$
- $I_x$  = area moment of inertia of foundation about x-axis.
- $I_y$  = area moment of inertia of foundation about y-axis.
- $I_t = I_x + I_y$ .
- $G$  = Soil shear modulus
- $\nu$  = Poisson ratio of the soil

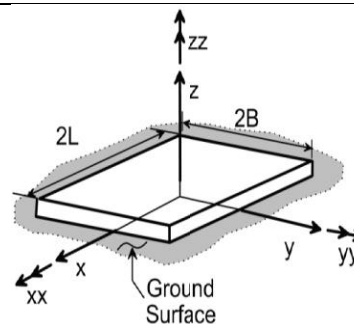


Table 3.2. Expressions for calculating the static stiffness of rigid rectangular footings [27]

<i>Degrees of Freedom</i>	<i>Pais and Causel (1988)</i>
Translation along z-axis	$K_{z, \text{sur}} = GB/(1-\nu) \left[ 3.1(B/L)^{0.75} + 1.6 \right]$
Translation along y-axis	$K_{y, \text{sur}} = GB/(2-\nu) \left[ 6.8(L/B)^{0.65} + 0.8(L/B) + 1.6 \right]$
Translation along x-axis	$K_{x, \text{sur}} = GB/(2-\nu) \left[ 6.8(L/B)^{0.65} + 2.4 \right]$
Rocking about y-axis	$K_{yy, \text{sur}} = GB^3/(1-\nu) \left[ 3.73(L/B)^{2.4} + 0.27 \right]$
Rocking about x-axis	$K_{xx, \text{sur}} = GB^3/(1-\nu) \left[ 3.2(L/B) + 0.8 \right]$
Rocking about z-axis	$K_{zz, \text{sur}} = GB^3 \left[ 4.25(L/B)^{2.45} + 4.06 \right]$

Not: the foundation dimensions and soil properties used in Table 3.1 and 3.2 are the same.

### **3.4. Implementation of SSI in Displacement-Based Analysis Procedure (Pushover Analysis) in view of the Seismic Building Codes**

Typically, in most seismic building codes SSI effects are ignored. The main cause of ignoring SSI effects may be due to its complicated analysis process and its probable beneficial effects which reduce the seismic responses such as base shear forces, lateral forces and overturning moments (FEMA-450, TEC-2018). Therefore not considering SSI leads to a conservative design and hence improves the building safety.

On the other hand, there is numerous evidence that shows SSI does not always have favorable effects on seismic responses of the buildings. It indicates that under severe earthquake motion, the nonlinear behavior of soil-foundation has significant effects on the overall seismic behavior of the structure-foundation system [32]. Consequently, the beneficial assumption of SSI is an oversimplification that may result in an unsafe design of the foundation and structure [33]. Taking these diversities into account, it worth to further study the SSI effects on seismic responses of the buildings, in order to find out by what means different studies ended up with such contrasting results.

Furthermore, recently some building codes, mostly American, have included simplified procedures to account for SSI effects in seismic evaluation and design of buildings. Some of the seismic provision that presents procedures to incorporate SSI in displacement-based analysis procedure are listed below:

1. ATC-40, Seismic Evaluation and Retrofit of Concrete Buildings (ATC, 1996).
2. FEMA 440, Improvement of Nonlinear Static Seismic Analysis Procedures (FEMA, 2005).
3. ASCE/SEI 41-06, Seismic Rehabilitation of Existing Buildings (ASCE, 2007)
4. PEER Report No. 2010/05, Guidelines for Performance-Based Seismic Design of Tall Buildings (PEER, 2010).



## 5. TEC-2018, Turkish Building Earthquake Regulation (TEC, 2018).

In this section, a brief description of implementing the SSI procedure is given in view of the available seismic codes. Since all codes listed above give a similar procedure for incorporating SSI effects except those for tall buildings, as an example the procedure given in FEMA-440 is described in further detail in the following subsection.

### **3.4.1. Including SSI effects into the displacement-based analysis method**

Displacement based analysis procedure is a new concept for the civil engineering community. In this method, the structural behavior is characterized by a base shear force versus roof displacement diagram which is calculated using pushover analysis. In the pushover analysis, the structure in which the lateral loads being distributed over its height is pushed up to a certain displacement. The best way to assess the performance of a building is to combine the structural capacity (pushover curve) with seismic demand. Examples of these approaches are: the capacity spectrum method of ATC-40, the displacement coefficient method given in FEMA-356 and a similar method to capacity spectrum is proposed by TEC-2018.

Generally, the methods described above are applied for fixed base condition, however in order to account for SSI effects, pushover analysis is implemented to a model with a flexible base, and then the pushover curve of the model with SSI system is constructed. After obtaining the pushover curve, one of the three methods mentioned above can be used to predict the performance of the model with a compliant base. The pushover analysis of a building with a flexible base is demonstrated schematically in Figure 3.9.

The nonlinear static analysis procedure in this study is performed in view of the latest Turkish building earthquake regulations (TEC-2018), which is described in detail in the next Chapter. In this section, the procedure of considering SSI in the nonlinear static analysis are described based on FEMA-440. These procedures can be

implemented for shallow foundations at the ground surface only. It should be noted that this method does not cover pile-supported foundation.

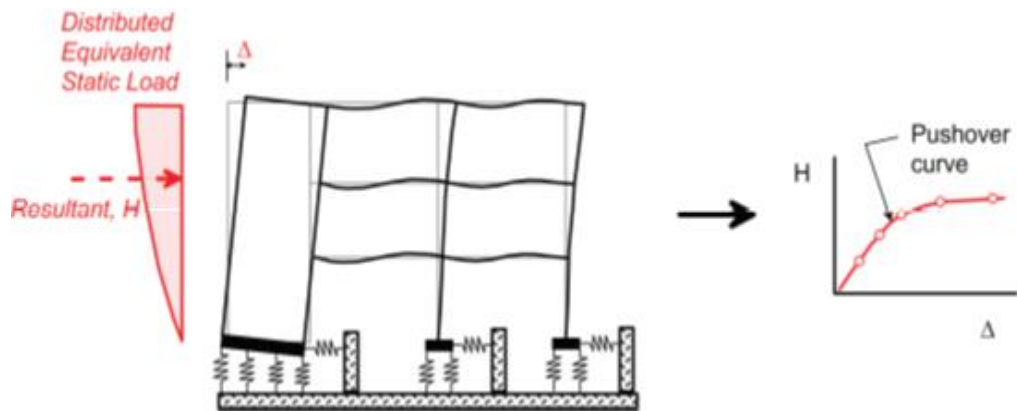


Figure 3.9. Application of static lateral loads to a flexible base model [27]

As mentioned in the former section, the SSI can be included in the displacement-based analysis procedure through:

- 1) Developing a flexible base model by utilizing foundation springs.
- 2) Taking into account kinematic interaction by reducing the free field response spectrum.
- 3) Normalization of the response spectrum curve using the calculated deformable base damping ratio,  $\beta_0$ .

Implantation of the above mentioned components in a displacement-based procedure is described in the following subsection.

#### 3.4.1.1. Developing a flexible base model

As stated by FEMA-440, soil-foundation springs for nonlinear static analysis can be generated by means of static stiffness equations listed in Table 3.1. or those given in Table 3.2. Generally, the way in which these springs are implemented in a pushover analysis model is either using uncoupled springs in which soil-foundation interaction

is represented by individual springs for each vibration mode of foundation or by distributing springs across the extent of the foundation which is also known as Winkler model. Both distributed and uncoupled spring models are schematically illustrated in Figure 3.10.

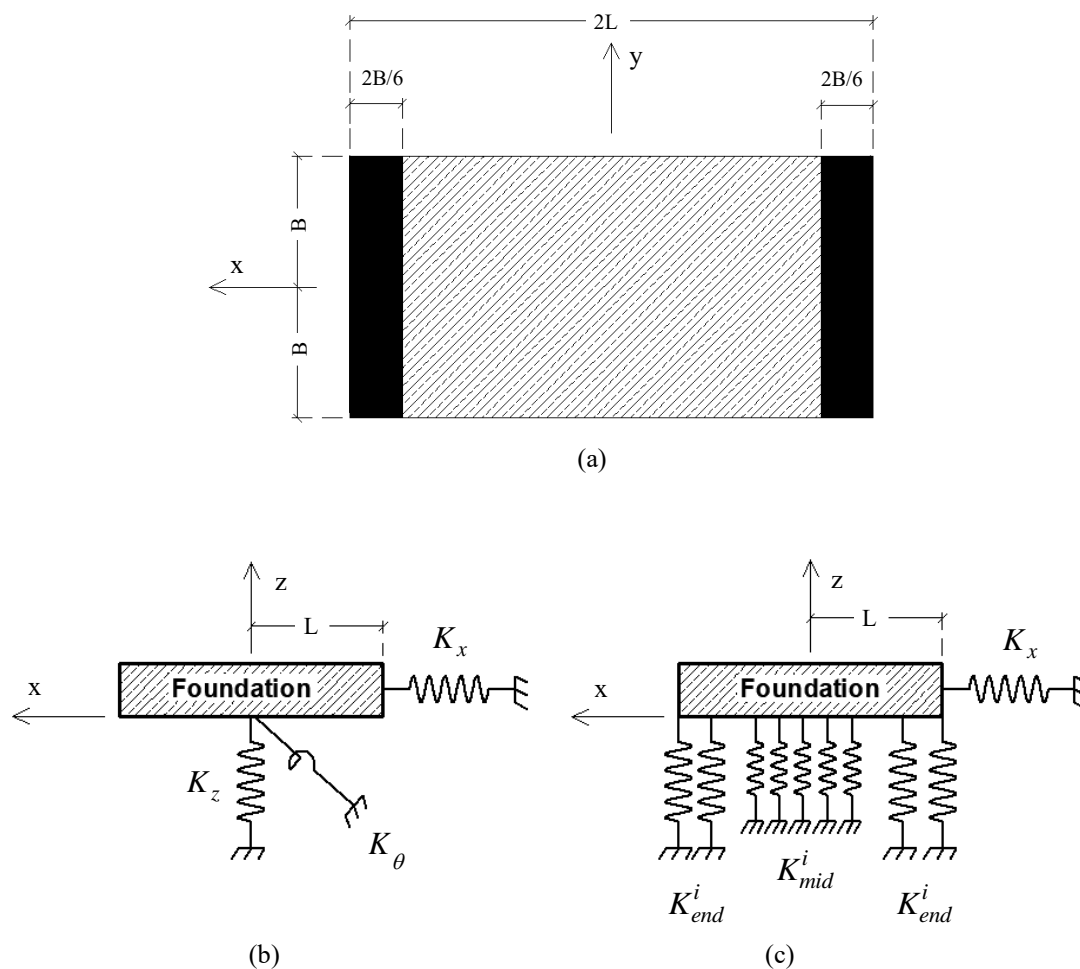


Figure 3.10. General representation of soil-foundation stiffness by equivalent springs: (a) geometry of foundation in-plane; (b) uncoupled spring model; (c) vertical spring distribution used to reproduce total rotational stiffness (Winkler model)

Basically, in practice for a rigid foundation, the uncoupled spring model is utilized to represent the interaction between foundation and soil, as illustrated schematically in Figure 3.10b. In this case, two steps of calculation are required. First, static stiffness  $K_j$  for each individual spring is calculated using, Table 3.1. or Table 3.2. for the surface foundation. Then, the embedment modifier  $\eta_j$  is calculated for each stiffness

term. The product of these two terms gives the stiffness of an embedded foundation. However, if the foundation depth is less than 3m (10 feet) or there is no basement considered for the building, embedment effects can be ignored [25]. In other cases, the embedment modifier values are calculated using the equation given by [13].

However, in reality, structural components of the SSI system including the foundation is not rigid. For non-rigid foundation, the vertical springs are distributed across the extent of the foundation, in such a way to reproduce the total rotational stiffness, as illustrated in Figure 3.9c. Using Figure 3.8. and Figure 3.10. the following basic steps are used to determine the stiffness characteristics of shallow foundation which is not rigid with respect to the supporting soil:

- 1) Total static stiffness,  $K_j$  for each individual spring, is calculated, for a rigid foundation at the surface of the ground, using the equation given in Table 3.1 or Table 3.2.
- 2) If embedment effects of the foundation are considered, then static stiffness  $K_j$  is adjusted by multiplying it by embedment modifier,  $\eta_j$  to obtain the embedded foundation stiffness.
- 3) Calculate and distribute the vertical and rotational stiffness under the footings using the following relationships;

$$k_z^i = \frac{K_{z,sur}}{4BL}; \quad k_{xx}^i = \frac{K_{xx,sur}}{I_x}; \quad k_{yy}^i = \frac{K_{yy,sur}}{I_y} \quad (3.12)$$

Where  $k_z^i$ ,  $k_{xx}^i$  and  $k_{yy}^i$  are the vertical stiffness density, rotational stiffness density about x-axis and rotational stiffness density about y-axis, respectively.  $I_x$  and  $I_y$  are the area moment of inertial of foundation around x and y-axis, respectively.

4) Typically, the rotational stiffness is not used in the Winkler model, instead the vertical springs are distributed in such a way that reproduces the total rotational stiffness. As illustrated in Figure 3.10c, the individual spring stiffness in the middle part of the foundation is calculated by multiplying appropriate stiffness intensity by spring's tributary area. However, since the reactions of soil in the vertical direction varies, intensifying in the edge side of the foundation, the spring intensity at this area is defined stiffer. The strip length, where the spring is defined stiffer, at the edge of the foundation is generally assumed as one-sixth of foundation width [34], which is shown in Figure 3.10a. The spring stiffness at the edge of the foundation and in the middle part of the foundation can be approximated using the following equations [27]:

$$K_{end}^i = R_k \times k_z^i \times dA \quad (3.13a)$$

$$K_{mid}^i = k_z^i \times dA \quad (3.13b)$$

Where, the superscript,  $i$ , indicate the number of produced springs,  $dA$  is the tributary area of spring and  $R_k$  is the correction factor for reproducing rotational stiffness and is expressed by FEMA-440 as follow:

$$R_{k,yy} = \frac{\left( \frac{3K_{yy}}{4k_z^i B L^3} \right) - (1 - R_e)^3}{1 - (1 - R_e)^3} \quad (3.14a)$$

$$R_{k,xx} = \frac{\left( \frac{3K_{xx}}{4k_z^i B^3 L} \right) - (1 - R_e)^3}{1 - (1 - R_e)^3} \quad (3.14b)$$

Where, the end length ratio,  $R_e = L_{end} / 2L$ , is defined as one-sixth of the foundation width ( $L_{end} = 2B / 6$ ) by [34] (also shown in Figure 3.10a.).

The horizontal spring is not distributed in the Winkler model for a two-dimensional analysis and is applied as concentrated spring as shown in Figure 3.10c. However, in the case of three-dimensional analysis, the horizontal springs are distributed uniformly in both x and y-directions around the foundation perimeter. The sum of the spring stiffness should then reproduce the total stiffness of the impedance function [27].

### 3.4.1.2. Reduction of response spectrum due to kinematic interaction

FEMA-440 states that kinematic interaction effects, in a displacement-based analysis procedure, can be represented by the ratio of response spectra (RRS). The RRS is defined as the ratio of free field spectral coordinates to response spectral coordinates applied to the foundation. Embedment and base-slab averaging effects, which are described in Section 3.1., are the two main phenomena of kinematic interaction. These two mechanisms of kinematic interaction are considered for evaluating the RRS.

FEMA-440 provided a simplified procedure for evaluating base-slab averaging and embedment effects of kinematic interaction as a function of the structural period (T). The following equation is suggested by FEMA-440 to estimate RRS for base-slab averaging and embedment effects as a function of the period:

$$RRS_{bsa} = 1 - \frac{1}{14100} \left( 2 \left( B_e^A \div 0.3048 \right) f_L \right)^{1.2} \quad T \leq \frac{1}{f_L} \quad (3.15a)$$

$$RRS_{bsa} = 1 - \frac{1}{14100} \left( \frac{2 \left( B_e^A \div 0.3048 \right)}{T} \right)^{1.2} \quad T > \frac{1}{f_L} \quad (3.15b)$$

$$RRS_{emb} = \cos \left( \frac{2\pi D}{TV_{sr}} \right) \quad T > \frac{1}{f_L} \quad (3.15c)$$

$$RRS_{emb} = \cos \left( \frac{2\pi D f_L}{V_{sr}} \right) \quad T \leq \frac{1}{f_L} \quad (3.15c)$$

Where:

$V_{sr}$  = strain reduced shear wave velocity

$B_e^A$  = the equivalent foundation dimension and is expressed in units of meters

$f_L$  = the limiting frequency and is given as  $f_L = 0.5 \text{ Hz}$  ( $T=0.2 \text{ sec}$ )

D = foundation embedment in units of meters

The total RRS for each period of interest is the product of  $RRS_{bsa}$  and  $RRS_{emb}$ . Accordingly, the values of RRS (in order to reduce the spectral coordinates) is then multiplied by the ordinates of spectral acceleration and a new spectrum curve is obtained which is used for the analysis (see FEMA-440 and NIST, 2012 for more details).

#### **3.4.1.3. Reduction of response spectrum due to foundation damping**

Foundation flexibility and foundation damping effects are the two main components of inertial interaction. Foundation flexibility effects, which represent the geotechnical components of the soil-foundation system, are incorporated into the soil-structure analysis by foundation impedance function as described previously in this chapter. On the other hand, foundation damping is caused due to relative movements of foundation and supporting soil. These effects of inertial interaction are ignored by most of the seismic codes. For example, FEMA-356 and ATC-40 only provide procedures for accounting foundation flexibility effects but are silent about the effects of kinematic interaction and foundation damping.

Although rarely used in practice, FEMA-440 introduced a simplified procedure to account for foundation damping and kinematic interaction effects for use in non-linear static analysis. Procedure for incorporating kinematic interaction effects is explained in Section 3.5.1.2., and in this section, the procedure proposed by FEMA-440 for evaluating foundation damping effects is explained briefly in the following.

In FEMA-440, the damping ratio of the complete SSI system,  $\beta_0$ , is defined as the combination of foundation damping ratio,  $\beta_f$ , and fixed base structural damping ratio  $\beta_i$  and is expressed by the equation given below.

$$\beta_0 = \beta_f + \frac{\beta_i}{(T_{SSI}/T)^3} \quad (3.16)$$

Where  $T_{SSI}$  and  $T$  are the linear periods of the structural model in a flexible base and fixed base conditions, respectively. To estimate,  $T_{SSI}$  the flexible model can be constructed using one of the procedures described in section 3.5.1.1. The symbol  $\beta_i$  is the initial damping for the structure, and generally five percent initial damping is considered in most seismic codes.

The real challenge here is to determine the soil-foundation interaction damping ratio,  $\beta_f$ , from the results of a pushover analysis of both flexible base and fixed base structural models.

According to FEMA-440, to estimate,  $\beta_f$  first the ratio of period lengthening is determined which is the ratio of flexible base and fixed base structural period ( $T_{SSI}/T$ ). By considering the shaking in the x-direction, the translational stiffness of the foundation,  $K_x$ , is then calculated using the formula presented in Table 3.1 or Table 3.2. The effective rotational stiffness,  $K_{yy}$ , is then represented by the following formula:

$$K_{yy} = \frac{K_{fixed}^* (h^*)^2}{(T_{SSI}/T)^2 - 1 - (K_{fixed}/K_x^*)} \quad (3.17)$$

Where  $h^*$  is the effective structural height, and can be approximated as 70% of total structure height and  $K_{fixed}^*$  is the equivalent effective structural stiffness of single



degree of freedom (SDOF) oscillator for fixed base condition and is evaluated as follow:

$$K_{fixed}^* = M^* \left( \frac{2\pi}{T} \right)^2 \quad (3.18)$$

In which  $M^*$  denote the effective mass associated the first mode.

The next step is to determine the effective lengthening period ratio,  $(T_{SSI}/T)_{eff}$ , which can be obtained as a result of pushover analysis of the structural model. By assuming  $\mu$  to represent the expected ductility of SSI system, the effective period lengthening ratio is expressed as follow:

$$\left( \frac{T_{SSI}}{T} \right)_{eff} = \left\{ 1 + \frac{1}{\mu} \left[ \left( \frac{T_{SSI}}{T} \right)^2 - 1 \right] \right\}^{0.5} \quad (3.20)$$

Depending on this effective period lengthening ratio, foundation damping ratio,  $\beta_f$ , can be approximated using Figure 3.11:

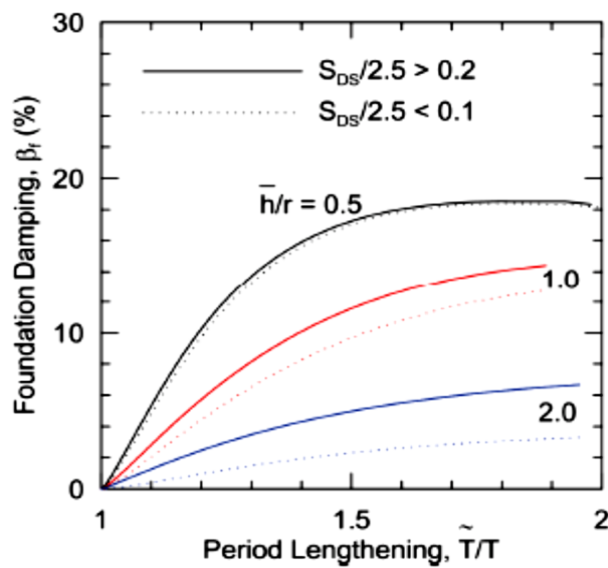


Figure 3.11. Relationship between foundation damping and period lengthening [25]

## **CHAPTER 4. NONLINEAR STATIC ANALYSIS**

This chapter describes the analytical procedures necessary to determine the performance levels of RC buildings for a given earthquake level. Generally, the analysis procedures for performance evaluations are categorized into two main analysis approaches, the first one is referred to as the force-based analysis method and the second one is denoted as the displacement-based analysis method.

In the conventional force based-methods, the seismic responses of structures are computed through linear analysis technique (linear static and linear dynamic). In this method, the force demand in each structural component is calculated and then compared with available member strength capacities. Although linear elastic methods can estimate the elastic capacity of the structures and predict the occurrence of the first yield, these methods are unable to follow the failure mechanism of the buildings and account for the redistribution of forces as yielding progress [5]. Furthermore, the damages of structural components due to earthquake motions depend on inelastic deformation capacities rather than the initial yield strength. Therefore, the design of structures by force-based methods is found undesirable and unpredictable during severe earthquake motions [23]. The shortcoming of force-based methods mentioned above leads the researchers to develop the displacement-based analysis method for seismic evaluation of the buildings.

In displacement-based approaches, the seismic evaluations of structures are performed through non-linear analysis methods and are mainly based on inelastic deformation rather than elastic forces. Since the buildings experience significant inelastic deformation against large seismic excitations, non-linear analysis procedures are required to investigate the performance of the buildings.

Therefore, this approach can provide more accurate results that help to estimate the real behavior of the buildings and to understand the failure modes of the buildings exposed to severe hazard motions. The displacement-based procedure includes non-linear time history analysis and non-linear static analysis (pushover).

To perform a non-linear analysis, first the mathematical model of the structure is constructed, and then it is exposed to the ground motion which is expected to occur during its lifetime (Figure 4.1.). As analysis results global seismic responses such as roof displacement and base shear, and local responses such as inter-story drift ratios and component forces are estimated. Eventually, the global and local responses are used to specify the building performance with comparing them to the available response limits. The nonlinear analysis procedure is schematically demonstrated in Figure 4.1.

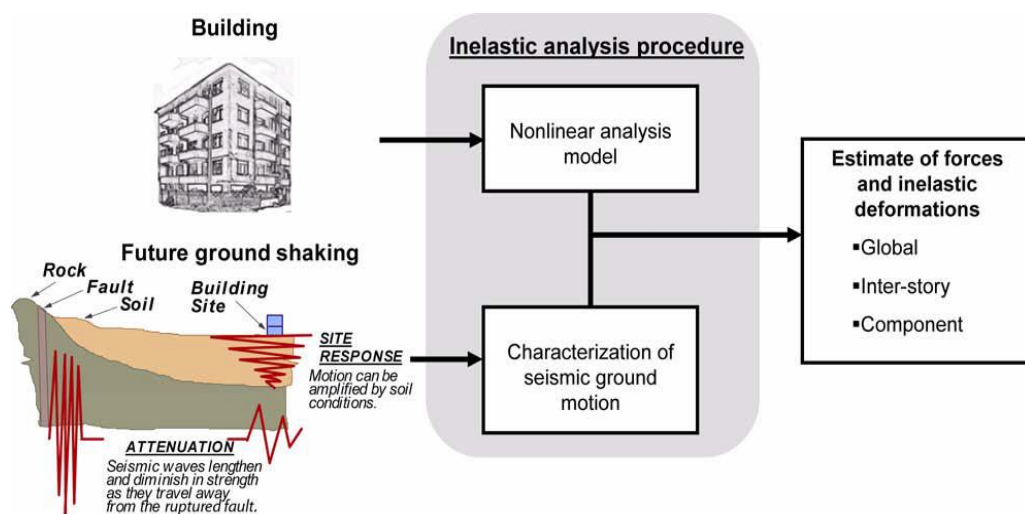


Figure 4.1. Schematic demonstration of nonlinear analysis procedure [25]

In order to conduct a non-linear analysis generally nonlinear static procedure (pushover) and nonlinear time history analysis is used. Although it is a general agreement that non-linear time history analysis is able to and has the greatest potential to validate the seismic performance of the buildings more accurately, there is also agreement that this method is expensive from computational standpoint and require

much more time which makes this method less practical and is rarely used for performance evaluation of the buildings.

Moreover, pushover analysis which is a simpler assessment approach is mostly preferred in practice. In this method, the structural model is pushed up to a given displacement by using a load pattern to distribute the horizontal forces along the height of the building. The cumulative resultant force is then related to a predefined displacement which forms the non-linear pushover curve. The pushover and capacity curves are then plotted in the same coordinate system and the seismic displacement demand which is the intersection of these two curve is identified (Figure 4.2.). Examples of these approaches are the capacity spectrum method of ATC-40, the displacement coefficient method given in FEMA-356 and a similar method to capacity spectrum is proposed by TEC-2018.

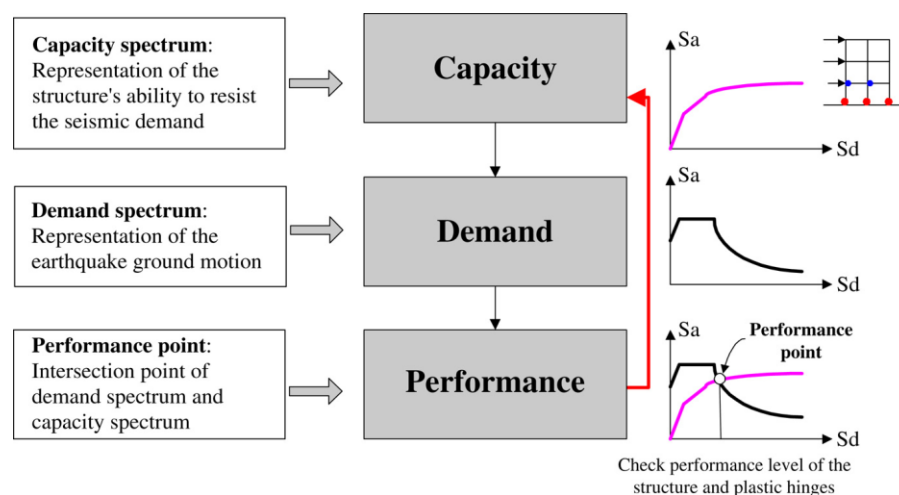


Figure 4.2. Static analysis procedure for performance evaluation of the buildings [35]

In this chapter, first, a brief explanation of pushover analysis is made it is followed by discussing the merits and shortcomings of this method. Then the implementation of this method for performance investigation of the RC building is introduced. As an example, the capacity spectrum method given in ATC-40 is briefly described and finally, a step by step description of the inelastic static analysis procedure for performance evaluation of the buildings proposed by TEC-2018 is reported.

#### 4.1. Evaluation of Pushover Analysis

Pushover analysis is a simplified nonlinear static analysis method in which the structure is pushed up to some desired target displacement by subjecting the buildings to monotonically increasing lateral load pattern. The lateral loads are distributed along the height of the structures and are increased continuously through elastic and inelastic behavior until it reaches a predefined target displacement or the building is failed to sustain further loads [5].

To perform a pushover analysis, first, a mathematical model of the building is constructed in 2D or 3D format. In the developed model, the nonlinear behavior of the structural elements is represented by the appropriate load-deformation relationship. The building is then analyzed under the gravity load (dead load +live load) and the result from this step is set to be the initial condition for the monotonic loading. The lateral load is then applied and increased step by step proportional to the defined load pattern (generally dominant mode shape in related direction). The horizontal loads are increased until some members reach their load-carrying capacities. The stiffness of yielded members is reduced and the lateral loads are increased again until the other member yields. At each loading step, the base shear is plotted against lateral deformation and the process is carried forward until the desired displacement (generally at the roof level) is reached or the building is failed to sustain further loads. The resulting base shear force and lateral roof displacement relationship are termed the pushover curve (Figure 4.3.).

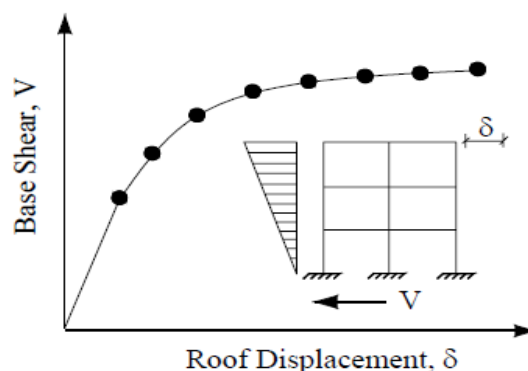


Figure 4.3. Pushover curve of the building [36]

The obtained capacity curve which characterizes the global response of the mathematical model is then bi-linearized in order to transform it into an equivalent single degree of freedom (SDOF) system. The bi-linearization step can be performed using the procedure given in TEC-2018, FEMA-356 or ATC-40. The next step is to compute the maximum displacement demand for SDOF system, using one of the methods proposed by the above mentioned seismic codes. Finally, the roof displacement demand of the multi-degree of freedom (MDOF) system is calculated by converting the maximum displacement of the SDOF system. At this stage of pushover analysis, the local seismic demands of the building such as deformations and forces are calculated which represents the inelastic behavior of structural members.

#### **4.1.1. Advantages and limitation of pushover analysis**

Static pushover analysis is a powerful tool for predicting the inelastic behavior of a building under seismic loads and is preferable over elastic analysis procedures. However, this method like any other analysis method is based on some assumptions and has limitations that should be identified. Some of the basic advantages and limitations of this method are outlined in the following [37]:

Advantages:

- a) This method is simple to implement in practice compared to non-linear time history analysis.
- b) It can estimate the seismic capacity of structural members of a non-linear system and is able to capture the failure mechanism under progressive yielding.
- c) It can help to identify the location of potential weakness governing in a building where the failure may occur.
- d) The sequence of plastic hinge formation can be observed in structural members.

- e) It is able to verify completeness and adequacy of the load paths within the structures as a whole by taking in to account all members of the system.
- f) It provides the possibility to accurately estimate the force demands in potentially brittle structural members. For example, axial force in columns, moments on column-beam joints and etc.
- g) Estimation of inter-story drifts by giving adequate information about local and global inelastic demands.
- h) The designer is given the possibility to make a comparison between the structural capacity and the seismic demand for the desired performance level, thus makes it easy to predict the performance of the structure.

Limitations:

- a) It is assumed that the first mode (or a few first modes) governs the seismic actions of the structures and the mode shapes remain constant during the whole analysis process regardless of deformation level.
- b) Implementation of this method is not recommended for the buildings where the torsional coupling prevails or there are irregularities or uneven mass distribution exists.
- c) This method is not reliable when the effects of higher modes are important.
- d) Distribution of inertia forces is represented by invariant lateral load patterns (generally according to the fundamental mode shape) and is assumed to be constant during the earthquake.
- e) This method is only applicable for seismic evaluation of low to midrise buildings while it is not recommended for high-rise buildings, in which the effects of higher modes are significant and axial deformation of columns plays an important role in the estimation of lateral drifts.

## **4.2. Implementation of Pushover Analysis for Determining Seismic Responses of RC Buildings**

The main objective of pushover analysis is to estimate the inelastic demands of a building such as deformation and strength against a given earthquake and comparing them to available capacity limits, in order to check the structural performance [38]. Although according to available literature, non-linear time history analysis is known as the most precise and complete analysis tool for predicting non-linear behavior of structures against seismic loading, this method as mentioned earlier is expensive from both computational standpoint and complexity. Instead, the application of non-linear static analysis (pushover) is also possible as a more practical analysis method. The inelastic static analysis method which is also known as pushover analysis has been also recommended by many seismic codes (FEMA-356, FEMA-440, ATC-40, TEC-2018 ...). Even though this method has been developed basically for performance evaluation of existing buildings, it can also be applied for seismic assessment and design of new buildings.

In the following sections, the application of the pushover analysis procedure for performance assessment of RC building based on TEC-2018 [24] is explained in detail. In addition, the capacity spectrum method of ATC-40 is also briefly discussed.

## **4.3. Capacity spectrum method of ATC-40**

Although the capacity spectrum method of ATC-40 is not used in this study, it is briefly reviewed in order to provide the readers with some extra information and perspective regarding the different methods of the non-linear analysis procedure. In addition, it is aimed to provide a conceptual comparison between the inelastic static procedure given in ATC-40 and TEC-2018. Therefore, the basic concept of this method is briefly explained in the following paragraphs.

Similar to other nonlinear static methods, the capacity spectrum method also requires pushover analysis to generate the force-deformation relationship (i.e. pushover curve)



of the building. The pushover curve which represents the nonlinear force-deformation behavior of the buildings can be computed using the procedure explained in Section 4.1 with the help of computer programs such as SAP2000 and ETABs. In addition, these programs are able to perform nonlinear pushover analysis directly according to ATC-40 and FEMA-440 procedures, with no iteration required.

In this method, the maximum inelastic displacement demand also referred to as performance point is computed by comparing the structural capacity with seismic demand of the structure. The maximum displacement demand, which represents the response of the building for a given earthquake is computed as the intersection point of these two curves. To achieve this goal, the pushover curve is transformed into spectral acceleration and spectral displacement domain, and the resulting diagram is termed as the capacity curve. Similarly, the demand curve which is represented in terms of the building period and spectral acceleration is also transformed to spectral acceleration and spectral displacement domain. Afterward, both curves are plotted in the same coordinate system called “acceleration-displacement response spectra (ADRS) format”, and the performance point is estimated (Figure 4.4.).

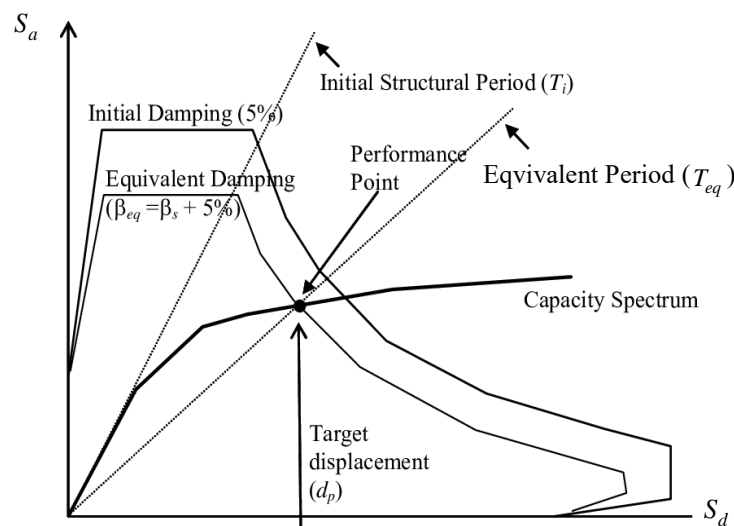


Figure 4.4. Graphical demonstration of the capacity spectrum method [5]

According to ATC-40, the pushover curve can be transformed into ADRS format using Equation (4.1). Similarly, the seismic demand curve is also can be transformed into an ADRS format using Equation (4.2).

$$S_a = \frac{V/W}{\alpha_1}; S_d = \frac{\Delta_{roof}}{PF_1 \times \phi_{1,roof}} \quad (4.1)$$

$$S_d = \frac{T^2}{4\pi^2} \times S_a \times g \quad (4.2)$$

Where,  $S_a$  and  $S_d$  are spectral acceleration and spectral displacement, respectively. The letter  $T$  shows the vibration period,  $g$  stands for gravitational acceleration,  $V$  is the base shear force,  $W$  is the total weight of the building,  $\Delta_{roof}$  is lateral displacement at the roof level. Similarly,  $PF_1$ ,  $\alpha_1$  and  $\phi_{1,roof}$  are the modal participation factor, the modal mass coefficient and the mode amplitude at the roof level associated with the first mode (dominant mode) of the buildign , respectively.

The next step in the capacity spectrum method is to estimate the inelastic displacement demand (i.e. performance point), for this propose the capacity curve which is obtained for the equivalent MDOF system is required to be converted in a bilinear form in order to represent the equivalent SDOF system. This bilinear representation of capacity curve is then used to estimate the period (termed as equivalent period,  $T_{eq}$ ) and the viscous damping (denoted as equivalent viscous damping,  $\beta_{eq}$ ) of the equivalent SDOF system.

According to ATC-40, the viscous damping is computed using the relationship between the amount of energy dissipated in one vibration cycle of the nonlinear system,  $E_D$ , and the equivalent linear system,  $E_{S0}$  (Figure 4.5.).

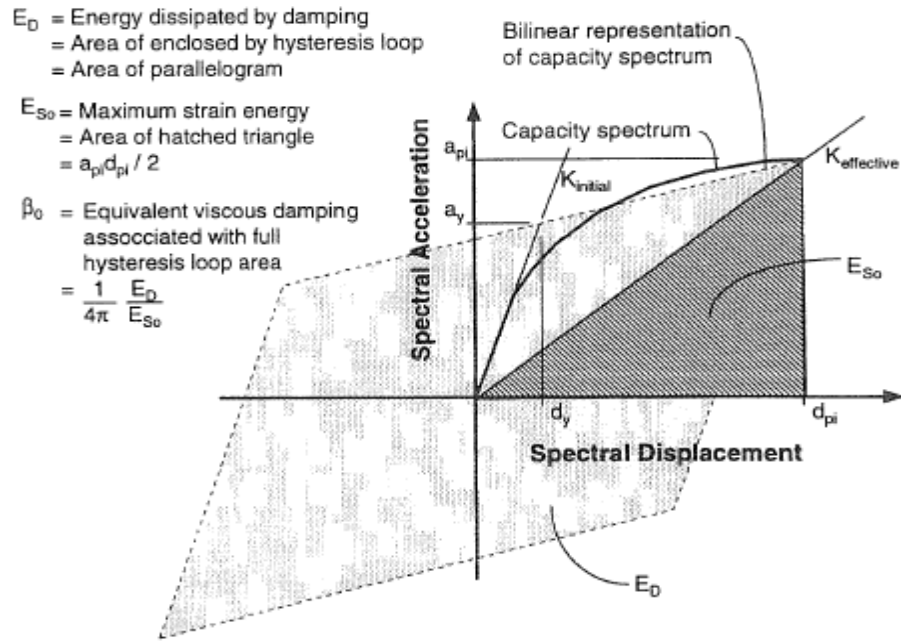


Figure 4.5. Derivation of damping for spectrum reduction [5]

Based on this concept, the total equivalent viscous damping corresponding to the maximum displacement,  $d_{pi}$ , for the bilinear system is given by Equation (4.3).

$$\beta_{eq} = 0.05 + k\beta_0; \quad \beta_0 = \frac{2}{\pi} \frac{(\mu-1)(1-\alpha)}{\mu(1+\alpha\mu-\alpha)} \quad (4.3)$$

Where  $\beta_0$  is the equivalent viscous damping associated with full hysteresis loop,  $\mu$  is the ductility ( $\mu = d_{pi}/d_y$ ),  $\alpha$  is the post-yield slope coefficient of the bilinear curve and  $k$  is an adjustment factor related to the hysteretic behavior of the RC structures (can be obtained from ATC-40).

Similarly, the equivalent period for the elastic SDOF system is computed from the initial period of the nonlinear system,  $T_0$  and ductility ratio,  $\mu$  and can be estimated using Equation (4.4).

$$T_{eq} = T_0 \sqrt{\frac{\mu}{1+\alpha\mu-\alpha}} \quad (4.4)$$

As it is clear from Equation (4.3) and (4.4) the estimation of equivalent damping ratio ( $\beta_{eq}$ ) and equivalent vibration period ( $T_{eq}$ ) depends on the displacement ductility ratio ( $\mu$ ). The values of  $\beta_{eq}$  and  $T_{eq}$  are then needed to compute the maximum displacement demand (i.e. performance point) of the SDOF system subjected to a given earthquake motion. Since the maximum ductility ratio of the building under evaluation is not known an iteration procedure is required to determine the maximum displacement demand.

ATC-40 has proposed three different iteration procedures, referred to as procedures A, B, and C, in order to reach the performance point. All the procedures are based on the same concepts but vary depending on application wither graphical or analytical techniques. Procedure A and B are described as analytical methods which are appropriate to implement in computer programs, whereas procedure C is designated for hand solution and is based on graphical technique. Furthermore, procedure A is recommended by ATC-40 to be the best of the three procedures, since it is more straightforward and is easy to apply than the other two. In this study, only the procedure A is summarized in the following steps:

- 1) Plot the capacity curve (transformed form of pushover curve) and demand curve (design elastic spectrum with 5% damping) in the ADRS format, both in the same graph.
- 2) Select a trail performance point, the equal displacement approximation rule might be used for the first iteration (any point can be chosen it depends on engineering judgment).
- 3) Compute the displacement ductility ratio,  $\mu = d_{pi} / d_y$  (Figure 4.5).
- 4) Estimate the equivalent damping ratio  $\beta_{eq}$  from Equation (4.3).

- 5) Plot the demand curve for  $\beta_{eq}$  calculated in Step 4 and record the displacement  $d_{pi}$  corresponding to the intersection of this diagram and capacity curve (Figure 4.4).
- 6) Check the tolerance between the two consecutive points (should be less than 0.05). If it is close enough then terminate the analysis and the selected point in step 6 is the performance point (i.e. maximum displacement demand) for the demand earthquake. If not, then chose another point and repeat step 4 to 6 until it reaches an acceptable tolerance.

In general, the capacity curve is developed to represent the first mode response of the structures assuming that this mode is predominant. Therefore, the procedure described above is restricted for buildings where their responses are dominated by the first mode (fundamental mode). According to ATC-40, for buildings where the effects of higher modes are significant or having a fundamental vibration period greater than one second, the effects of higher modes should also be considered.

#### **4.4. Nonlinear static procedures based on TEC-2018**

Recently updated Turkish earthquake code (TEC-2018) has recommended two main analysis approach for seismic performance evaluation of new/existing buildings. They are force-based and displacement-based analysis approaches. The force-based approach is used to determine the seismic responses such as axial forces, bending moments and element shear forces through linear analysis methods (linear static analysis and linear dynamic analysis) and are then compared to the element strength capacities. Accordingly, the preliminary-sizing of the structural elements and reinforcement ratios (for RC structures) of the buildings are determined. TEC-2018 provision has limited the linear analysis methods to estimate only the normal performance levels (i.e. damage control performance level) of the buildings (refer to Chapter 2).

Furthermore, as explained earlier, buildings undergo large deformations when subjected to severe earthquake motions. Besides, the damage of buildings is more related to deformation capacities rather than strength capacities. Therefore, the force-based analysis methods are found insufficient and unrealistic for the seismic evaluation of the buildings. To overcome this problem, TEC-2018 suggests that after a preliminary design of the buildings using linear analysis methods, the displacement-based analysis approach should be implemented for performance check.

According to the TEC-2018, the displacement-based approaches are classified into non-linear static procedures (i.e. pushover analysis) and non-linear dynamic analysis (i.e. non-linear time history analysis). The non-linear static analysis procedures are also divided into single-mode pushover analysis (SMPA) and multi-mode pushover analysis procedures (MMPA). Using one of these methods, the seismic performance of new/existing structures can be investigated. In this study, since only single-mode pushover analysis is used, this method is explained in detail, and the other methods are not covered. In addition, brief information is given regarding the non-linear modeling and acceptance criteria contained in TEC-2018 for the design of RC frame structures.

#### **4.4.1. Non-linear modeling of structural system**

Modeling strategies that clearly explain geometric and material nonlinearity of the structure and the structural element is an important factor in the non-linear static analysis procedures. The structure should be modeled in such a way that the inherent non-linear strength and deformation properties of each structural element are accounted for. In this regard, for non-linear static procedures, the inelastic behavior of the structural members is commonly represented by a backbone curve, which is a plot of force versus deformation. This curve is assumed to define the component behavior under monotonically increasing deformation. In other words, this curve is used to measure the strength against translation or rotation of the element. The generalized force-deformation relation (an idealized form of the generalized force-deformation curve) for concrete element or component is shown in Figure 4.6.

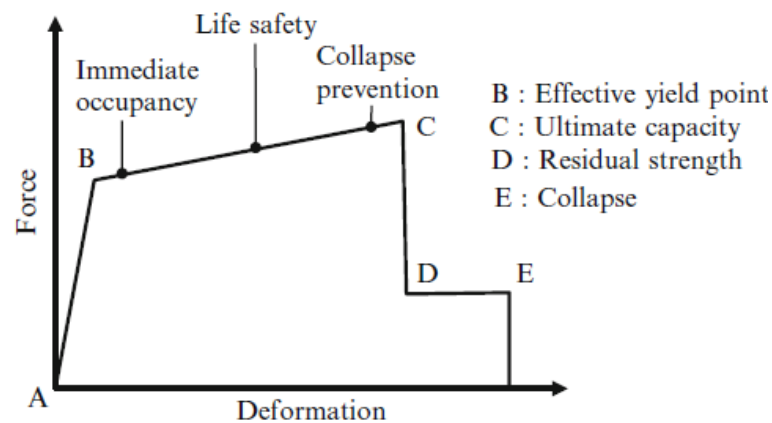


Figure 4.6. Generalized force-deformation curve (backbone curve) for concrete elements [37]

The associated physical components of the force-deformation relationship shown in Figure 4.6., include stress-strain relationship for defining the axial responses, moment-curvature relationship for flexural responses, and plastic-hinging for measuring rotational responses.

The numerical modeling of nonlinear behavior of RC frame elements contained in the Turkish Earthquake Code (TEC-2018) basically falls into two categories. They are distributed plasticity models, where the inelastic deformations are distributed along the whole element length, and concentrated plasticity models, where the inelastic deformations are assumed to be lumped at the critical sections, where the internal forces are expected to be the maximum (generally the maximum internal forces occur at the end of the element when the building is subjected to seismic loading) and the other portion of the element is assumed to behave elastically.

In concentrated plasticity models which are more practical than the distributed plasticity models, it is assumed that plastic deformations are uniformly distributed in a small zone namely plastic hinge length, where the internal forces are expected to have reached to their plastic capacities. The length of the plastic hinge ( $L_p$ ) can be taken approximately as half of the cross-section height ( $h$ ) in direction of loading ( $L_p \approx 0.5h$ ). However, for elements in which plastic deformations are caused only by axial loadings, plastic hinge length should be taken equal to the element length. The

inelastic deformations, distributed along this length, are characterized by plastic hinges, which are placed right before the intersection zone of the elements (for beams and columns).

#### 4.4.2. Acceptance criteria for modeling of the RC structures

In order to implement a nonlinear static analysis, the general obligations and acceptance criteria for nonlinear modeling of structural components (columns and beams) recommended by TEC-2018 are summarized in the following:

- 1) The building should always be modeled in 3D format, and the analysis should be performed by taking into consideration the two horizontal components of earthquake effects perpendicular to each other.
- 2) Beam and columns should be modeled as finite elements. The material nonlinearity of this finite element can be modeled using whether concentrated plasticity model or distributed plasticity model (as explained in Section 4.2.2.1.). However, for practical use, the concentrated plasticity model is generally preferred due to its simplicity and applicability. Using this plasticity model, the plastic hinge which represents the inelastic deformations of the elements should be placed at the end of the elements (just before the intersection zone of columns and beams). The other part of the element (the portion remained between two plastic hinges) can be modeled as an elastic system, and the section stiffness ( $EI$ ) for the elastic part should be modified using effective cross-section stiffness  $(EI)_e$ . For nonlinear analysis of new buildings, the values of  $(EI)_e$  can be calculated using the following formula:

$$(EI)_e = \frac{M_y L_s}{\theta_y 3} \quad (4.5)$$

Where  $M_y$  and  $\theta_y$  is the average value of effective yield moment and yield rotations of plastic hinges at the end zone of the elements, respectively.  $L_s$  is



the shear span (the ratio of bending moment divided by shear force of the element); the value of shear span can be taken as half of the element length for columns and beams.

For inelastic analysis of existing buildings, the value of  $(EI)_e$  is directly related to the initial stiffness of the element ( $EI$ ) and can be assumed as 35% and 70% of initial stiffness of beams and columns, respectively.

- 3) The geometric nonlinearity also known as the P-Delta effects should be considered. P-Delta effects involve the lateral deformation of the structural system (i.e. second-order effects) caused by the application of gravity loads (axial loads) on the laterally displaced state of the structure.
- 4) The modeling process should be accomplished using the expected (average) strength of concrete ( $f_{ce}$ ) and the expected strength of steel ( $f_{ye}$ ). The expected (average) strength of concrete and steel is expressed in terms of their characteristic strengths by the following equation:

$$f_{ce} = 1.3f_{ck}, \quad f_{ye} = 1.2f_{yk} \quad (4.6)$$

Where  $f_{ck}$  and  $f_{yk}$  are the characteristic strength of concrete and steel, respectively.

The acceptance criteria described above only covers the RC frame structures, where their load-bearing members consist of column and beam elements. The details of modeling criteria for other types of buildings can be found in the TEC-2018 document. Furthermore, the effects of soil-structure interaction (SSI) for shallow foundations in the TEC-2018 document are ignored. However, in this study, the SSI effects of the buildings founded on the shallow foundation are included in the displacement-based analysis method using the procedure described in Chapter 3.

#### 4.4.3. Single-mode pushover analysis (SMPA)

In this method, like any other non-linear static procedure, the pushover curve of the buildings which is a plot of base shear versus roof displacement is developed. The process begins by subjecting the building first to gravity loads, afterward, the lateral loads are applied step by step proportional to the first mode shape (fundamental mode) in a specified earthquake direction. The lateral loads are increased incrementally until the building reaches a target displacement (seismic displacement demand). At every increment of lateral load, the seismic responses of structural members such as displacement, plastic rotations, and internal-forces along with their cumulative values are recorded. In the last step, the cumulative values corresponding to the seismic demand are obtained, and then these values are used for performance assessment of the building by comparing them to the available member capacities (refer to Chapter 2.).

The basic assumption of this method is that the response of the structure is governed by the first mode (fundamental mode) and thus the effects of higher modes are ignored. Therefore single-mode pushover analysis is not allowed for performance assessment of tall or highly irregular buildings, in that the contribution of higher modes of vibration is significant.

According to TEC-2018, single-mode pushover analysis method can be applied for performance evaluation of the building that meets the following conditions:

- a. This method can be applied for performance evaluation of the building in that the building height classes (BYS) corresponds to  $BYS \geq 5$ .
- b. The building's torsional irregularity coefficients ( $\eta_{bi}$ ) for each floor must not exceed 1.4 ( $\eta_{bi} \leq 1.4$ ).
- c. The modal mass participation ratio contributed to the first mode of vibration in related direction should be greater than 70% of the total mass of the building.

The performance assessment of the buildings, considering the above-mentioned conditions and limits recommended by TEC-2018 can be accomplished by conducting single-mode pushover analysis.

As explained before, the primary objective of the nonlinear analysis is to estimate the inelastic demand of the buildings for a given earthquake level. In order to achieve this goal using SMPA, the determination of three basic phenomena, capacity curve, demand curve, and performance point is required. First, the capacity curve, which is a plot of spectral acceleration versus spectral displacement is obtained from the pushover curve. Then, the elastic response spectrum curve, representing the earthquake ground motion, is obtained. This curve is generally given in terms of spectral acceleration and building period for a 5% damping ratio. The demand curve is then, determined by transforming the elastic response spectrum curve into the acceleration displacement response spectrum (ADRS) format. Finally, the performance point (inelastic demand in terms of spectral displacement) is obtained by intersecting the capacity curve and demand curve (see Figure 4.2.). Once the inelastic displacement demand is achieved, pushover analysis is performed again up to this displacement and the seismic responses of the building corresponding to this demand are calculated. The procedures for estimation of inelastic displacement demand (i.e. performance point) are discussed step by step in the following sub-sections.

#### **4.4.3.1. Step by step procedure to estimate the capacity curve**

The capacity curve of a multi-degree freedom system can be obtained by pushing the structure up to a predefined displacement. For this purpose, TEC-2018 recommended different nonlinear static analysis methods (single-mode pushover analysis and multi-mode pushover analysis) also described earlier. In order to obtain structural capacity using single-mode pushover analysis method, the following steps can be applied;

- 1) Construct the mathematical model of the building, using the modeling procedure described in Section 4.2.2.2. It should be noted that for seismic

assessment of new building the preliminary design (determination of the size of structural members and reinforcement ratios) should be performed using one of the linear analysis methods suggested by TEC-2018.

- 2) Develop a flexible base model by assuming a rigid foundation at the surface of the ground to account for soil-structure interaction using the procedure explained in Chapter 3. This step is not covered in the TEC-2018 document.
- 3) Assume the floor system as a rigid diaphragm, and the mass properties of each diaphragm should be lumped at its center of mass (reducing the in-plane degree of freedom to three per floor, namely, two horizontal displacements along x and y-axis and rotation around the z-axis).
- 4) Perform a modal analysis and compute the natural frequency ( $\omega_1$ ) and mode shape ( $\Phi_1$ ) for the first mode of vibration of the linear elastic system.
- 5) Perform a nonlinear static analysis under gravity loads ( $G + nQ$ ) before applying lateral loads, and set the result of this analysis as an initial condition for the pushover analysis.
- 6) Apply the lateral load/displacement increment continuously proportional to the first mode shape (obtained in Step 4) until a control node at the roof level reaches a target displacement. Develop the pushover curve by plotting the roof displacement and its corresponding base shear at every load/displacement increment (Figure 4.7a.). The mode shape remains constant during the whole process of the analysis.
- 7) Convert the ordinates of the pushover curve into modal spectral acceleration and modal spectral displacement, using Equation (4.7) and (4.8), respectively. This curve is termed as a modal capacity diagram which represents the behavior of an equivalent single degree of freedom system (Figure 4.7b).

$$a_1^{(X,k)} = \frac{V_{tx1}^{(X,k)}}{m_{tx1}^{(X,1)}} \quad (4.7)$$

$$d_1^{(X,k)} = \frac{u_{tx1}^{(X,k)}}{\Phi_{tx1}^{(1)} \Gamma_1^{(X,1)}} \quad (4.8)$$

Where  $a_1^{(X,k)}$  is the modal spectral acceleration and  $d_1^{(X,k)}$  is the modal spectral displacement associated with the first mode of vibration (fundamental mode). Superscript  $(X)$  and  $(k)$  denotes the direction of earthquake loading and the pushover steps ( $k = 1, 2 \dots$ ), respectively.  $V_{tx1}^{(X,k)}$  is the base shear force calculated at step  $k$  of pushover analysis in the direction of the x-axis,  $m_{tx1}^{(X,1)}$  represent the participation of the modal mass for the first mode of vibration along the same axis, calculated at the first pushover step ( $k = 1$ ) and kept constant throughout the whole process of the pushover analysis. Similarly, for an earthquake in  $(X)$  direction,  $u_{Nxl}^{(X,k)}$  denotes the roof displacement, calculated at step  $k$  of pushover analysis,  $\Phi_{Nxl}^{(1)}$  is the amplitude of the first mode shape (calculated in Step 4) at the roof level and  $\Gamma_1^{(X,1)}$  is the modal participation factor for the first mode, computed at the first step of pushover analysis ( $k = 1$ ).

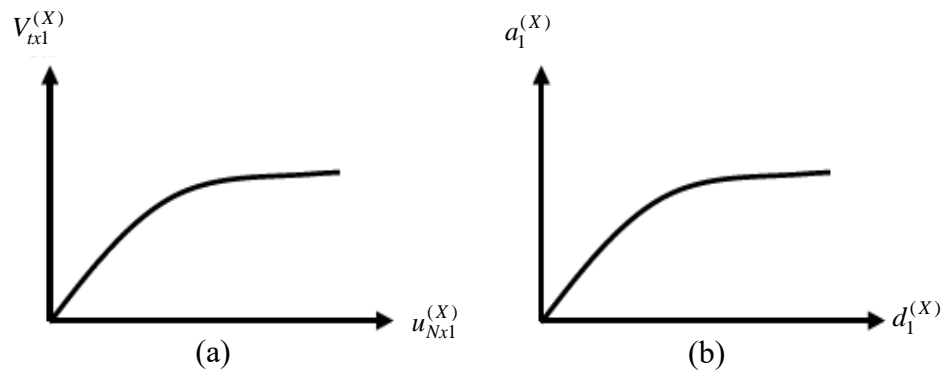


Figure 4.7. Schematic representation of structural capacity in the direction of the x-axis; (a) Pushover curve, (b) modal capacity diagram

The procedure described above is for estimation of the modal capacity diagram (capacity curve) in the direction of the x-axis, a similar procedure can be applied for the y-direction.

#### 4.4.3.2. Estimation of the demand curve

Our understanding of the response of structures to the earthquake, mainly depends on the importance and level of the seismic motion that a building is subjected to. Two basic terms magnitude and intercity are generally used to measure the importance of a particular earthquake. For practical design, the latest version of the Turkish earthquake code (TEC-2018) classified the earthquake hazard motions based on their magnitude and exceedance probability (return period) into four different hazard levels as is explained in Chapter 2. The effects of these earthquake ground motions are represented by the design elastic spectrum diagram, given in standard format for 5% damping ratio, in terms of design elastic spectral acceleration ( $S_{ae}$ ) and building natural vibration period ( $T$ ) as shown in Figure 4.8.

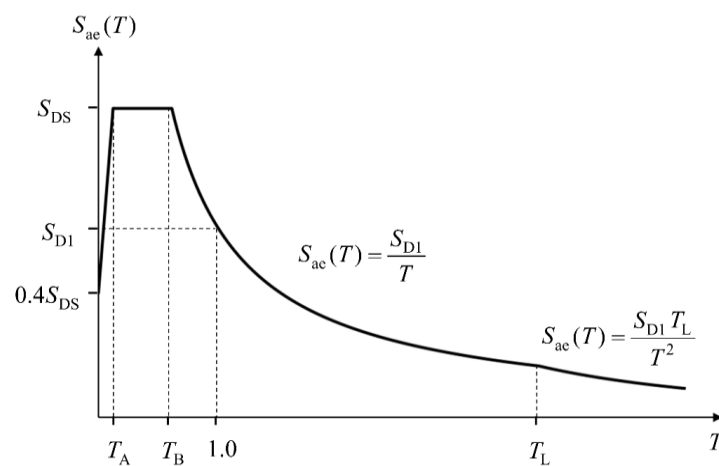


Figure 4.8. Design elastic spectrum diagram

The design elastic spectrum, presented in Figure 4.8, is specified as spectral shape related to local soil conditions, modified by the design spectral acceleration coefficients ( $S_{DS}$  and  $S_{D1}$ ), reflecting the assessed seismicity of the region where the

structure is to be built. The procedure for the construction of design elastic spectrum is provided in Chapter 2., and also for a wider explanation refer to TEC-2018 [24].

To ensure consistency with a given performance level, displacement consistent with seismic demand across the capacity curve should be determined. For this purpose, the design elastic spectrum, presented in Figure 4.8., required to be also plotted in the acceleration displacement response spectrum (ADRS) format, in order to have the same ordinates as the capacity curve (Figure 4.7b.). The horizontal ordinates of the design elastic spectrum diagram can be converted to spectral displacement ( $S_{de}$ ) using Equation (4.9).

$$S_{de}(T) = \frac{T^2}{4\pi^2} g S_{ae}(T) \quad (4.9)$$

Where  $S_{ae}$  is the spectral acceleration,  $T$  is the natural period of the building and  $g$  is the gravitational acceleration.

The resulting curve is then referred to as demand diagram ( $S_{ae}$ - $S_{de}$  curve) and is illustrated in Figure 4.9.

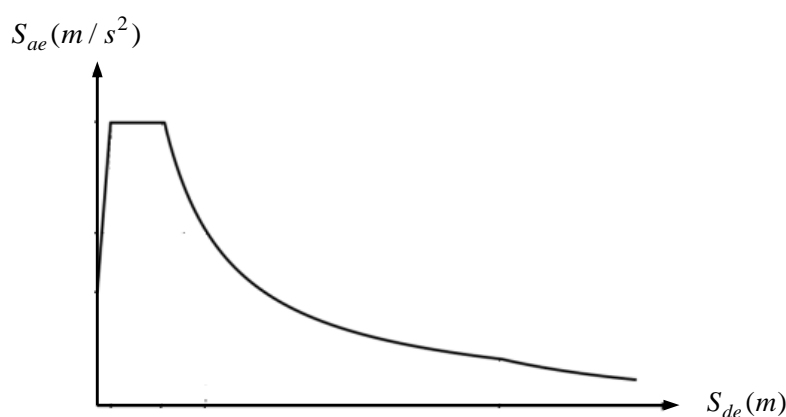


Figure 4.9. Demand diagram (transformation of design elastic spectrum in ADRS format)

#### 4.4.3.3. Determination of modal displacement demand

In the Turkish earthquake code (TEC-2018), the inelastic seismic demand of a MDOF system building is also estimated from the maximum displacement of an equivalent SDOF system. Based on the procedure presented in this document, the seismic demand (i.e. performance point) is determined in terms of modal spectral displacement. The process begins simply by plotting the modal capacity curve (Figure 4.7b) and the demand diagram (Figure 4.9.) associated with the first mode of vibration, in the ADRS format, in the same axis as is presented in Figure 4.10.

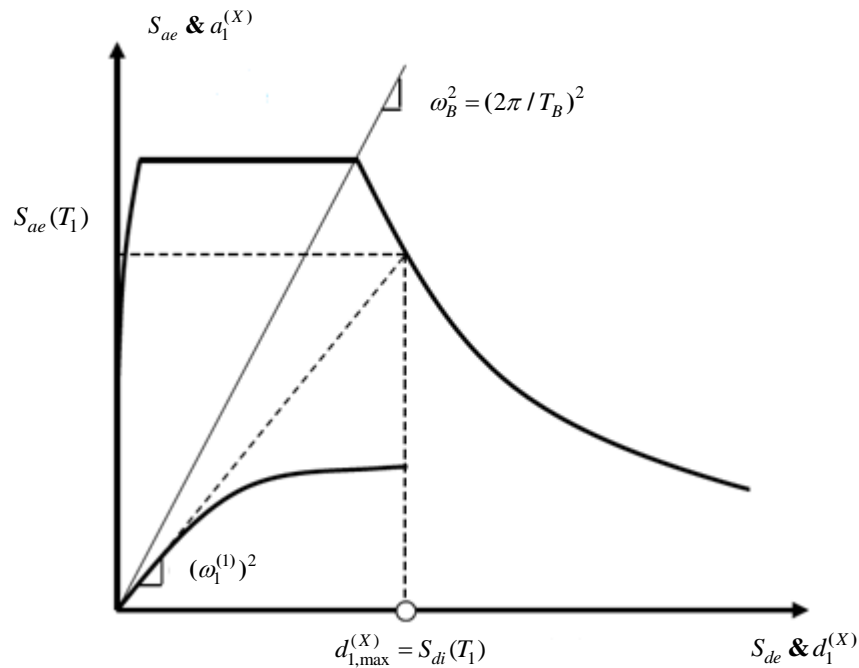


Figure 4.10. Illustration of the modal capacity curve and demand diagram in ADRS format

According to TEC-2018 document, the maximum modal displacement of the equivalent SDOF system, obtained at the last step of pushover analysis, is equated to the inelastic spectral displacement of the structural system (Figure 4.10.) and is expressed by Equation (4.10):

$$d_{1,\max}^{(X)} = S_{di}(T_1) \quad (4.10)$$



Where  $d_{1,\max}^{(X)}$  is the maximum modal displacement of the equivalent SDOF, calculated at the last step of pushover analysis and  $S_{di}(T_1)$  is the inelastic spectral displacement corresponding to the first mode of vibration ( $T_1$ ). The inelastic first-mode spectral displacement,  $S_{di}(T_1)$ , is defined using a simple procedure based on the equal displacement rule:

$$S_{di} = C_R S_{de}(T_1) \quad (4.11)$$

In which  $S_{de}(T_1)$  represents the elastic spectral displacement associated with the fundamental mode of the building, defined by Equation (4.9), and  $C_R$  is the spectral displacement ratio (i.e. spectral displacement amplification factor).

To estimate the value of spectral displacement ratio ( $C_R$ ), first, the modal capacity curve and the demand curve is plotted in the same graph as shown in Figure 4.10. and Figure 4.11, then the value of fundamental vibration period ( $T_1$ ) is compared with the characteristic period of the elastic spectrum ( $T_B$ ). The characteristic period ( $T_B$ ) is the transition period between constant velocity and constant acceleration in the elastic spectrum diagram. If  $T_1 > T_B$  then the value of spectral displacement ratio always equals unity ( $C_R = 1$ ), in other words, inelastic spectral displacement equals the elastic spectral displacement (see Figure 4.10.).

$$C_R = 1 \quad T_1 > T_B \quad (4.12)$$

In the case of  $T_1 \leq T_B$  as shown in Figure 4.11, inelastic spectral displacement is greater than the elastic spectral displacement of equivalent SDOF system, therefore the value of  $C_R$  is also greater than the unity ( $C_R \geq 1$ ) and is computed using the following relationship:

$$C_R = \frac{1 + (R_y - 1) \frac{T_B}{T_1}}{R_y} \quad T_1 \leq T_B \quad (4.13)$$

Where  $R_y$  is the yield reduction factor and is expressed as follow:

$$R_y = \frac{S_{ae}(T_1)}{a_{y1}} \quad (4.14)$$

Where in Equation (4.13),  $S_{ae}(T_1)$  is the elastic spectral acceleration corresponding to the elastic strength demand and  $a_{y1}$  represents the yield spectral acceleration corresponding to the yield strength of the equivalent SDOF system (representation of MDOF system). In this case, since the value of  $a_{y1}$  is not known at the beginning an iterative procedure is required to estimate the value of  $C_R$  using the following steps:

1. Develop the bi-linear representation of the modal capacity curve, assuming that  $C_R=1$  at the first step, as shown in Figure 4.11. The bi-linearization should be performed based on the assumption that the area under the two diagrams is approximately equal.
2. Using the bi-linear curve, approximate the first value for the yield spectral acceleration,  $a_{y1}^0$ .
3. Compute the value of  $R_y$ , using  $a_{y1}^0$  which is obtained in Step 2, from Equation (4.14) and accordingly estimate  $C_R$  and  $S_{di}(T_1)$  from Equations (4.13) and (4.11), respectively.
4. Develop a new bi-linear curve and estimate a new value for  $a_{y1}$  as is graphically presented in Figure 4.11. The procedure in Step 3 is repeated for

the new value of  $a_{y1}$ . The iteration process is continued until the results of the two consecutive Steps are close enough.

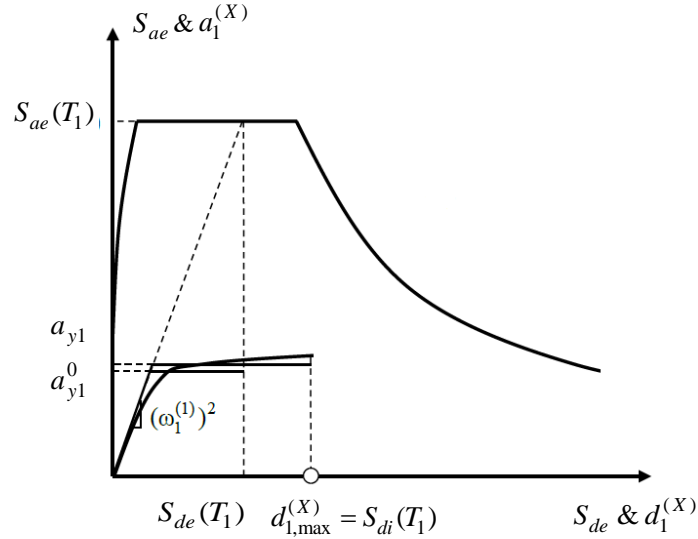


Figure 4.11. Estimation of inelastic spectral displacement through the iterative process.

The inelastic spectral displacement,  $S_{di}(T_1)$ , obtained using Equation (4.11) also defines the maximum modal displacement,  $d_{1,max}^{(X)}$  (computed at the last step of pushover analysis) of the equivalent SDOF system. The roof (global) displacement of MDOF system is then computed, converting the maximum modal displacement of the SDOF system using the following relationship:

$$u_{Nx1}^{(X)} = d_{1,max}^{(X)} \Phi_{Nx1}^{(1)} \Gamma_1^{(X,1)} \quad (4.15)$$

In which,  $u_{Nx1}^{(X)}$  is the total displacement demand (i.e. performance point) at the roof level,  $\Phi_{Nx1}^{(X)}$  and  $\Gamma_1^{(X,1)}$  is as defined in Equation (4.8). The seismic responses of MDOF system such as deformation and strength demands of the structural members and inter-story drift demands corresponding to this roof displacement are calculated and are compared to the available element deformation/strength capacities and acceptance criteria (see Chapter 2.), in order to estimate the performance levels of the buildings.

## **CHAPTER 5. NUMERICAL EXAMPLES AND RESULTS**

In this chapter, it is aimed to present a numerical example, based on the theoretical concepts described in the former chapters. In this numerical example, it is intended to investigate the effects of soil-structure interaction on the seismic performance of the 3D reinforced concrete (RC) moment-resisting frames (MRFs) buildings. The study includes buildings of 2, 4 and 8 stories where the preliminary design of them was performed using linear analysis (force-based) method, based on the minimum requirement of the Turkish Earthquake Code (TEC-2018). However, since this study is concentrated on the application of non-linear static methods, the linear analysis procedure is not included here.

The seismic evaluations of the studied buildings are performed as a result of a parametric investigation, in which the soil properties, the base conditions and the heights of the structures vary. Two different support cases are considered as (1) fixed base and (2) flexible base conditions. As concerns the soil properties, different soil properties for Aapazari region is considered and the single-mode pushover analysis, one of the nonlinear analysis method purposed by Turkish Earthquake Code (TEC-2018), is employed for performance evaluation. As an analysis tool SAP2000 software package is used.

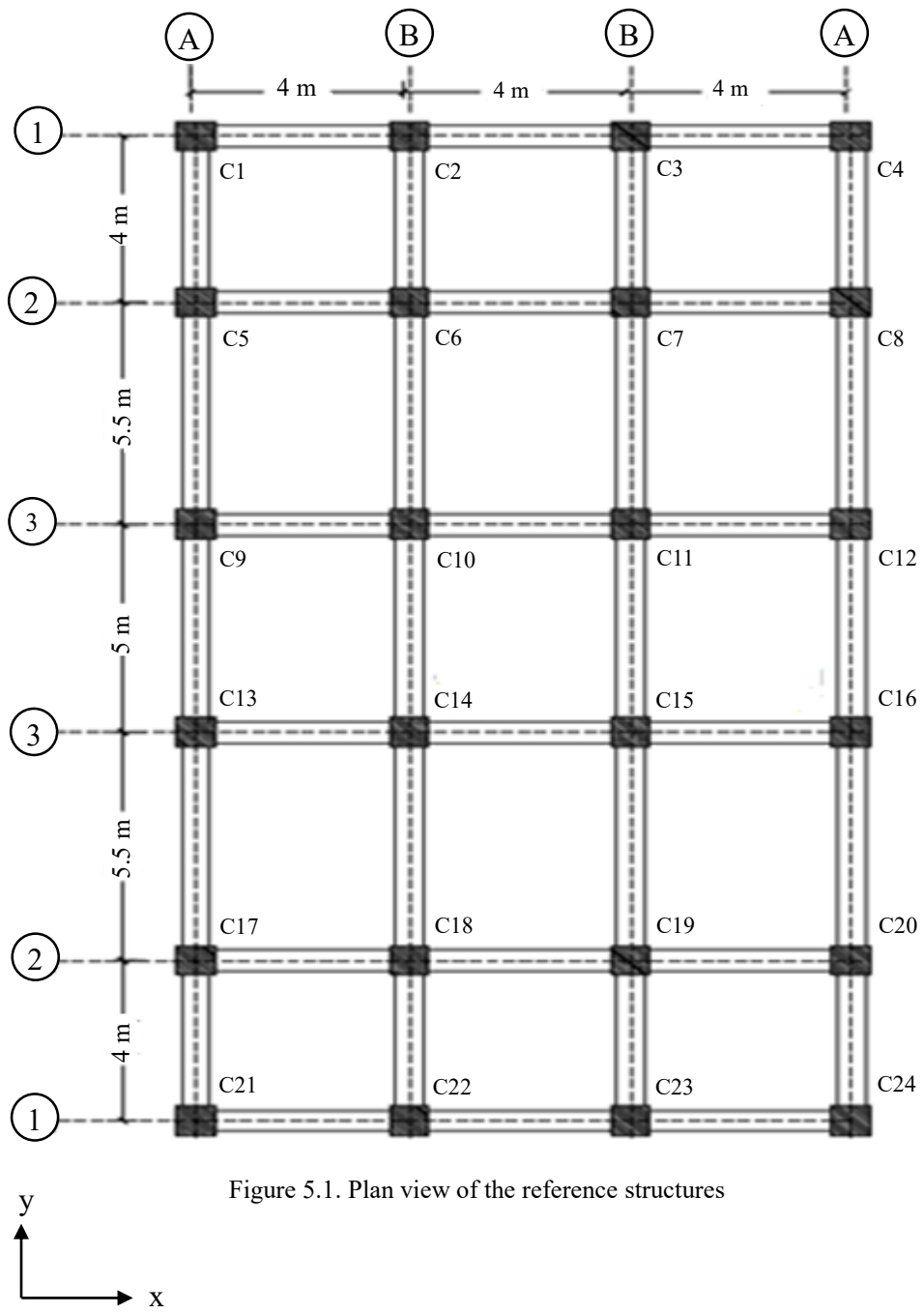
In addition, before presenting the results a brief explanation of the modeling strategies in SAP2000 is provided. The non-linear behavior of the superstructure is modeled based on the requirements of TEC-2018 (see Chapter 4.), while the substructure (foundation) is modeled by means of the impedance function described in Chapter 3.

Finally, the obtained numerical results are evaluated comparatively in terms of roof displacement-base shear force relationships, vibration periods, inter-story drifts and

the damage states of ground floor columns. Accordingly, in order to better realize the SSI effects, both global and component-based damage states of the buildings are studied. The global performance of the buildings is evaluated by comparing the inter-story responses at the performance point with the corresponding limit states reported in Chapter 2. Similarly, the plastic rotation of the ground columns at the target displacement is utilized to check the component-based performance levels by comparing them to the acceptability criteria described in the same chapter.

### **5.1. General Description of the Case Study**

Three different RC moment resisting frames with 2, 4 and 8 stories are selected as reference structures, which can be considered as regular residential buildings. All of the reference structures have the same plan dimension which is symmetric both in x and y directions. As well as the story heights are 3m for all the buildings. The typical plan view of the case studies which is 12 m by 24 m is shown in Figure 5.1.



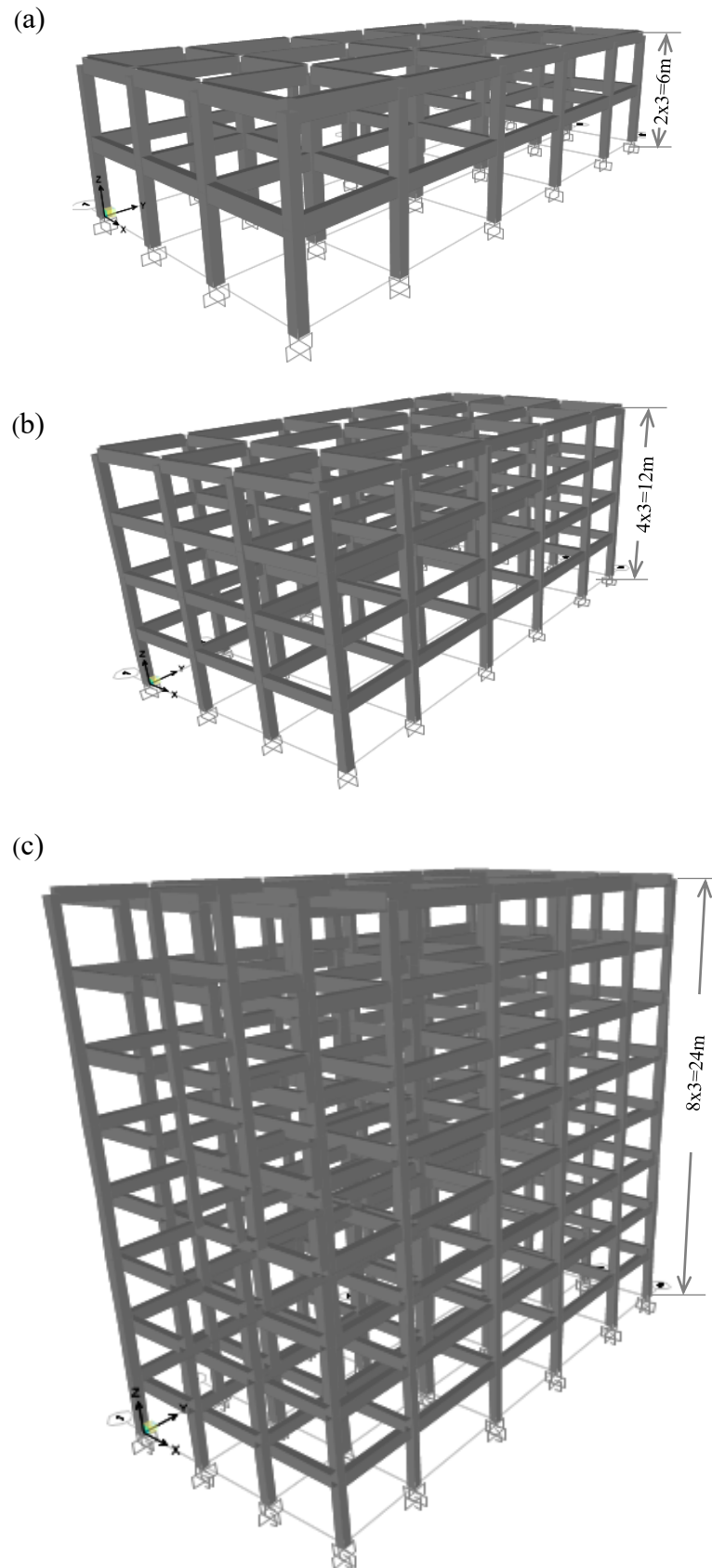


Figure 5.2. 3D view of the case studies: (a) two-story, (b) four-story and (c) eight-story models

The preliminary design of the studied buildings was performed under the design earthquake (DD-2) based on the minimum requirement of TEC-2018. Originally, it has been designed as an eight-story residential building. Then, in order to investigate how the SSI affects seismic performance as the building heights changes, it is modified to two and four-story structures by removing the top six and four floors, respectively. Whereas the structural member's properties such as dimensions and component reinforcement remained the same. The compressive strength of concrete and tensile strength of steel bars was considered 25 Mpa (C25) and 420 Mpa (S420), respectively.

According to TEC-2018, buildings are classified based on their height ranges into eight different categories where these structures can be considered as low to mid-rise RC buildings. The typical 3D view of the case studies is presented in Figure 5.2. The load resisting members of the structural system only consist of beams and columns. Effects of stairs are omitted in this study, while loads of infill walls are included by distributing them uniformly along the length of beams. The slab thickness of all models is the same and is assumed 180 mm, the slab loads are also distributed along the surrounding beams using whether trapezoidal or triangular load distribution. Two types of columns (internal and external) are considered where the internal and external column dimensions are  $500 \times 500 \text{ mm}^2$  and  $400 \times 400 \text{ mm}^2$ , respectively. Whereas member dimension for beams are  $300 \times 600 \text{ mm}^2$  and are assumed to be the same for all stories. Details of member cross-section dimensions and reinforcements are summarized in Table 5.1.

Table 5.1. Details of structural members and reinforcement ratios

Column/Beam	Dimension		Reinforcement
	b (m)	h (m)	
C <sub>ex</sub>	0.40	0.40	12Φ16 = 2413 mm <sup>2</sup>
C <sub>in</sub>	0.50	0.50	16Φ16 = 3217 mm <sup>2</sup> (Bottom) 4Φ16 = 804 mm <sup>2</sup>
Beam	0.30	0.60	(Top) 3Φ16 = 603 mm <sup>2</sup>



Where in Table 5.1.,  $b$  and  $h$  represent the width and height of the element cross-section, respectively. The abbreviation  $C_{ex}$  stands for the external columns and  $C_{in}$  for the internal columns.

General information considered for the current project including building information, material properties, load participations, earthquake level, as well as local soil types and other required parameters which are used in this study are summarized in Table 5.2.

Table 5.2. General requirements and assumption of the project

Items in project	Parameters definition	Parameters quantity
<b>General information of the case study</b>	Number of stories	2, 4, 8
	Story height	3 m
	Total heights (H)	6 m, 12 m, 24 m
	Total width in x-direction (B)	12 m
	Slenderness ratio (H/B)	0.5, 1, 2
	Plane area of the structure	288 m <sup>2</sup>
	Building type	Residential
<b>Material properties</b>	Compressive strength of concrete	25 MPa (C25)
	Yield strength of steel	420 MPa (S420)
	Concrete elastic modulus	30 GPa
	Steel elastic modulus	200 GPa
<b>Building self loads and live loads</b>	Unit weight of concrete	25 kN/m <sup>3</sup>
	Interior wall loads	2.5 kN/m <sup>2</sup>
	Exterior wall loads	4.2 kN/m <sup>2</sup>
	Live loads for roof floor	1.5 kN/m <sup>2</sup>
	Live loads for normal floors	2.0 kN/m <sup>2</sup>
<b>Project Parameters</b>	Earthquake ground shaking hazard level	2 (DD-2)
	Design zone of seismicity (DTS)	1, 1a
	Building importance factor (I)	1
	Local soil types	ZA, ZB, ZC, ZD, and ZE
	Live load participation factor (n)	0.3

The project is developed in Sakarya, Turkey. Based on the latest Turkish earthquake hazard map this region is located in a high seismic zone, where the design zone of seismicity (DTS) for this area corresponds to DTS 1, 1a (Table 5.3.). It should be noted that in the latest version of the Turkish earthquake coed (TEC-2018) different design zone of seismicity has been defined, depending on the short-period design response acceleration parameter,  $S_{DS}$ , for design earthquake (DD-2) and building types or their usage purposes (BKS). The different zone of seismicity described in the TEC-2018 is summarized in Table 5.3.

Table 5.3. Design seismicity zone classification (TEC-2018)

Short-period design response acceleration parameter for hazard level DD-2 ( $S_{DS}$ )	Building classes (BKS)	
	BKS = 1	BKS = 2, 3
$S_{DS} < 0.33g$	DTS = 4a	DTS = 4
$0.33g \leq S_{DS} < 0.50g$	DTS = 3a	DTS = 3
$0.5g \leq S_{DS} < 0.75g$	DTS = 2a	DTS = 2
$0.75g \leq S_{DS}$	DTS = 1a	DTS = 1

## 5.2. Selection of the Local Soil Properties

For what concerns the geologic condition of the site, five different ground conditions for the Adapazari region are considered in this study, in order to investigate the effects of different site conditions on the damage levels of RC buildings under strong ground shaking. The selected soil profile corresponds to ZA, ZB, ZC, ZD and ZE soil types of TEC-2018 provisions. Furthermore, the dynamic interaction between the foundation and underlying soils is generally modeled using three basic characteristics of the soil stratum including soil shear velocity ( $V_s$ ) Poison ratio ( $\nu$ ), soil shear modulus ( $G_0$ ), and soil density ( $\rho_s$ ). The mechanical properties of the selected local soil profiles are presented in Table 5.4.

Table 5.4. Mechanical properties of selected soils

Local soil types	Test site	$V_s$ (m/s)	$\rho_s$ (kN/m <sup>3</sup> )	$G_0$ (kN/m <sup>2</sup> )	$\nu$
ZA	-	1500	20	4500000	0.49
ZB	-	800	20	1280000	0.49
ZC	-	400	20	320000	0.49
ZD	Adapazari _Site B	185	20	68450	0.49
ZE	Adapazari _Site A	85	20	14450	0.49

The non-linear analysis of the buildings and consequently the seismic performance investigation is carried out in Adapazari region. Therefore, the actual soil properties of the region were needed for the verification of the established model with static stiffness. For this purpose, mechanical soil properties for ZD and ZE are obtained from geotechnical studies, after 1999 Kocaeli earthquake, at different points in central part of the Adapazari region [39]. The points, where the field investigation was performed are shown in Figure 5.3. In this study, only the results of the field test at points A and B (Figure 5.3.) in which the soil parameters correspond to soil types ZE and ZD (Table 5.4.) of the TEC-2018 standard are used, respectively. The local soil properties for ZA, ZB, and ZC are adopted from the TEC-2018 provision.



Figure 5.3. Location of ground investigation for different points at the central part of the Adapazari region [14]

### **5.3. Modeling of the Case Studies in SAP2000**

The buildings are modeled, in SAP2000 software packages based on the existing plan (Figure 5.1.) as 3D reinforced concrete MRF considering two different support conditions: (1) the buildings are assumed to be fixed at their bases and (2) in order to account for soil-structure interaction the foundation stiffness and underlying soil stiffness are represented by springs (i.e. foundation impedance) at each degree of freedom. The beams and columns are modeled using frame elements, with rectangular cross-sections. Slabs and infill walls are omitted in the analytical model and their effects are contributed to the system by transforming their loads to the surrounding beams as trapezoidal and uniform loads, respectively.

#### **5.3.1. Material models**

In continuum finite element models, component parameters such as strength and deformations as well as the anticipated nonlinear behavior of the structures subjected to external forces like earthquake ground motions are directly computed from material stress-strain relationships defined for the components. Therefore, selecting an appropriate hysteresis material model is important for the non-linear analysis of the buildings. In this study, the material models for concrete and steel are specified according to TEC-2018 documents and are implemented in the SAP2000 program. Details of material models and material properties available in TEC-2018 is discussed in the following sub-sections.

##### **5.3.1.1. Concrete model**

A unified strain-stress relationship is used in this study, proposed by the Turkish earthquake code (TEC-2018), for both confined and unconfined concrete materials. The considered stress-strain diagram for concrete material is illustrated in Figure 5.4. Generally, unconfined concrete strain corresponding to the maximum unconfined stress is assumed 2% which is also known as yield strain. As it is apparent from Figure 5.4a., after 2% strain is reached, unconfined concrete strength is decreasing until the

section is crushed (losing the load-carrying capacity) and the strain corresponding to this point in the model is referred to as crushing strain. The crushing strain in TEC-2018 is specified 3.5% and the falling part where the strain is greater than 3.5% is represented by a straight line that reaches zero stress at a spalling strain of 5%.

The stress-strain diagram for confined concrete is then constructed by taking in to account the peak compressive strength of unconfined concrete, the crushing strain, tensile strength and cross-section properties such as transverse and longitudinal reinforcement ratios, the lateral and longitudinal bar spacing and etc. Confined and unconfined material models used for nonlinear analysis in this study are shown in Figure 5.4.

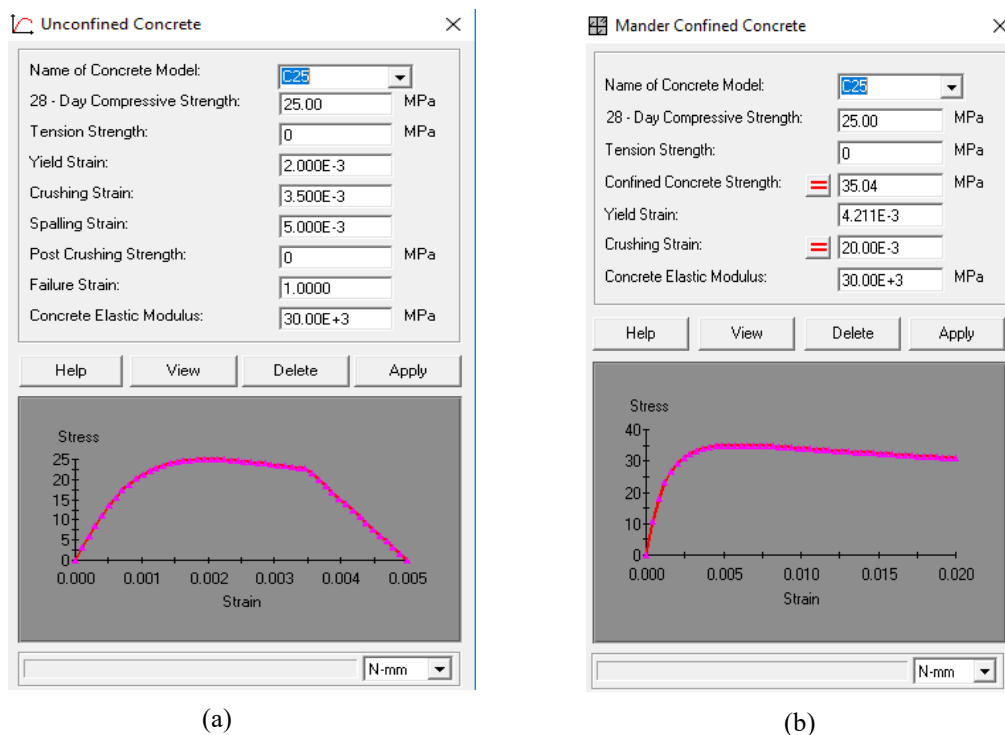


Figure 5.4. Material model for concrete C25 developed in XTRACT program, a) unconfined concrete model, b) confined concrete model

### 5.3.1.2. Steel model

The S420 steel type is used in this project for both main bars and transverse reinforcement. The steel model for S420 steel is constructed according to the strain

and stress limits given in TEC-2018. According to this code, yield strength for S420 steel is given as  $\epsilon_{sy} = 0.0021$ , strain limit at strain hardening is specified as  $\epsilon_{sh} = 0.008$  and ultimate strain is limited to  $\epsilon_{su} = 0.08$ . The elastic modulus for S420 structural steel bar is considered as  $E_s = 2 \times 10^5$  Mpa and fracture stress,  $f_{su}$ , can be assumed between  $1.15f_{sy} \leq f_{su} \leq 1.35f_{sy}$  which in this study  $f_{su} = 550$  Mpa is considered. Based on this information steel model developed for S420 steel is illustrated in Figure 5.5. and is employed later in the SAP2000 program.

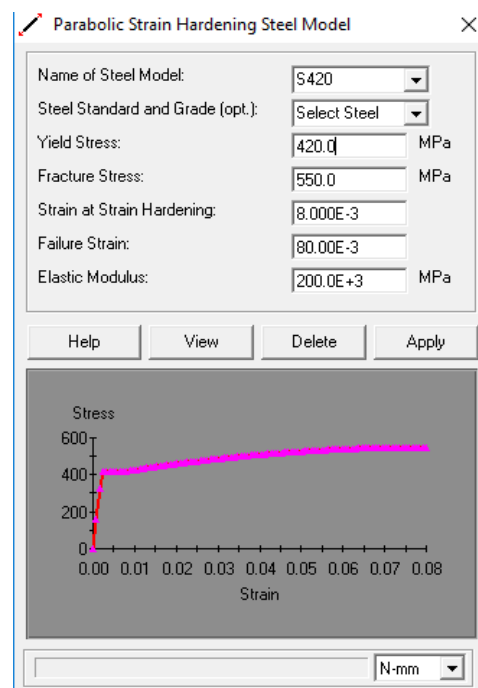


Figure 5.5. Steel Model for S420 steel type developed in the XTRACT program

### 5.3.2. Modeling of the superstructure

Three different, 2-story, 4-story and 8-story reinforced concrete Moment Resisting Frame buildings (MRF), are modeled (Figure 5.2.) using the geometric features and material properties defined in the former sections. The beam and columns are defined as frame elements which are available in SAP2000 workbench. Whereas, the slab and infill walls are omitted and their effects are contributed to the system by transforming their loads to the surrounding beams as trapezoidal and uniform loads, respectively.

The floors and roof of the buildings are designed as a rigid diaphragm. In this way, the structures are tied together as a single entity in which all constrained joints at each floor level are moved together as a planar diaphragm during the seismic motions. In addition, a rigid diaphragm causes the distribution of lateral forces to the vertical components of structures such as columns and shear walls in direct proportion to the relative rigidities. Assuming that the diaphragm is rigid against membrane deformations and provides the same amount of deflection for vertical elements.

In order to account for material nonlinearity, SAP2000 provides a series of hinge properties that can be assigned at any number of locations along the clear length of the frame element. Both coupled and uncoupled hinges are available in SAP2000 workbench. The uncoupled hinges are used to represent the concentrated post-yield (inelastic) behavior associated with moments, torsions, axial and shear forces. They can be defined in the same frame element, but no interaction exists between them. The uncoupled hinge property is useful for nonlinear modeling of beams where only pure bending moment is effective (axial forces for beams are negligible in most cases). On the other hand, in structural members such as columns where the nonlinear behavior is highly affected by the interaction of axial force and moments about the two major axes ( $M_2$  and  $M_3$ ), the usage of uncoupled hinge property is found unreliable. Therefore, the coupled P-M<sub>2</sub>-M<sub>3</sub> frame hinge type which yields based on the interaction of bi-axial bending moments and axial forces at the plastic hinge location is used to define the nonlinear behavior of columns.

As explained in Chapter 4., both concentrated and distributed plasticity models can be used for nonlinear modeling of the structural components. In SAP2000, fiber hinges are available which can be used to represent the distributed plasticity along the frame element and also the cross-sections. However, in this study the non-linearity of frames (columns and beams) are modeled by lumped plasticity model (plastic hinges), which means that the entire inelastic behavior is assumed to concentrate at some specific location, typically at the end zone (plastic hinge length) of the components where nonlinear responses are expected to have significant impact on the analysis and design.

Accordingly, the monotonic force-deformation relationship which is also called the backbone curve is used to specify the behavior of each plastic hinges. In SAP2000, the backbone curve is defined based on the FEMA-356 requirements. The generalized force-deformation relationship available in SAP2000 is shown in Figure 5.5.

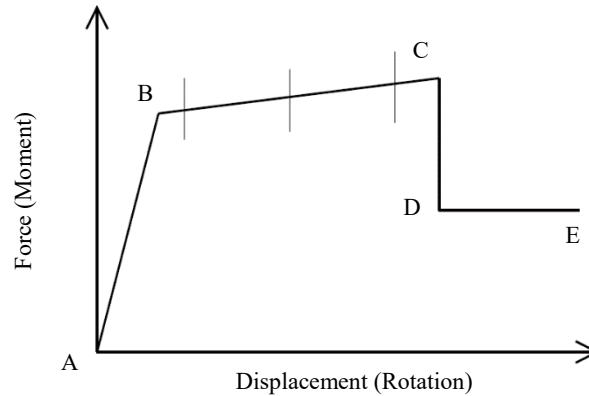


Figure 5.6. A generalized monotonic force-deformation curve representing plastic hinge behavior [40]

This curve is intended to represent the boundary capacity of the components under monotonic loadings. Based on this curve, point A is always the origin and point B represents the yielding and no deformation will be recorded in the hinge between these two points. Only the displacement or rotation beyond point B is demonstrated by the hinge. In other words, the line A-B represents the elastic behavior of the structural members. After that, a reduction in the stiffness is observed until point C which is the ultimate capacity of the member. Point D demonstrates the residual strength of the component and point E is a representative of the total failure, beyond this point the hinge is expected to lose its load-carrying capacity completely and directly drop below point E on the horizontal axis.

Furthermore, different force-deformation options are available in SAP2000, depending on the anticipated controlling behavior of members under the expected loading. This flexibility, provide the analyst to define their desired backbone curve. For example, if the component failure is expected from the bending (flexure) then the ordinates of this curve are defined in terms of a moment-rotation relationship.

In addition, based on the requirements of different seismic codes the force-deformation relationship (Figure 5.6.) can be normalized. The normalization process may differ



from one seismic code to the others, but the key parameters up to the ultimate capacity of the hinge (point C) usually remain the same. For example, the Turkish earthquake code (TEC-2018) uses moment-rotation relationship to define the boundary capacity of the structural components. In this standard, all the key parameters including yield and ultimate moments as well as the rotations corresponding to these points are obtained by moment-curvature analysis. However, the inelastic behavior after the ultimate capacity of the hinge is not specified in TEC-2018. The typical backbone curve based on this provision is illustrated in Figure 5.7.

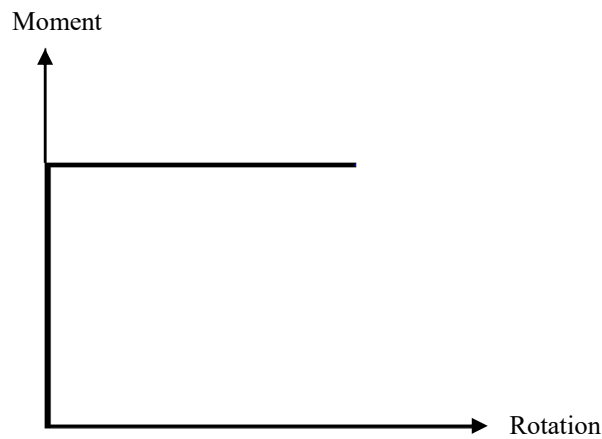


Figure 5.7. Backbone curve purposed by TEC-2018

As can be seen from the Figure above, no rotation will occur up to the yield point and the post-yield stiffness is assumed to be zero (generally the post-yield stiffness can be assumed between zero and 10% of the initial stiffness).

In this study, the normalized moment-rotation (backbone) diagram proposed by TEC-2018 is utilized and employed in SAP2000 to represent the behavior of plastic hinges, defined at the end zone of columns and beams. The definition of plastic hinges for beams and columns in SAP2000 is explained step by step in the following subsections.

### 5.3.2.1. Plastic hinge definition for columns

The coupled P-M2-M3 frame hinge type which yields based on the interaction of bi-axial bending moments and axial forces at the plastic hinge location is used to define

the nonlinear behavior of columns. Since the column cross-sections are created using section designer command in SAP2000, surface interaction diagram is directly developed by the program based on the defined reinforcement model, material properties, and on the provision of FEMA-356. Both external and internal columns have square cross-section, therefore, the interaction of biaxial moments with axial force (P-M2 and P-M3) is the same in both directions. The interaction surface for the coupled P-M3 hinge is as shown in Figure 5.8.

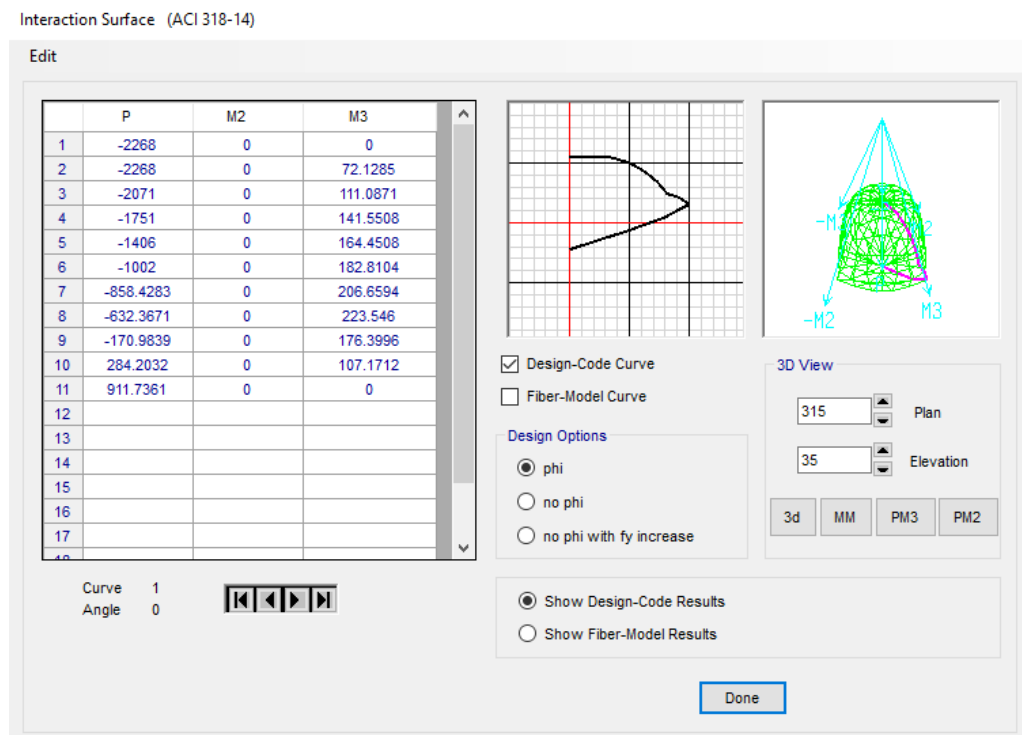


Figure 5.8. Normal force moment interaction surface (P-M3) for the columns

The normalized moment-rotation (backbone) diagram proposed by TEC-2018 is utilized and employed in SAP2000 to represent the behavior of plastic hinges, defined at the end zone of columns. The backbone curve defined for columns in SAP2000 is illustrated in Figure 5.9.

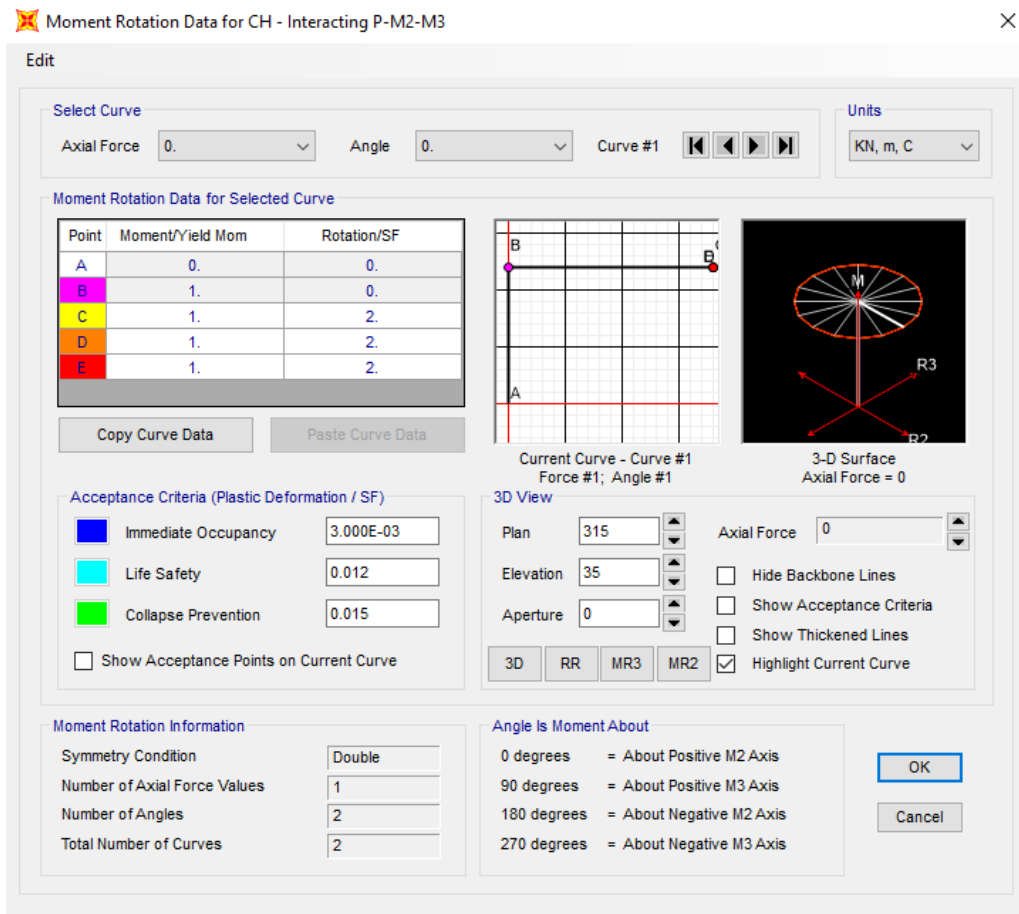


Figure 5.9. Idealized moment rotation (P-M2-M3) diagram (backbone curve) for columns

### 5.3.2.2. Plastic hinge definition for beams

The axial load carried by RC beams is very low which can be ignored. For this reason, only the pure bending moments ( $M_3$ ) is used to set up the beam hinges. As a result of moment-curvature analyses performed with XTRACT program [41], moment-curvature relationships of the beam section is determined considering both negative and positive loading conditions. Positive and negative bending moment of the beam obtained from curvature analysis is as follow:

Positive bmoment (tension at the bottom):  $(+)M = 168.20 \text{ kNm}$

Negative bending moment (tension at the top):  $(-)M = 191.10 \text{ kNm}$

Using this information, the properties of plastic hinge including the backbone curve defined for beams are presented in Figure 5.10.

Frame Hinge Property Data for BH - Moment M3

Edit

Displacement Control Parameters

Point	Moment/SF	Rotation/SF
E-	-1.	-2.
D-	-1.	-2.
C-	-1.	-2.
B-	-1.	0.
A	0.	0.
B	1.	0.
C	1.	2.
D	1.	2.
E	1.	2.

Symmetric

Type

Moment - Rotation

Moment - Curvature

Hinge Length

Relative Length

Hysteresis Type And Parameters

Hysteresis Type

No Parameters Are Required For This Hysteresis Type

Load Carrying Capacity Beyond Point E

Drops To Zero

Is Extrapolated

Scaling for Moment and Rotation

Use Yield Moment

Moment SF

Positive	Negative
168.2	191.1

Use Yield Rotation

Rotation SF

Positive	Negative
1.	1.

(Steel Objects Only)

Acceptance Criteria (Plastic Rotation/SF)

Immediate Occupancy

Positive	Negative
3.000E-03	-3.000E-03

Life Safety

Positive	Negative
0.012	-0.012

Collapse Prevention

Positive	Negative
0.015	-0.015

Show Acceptance Criteria on Plot

OK Cancel

Figure 5.10. Pure bending moment hinge definition for beam in SAP2000

### 5.3.2.3. Effective cross-section stiffness of RC columns and beams

During the analyze process of a building, the rigidity of its elements is taken as the basis for the transmission of the loads. The elements with high stiffness took more load than those with low stiffness. Based on the studies devoted to this subject, it has been determined that the stiffness values of the reinforced concrete structural elements under the influence of earthquakes were different from those predicted during the design phase. For this reason, the rigidity of the cracked section is taken into consideration for seismic analysis. In this regard, TEC-2018 suggests some effective stiffness values for RC members including shear walls, slabs, beams, tie beams and

columns. In this provision, the quantity of effective stiffness of the RC components is defined in terms of the corresponding initial stiffness. The effective stiffness coefficient proposed by this seismic code for frame elements is presented in Table 5.4.

Table 5.4. Effective stiffness coefficient proposed by TEC-2018

Element Type	Effective stiffness coefficients	
	Bending	Shear
Tie beams	0.15	1
Beams	0.35	1
Columns	0.7	1
Shear walls	0.5	0.5

The values of the effective stiffness coefficient given in Table 5.4., are then introduced in the SAP2000 program for each member (columns and beams) by multiplying them with the area moment of inertia of the sections as is shown in Figure 5.11.

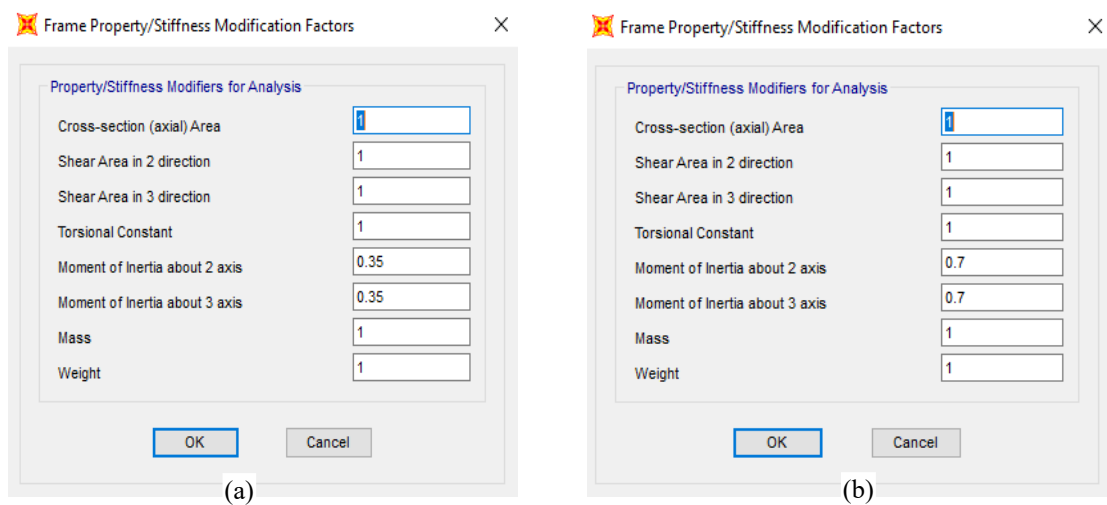


Figure 5.11. Effective Cross-Section stiffness coefficient assigned in SAP2000, (a) stiffness coefficient of columns, (b) stiffness coefficient of beams

### 5.3.3. Calculation of gravity loads and masses

Gravity loads directly affect the results of nonlinear analysis, therefore it is important to select the gravity loads appropriately. Generally, it is assumed as dead loads ( $G$ ) and

some portion of the design live loads ( $Q$ ). In this study, the total dead loads and 30% of live loads are used to define the gravity loads.

To calculate the dead load (self-weight of the building) the unit weight of concrete is assumed to be  $25.00 \text{ kN/m}^3$ . In calculating the self-weight of the slab, the thickness of slabs for all floors including the roof floor is considered to be  $0.18 \text{ m}$  (based on the preliminary design of the building), and an additional  $1.6 \text{ kN/m}^2$  self-load for finishing work is assumed. The internal and external wall loads are obtained from the Turkish building standard also known as TS-500 [42], where  $2.50 \text{ kN/m}^2$  for internal walls and  $4.20 \text{ kN/m}^2$  for external walls are presumed. The design live loads on slabs, considered for residential buildings, are also obtained from TS-500. Based on this standard, a design live load of  $1.5 \text{ kN/m}^2$  for roof floor and  $2 \text{ kN/m}^2$  for normal floors is considered.

Since the slabs are not modeled in SAP2000, the calculated gravity loads on them (slab self-weight and 30% of live loads) are then distributed to the surrounding beams as shown schematically in Figure 5.12.

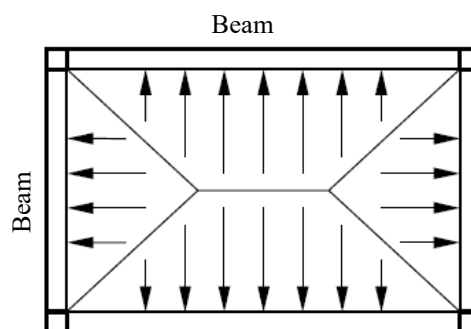


Figure 5.12. Schematic distribution of gravity loads

The infill walls are also not modeled in SAP2000, therefore the calculated dead loads of infill walls (both external and internal walls) are normalized to force per unit length, and then defined to the beams as uniform loads.

In this study, masses are computed from defined gravity loads ( $G+0.3Q$ ) by dividing them to the gravity acceleration ( $g$ ). To do this, there is an option in the SAP2000 program called “Define Mass Source” which can be used to calculate masses from the specified linear combination of load cases (Figure 5.13.).

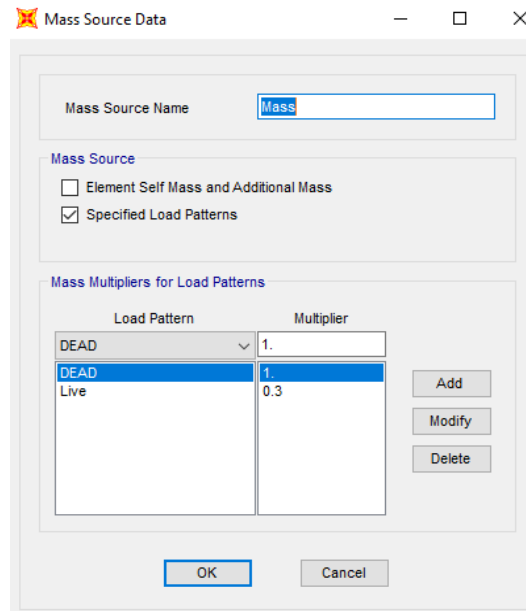


Figure 5.13. Definition of mass source in SAP2000

#### 5.3.4. Modeling of SSI in SAP2000: Sub-structures approaches

The theoretical basis of incorporating SSI in the displacement-based analysis procedure is explained in Chapter 4. The two main effects of SSI on seismic responses including inertial interaction and kinematic interaction were explained explicitly. However, in this study, only inertial interaction effects are considered. For this propose the influence of different soil parameters (Section 5.2.) is investigated. In this section, it is intended to model the SSI system in SAP2000 based on the assumed ground conditions parameters and theoretical aspects.

To include the soil-structure interaction in pushover analysis, the soil and foundation are modeled using elastic springs, available in SAP200 workbench. The stiffness coefficients of the springs (representative of the soil-foundation system) for each degree of freedom are obtained by means of impedance functions at the surface of the

ground (refer to Chapter 3.). As explained earlier, the foundation impedance (spring stiffness) can be calculated depending on mechanical soil properties and foundation size. For what concerns the foundation dimensions, isolated square footings of 1.5m x 1.5m are assumed under each column. The footings are accepted to be rigid and their embedment effects are ignored. As an example, a typical representation of the soil-foundation system by equivalent springs for the 4-story model is demonstrated in Figure 5.14.

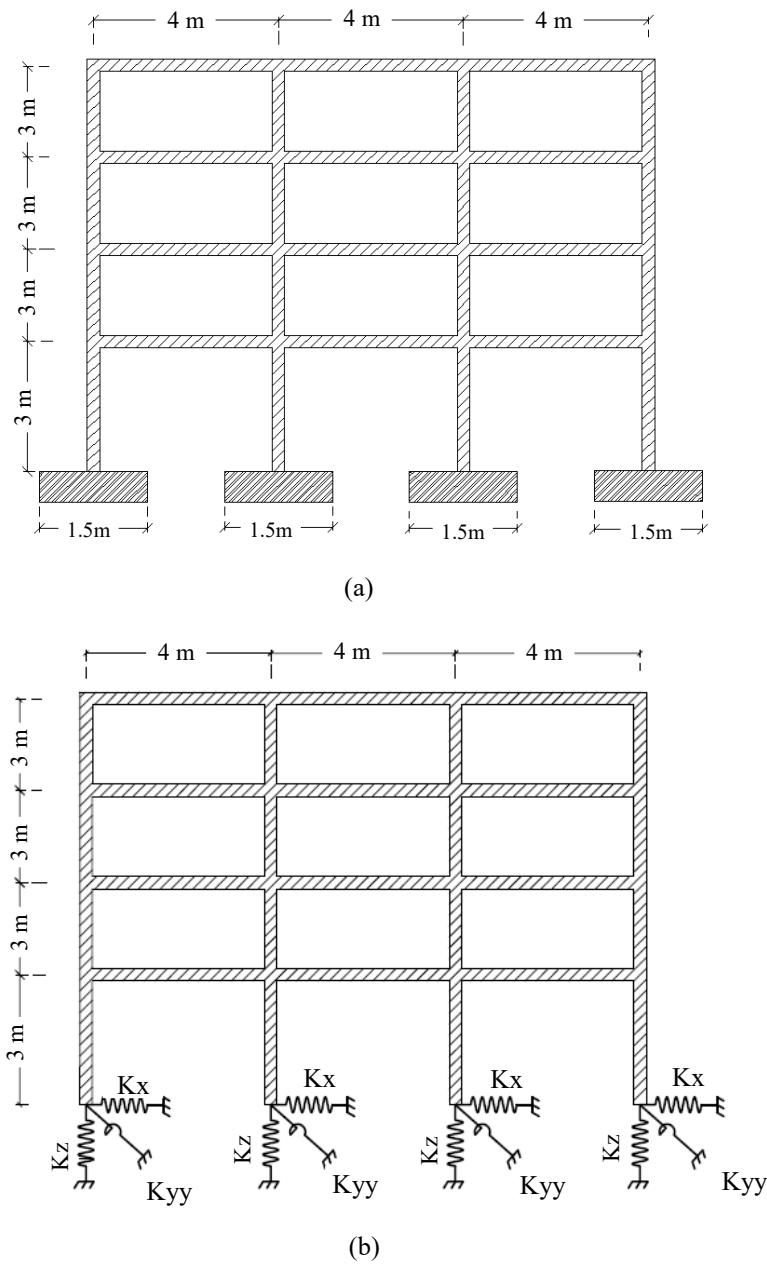


Figure 4.13. Front view of the 4-story model, (a) footing dimensions and (b) representation of the soil-foundation system with equivalent springs



### 5.3.4.1. Calculating soil static stiffness

Also explained in the former chapters, Gazetas [13], and Mylonakis et al.[31] presented equations for computing the stiffness and damping terms of the soil-foundation system. These impedance solutions are also recommended by many seismic codes such as ATC-40 and FEMA-356 which can be used to incorporate SSI effects in static pushover analysis. In this study, the above-mentioned impedance functions (explained in Chapter 3) are utilized to compute the equivalent spring stiffness. The calculated static stiffness for each degree of freedom (three translation along x, y and z-axis and three rotations about the same axis) is then employed in SAP2000 to define the spring stiffness. As it is stated in Chapter 3, the SSI effects can be incorporated to static pushover analysis through: (1) defining foundation springs (Figure 4.13); (2) accounting for kinematic interaction and (3) reduction of the response spectrum for flexible base damping ratio. Nevertheless, in this study kinematic interaction of the SSI is neglected and as concerns the damping ratio a constant 5% damping for the complete structural system is assumed in the analysis. Based on this information and considering the soil properties (Section 5.2), the values of spring stiffness alongside the footing dimensions used in this study for each degree of freedom are summarized in Table 5.5.

Table 5.5. Footing dimensions and equivalent spring stiffness for different soil types used in this study

Soil type	ZA	ZB	ZC	ZD	ZE
Footing dimensions					
2L, (m)	1.50	1.50	1.50	1.50	1.50
2B, (m)	1.50	1.50	1.50	1.50	1.50
The values of static stiffness for each degree of freedom					
K <sub>x</sub> , (kN/m)	2.01E+07	5.72E+06	1.43E+06	3.06E+05	6.64E+04
K <sub>y</sub> , (kN/m)	2.01E+07	5.72E+06	1.43E+06	3.06E+05	6.64E+04
K <sub>z</sub> , (kN/m)	3.00E+07	8.55E+06	2.14E+06	4.57E+05	9.65E+04
K <sub>yy</sub> , (kNm/rad)	1.39E+07	3.94E+06	9.85E+05	2.11E+05	4.45E+04
K <sub>xx</sub> , (kNm/rad)	1.34E+07	3.81E+06	9.53E+05	2.04E+05	4.30E+04
K <sub>zz</sub> , (kNm/rad)	1.58E+07	4.51E+06	1.13E+6	2.41E+05	5.09E+04

### 5.3.5. Assumptions made in modelling

In this section, some of the basic assumptions made regarding the modeling of the case studies described in the former sections as well as some other assumptions which are not explained before are summarized in the following;

- a) Joints (column and beam connections) are assumed to be rigid.
- b) The dimensions of the structural components including beams and columns are considered to be the same for all models.
- c) The slabs and infill walls are omitted and diaphragm constraints are defined at each story level.
- d) Material nonlinearity is included in the model by means of lumped plasticity (plastic hinges) model and is assumed to concentrate at the end zone of the elements.
- e) Geometric non-linearity, which is also known as P-Delta effects, are considered. This type of non-linearity are caused due to the application of external loading such as gravity loads upon the displaced configuration of a structure which results in adding an extra moment forces on the structural components.
- f) In the case of the flexible base model, the foundation is assumed to be rigid which is located at the surface of the ground. As well as, square type footings with plane dimensions of 1.5x1.5 m are considered and remained the same for all models.
- g) The soil beneath the foundation is assumed to be elastic and the interaction between soil and foundation is modeled by linear springs.
- h) The impedance values are computed by using frequency independent impedance functions.

## **5.4. Conducting Pushover Analysis in SAP2000**

This section deal with the analysis of the selected building which is built based on the analytical procedures explained in the former sections. In order to investigate the seismic responses of the selected buildings, single-mode pushover analysis, based on the TEC-2018 requirements (see Chapter 4.), is conducted in both x and y directions using the SAP2000 software package.

As explained in the former chapters, pushover analysis can be performed either displacement-controlled or force-controlled, both options are available in SAP2000. In this study, the displacement controlled option is selected and a control point at the roof level is designated, then the structure is pushed up to a predefined displacement at this point. Displacement-controlled is most suitable for buildings that become unstable and lose load-carrying capacity during the course of the analysis.

Furthermore, in order to perform a non-linear static analysis, both acceleration and modal load patterns are available in SAP2000 where the modal load is a specialized loading type for pushover analysis. Therefore, before applying the lateral loads a modal analysis is performed and then the lateral loads are distributed along the height of the buildings proportional to their first mode shapes, which is the dominant mode shape. In addition, to perform a pushover analysis, the definition of gravity loads is also required. Therefore, the structures are analyzed under the gravity loads and the results from this analysis are set as an initial condition for the pushover analysis. It should be noted that plastic deformations are not allowed under gravity loads. The procedure for performing single-mode pushover analysis in SAP2000 is summarized in the following sub-sections.

### **5.4.1. Definition of modal load cases**

As mentioned earlier, the lateral loads can be applied to the structure using the modal load pattern available in SAP2000. It is a load pattern on the joints where its shape and magnitude changes depending on the joint masses, mode shape, and angular frequency.

Therefore, before pushing the structures laterally, the modal load case is defined and employed in order to distribute the lateral loads and calculate base shear. In this study, the first (dominant) mode shape is used and the lateral loads are distributed according to this mode shape. Since the reference structures considered in this study is low to mid-rise buildings, where the total height of the structures is less than 25m, the responses of them are governed by the fundamental mode therefore the higher modes effects are ignored. The definition of the modal load case in SAP2000 is shown in Figure 5.13.

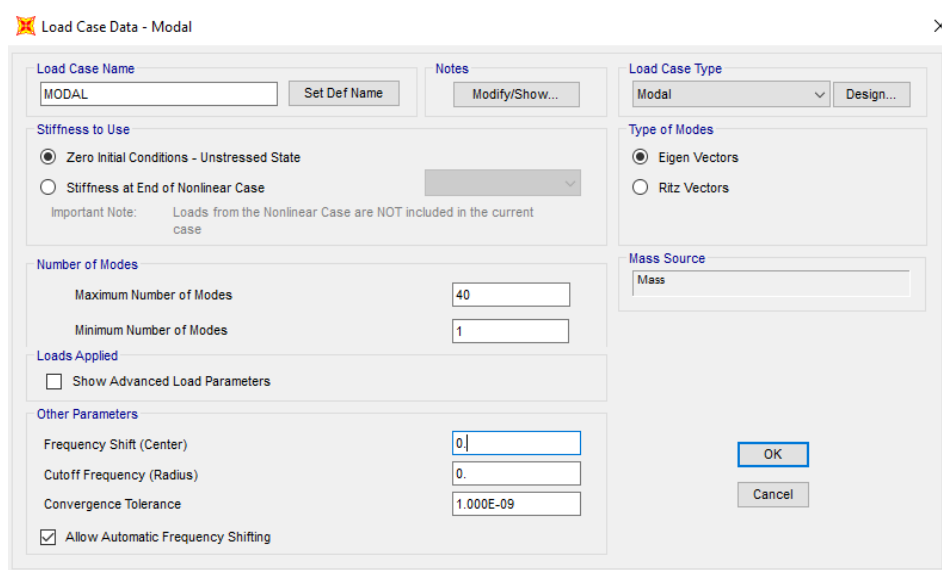


Figure 5.14. Definition of modal load case in SAP2000

#### 5.4.2. Definition of gravity load case (vertical loads)

Nonlinear static pushover analysis in SAP2000 can be applied either with zero initial condition or continued from a previous nonlinear analysis. The option “zero initial condition” indicates that no deformation has occurred to the structures and all of the elements are unstressed. Whereas the command “continue from a previous nonlinear analysis” states that the buildings are already deformed, the elements are stressed, and the forces are distributed on the components as a result of a previous nonlinear load application.

In the prescriptive requirements of the TEC-2018, the non-linear static pushover analysis is needed to start from the end of gravity loads. Therefore, the buildings are first analyzed under the gravity loads ( $G+0.3Q$ ), where  $G$  is the total dead load (self-weight of the building) and  $Q$  is the total live load, which are computed as is explained in Section 5.3.3. Accordingly, the result of this analysis is set to be the initial condition for pushover analysis. In addition, the gravity loads are applied with zero initial condition and no plastic hinges are formed in the components during this analysis, which is also not allowed by the TEC-2018 standard. The definition of gravity load case in SAP2000 is presented in Figure 5.15.

The screenshot shows the 'Define Gravity Load Case' dialog box in SAP2000. The 'Load Case Name' is 'Gravity'. The 'Initial Conditions' are set to 'Zero Initial Conditions - Start from Unstressed State'. The 'Analysis Type' is 'Nonlinear'. The 'Geometric Nonlinearity Parameters' are set to 'P-Delta'. The 'Mass Source' is 'Mass'. The 'Loads Applied' table is as follows:

Load Type	Load Name	Scale Factor
Load Pattern	DEAD	1.0
Load Pattern	LIVE	0.3

The 'Other Parameters' section shows 'Load Application' as 'Full Load', 'Results Saved' as 'Final State Only', and 'Nonlinear Parameters' as 'Default'.

Figure 5.15. Definition of gravity load case in SAP2000

After the definition of the modal and gravity load cases, the mathematical models including fixed and flexible base conditions are solved under these load cases, accordingly, the predominant modes in x and y-directions have been determined. Consequently, the buildings masses and mass participation ratios are calculated for the dominant modes which are shown in Table 5.6. and 5.7. for the x and y-directions, respectively.

Table 5.6. Total masses and mass participation ratios of the models associated with the fundamental modes of vibration ( $T_1$ ) in the direction of x-axis

Model	Base condition	Total mass and mass participation ratios in the x-direction					
		Soil types	ZA	ZB	ZC	ZD	ZE
2-Story		Total mass (kN s <sup>2</sup> /m)	745.5	745.5	745.5	745.5	745.5
	Fixed base	Mass participation ratio (%)	91.89	91.89	91.89	91.89	91.89
	Flexible base	Mass participation ratio (%)	89.81	89.97	90.57	92.44	94.82
4-Story		Total mass (kN s <sup>2</sup> /m)	1628.2	1628.2	1628.2	1628.2	1628.2
	Fixed base	Mass participation ratio (%)	86.32	86.32	86.32	86.32	86.32
	Flexible base	Mass participation ratio (%)	85.45	85.58	86.10	0.88	90.62
8-Story		Total mass (kN s <sup>2</sup> /m)	3393.5	3393.5	3393.5	3393.5	3393.5
	Fixed base	Mass participation ratio (%)	82.72	82.72	82.72	82.72	82.72
	Flexible base	Mass participation ratio (%)	82.72	82.40	82.66	83.60	84.81

Table 5.7. Total masses and mass participation ratios of the models associated with the fundamental modes of vibration ( $T_1$ ) in the direction of y-axis

Model	Base condition	Total mass and mass participation ratios in the y-direction					
		Soil Types	ZA	ZB	ZC	ZD	ZE
2-Story		Total mass (kN s <sup>2</sup> /m)	745.5	745.5	745.5	745.5	745.5
	Fixed base	Mass participation ratios (%)	91.45	91.45	91.45	91.45	91.45
	Flexible base	Mass participation ratios (%)	89.38	89.54	90.15	92.09	94.89
4-Story		Total mass (kN s <sup>2</sup> /m)	1628.2	1628.2	1628.2	1628.2	1628.2
	Fixed base	Mass participation ratios (%)	86.01	86.01	86.01	86.01	86.01
	Flexible base	Mass participation ratios (%)	85.14	85.28	85.79	87.66	91.20
8-Story		Total mass (kN s <sup>2</sup> /m)	3393.4	3393.4	3393.4	3393.4	3393.4
	Fixed base	Mass participation ratios (%)	82.73	82.73	82.73	82.73	82.73
	Flexible base	Mass participation ratios (%)	82.73	82.41	82.70	83.85	86.46

### 5.4.3. Pushover Load cases

After the definition of modal and gravity Load Cases, the lateral loads (earthquake equivalent loads) are applied consistent with the dominant mode shape and are set to

initially start from the end of the gravity load case. This loading type is termed as the pushover Load Case and is defined in SAP2000 as shown in Figure 5.16.

The screenshot shows the 'Load Case Name' dialog box in SAP2000. The 'Load Case Name' field is set to 'Push\_X'. The 'Initial Conditions' section has 'Continue from State at End of Nonlinear Case' selected, with 'Gravity' chosen in the dropdown. The 'Modal Load Case' section has 'All Modal Loads Applied Use Modes from Case' selected, with 'MODAL' in the dropdown. The 'Loads Applied' table is as follows:

Load Type	Load Name	Scale Factor
Mode	2	1.
Mode	2	1.

The 'Analysis Type' section has 'Nonlinear' selected. The 'Geometric Nonlinearity Parameters' section has 'P-Delta' selected. The 'Mass Source' is set to 'Mass'. The 'Other Parameters' section has 'Displ Control' for Load Application, 'Multiple States' for Results Saved, and 'User Defined' for Nonlinear Parameters. The 'OK' and 'Cancel' buttons are visible at the bottom right.

Figure 5.16. Definition of nonlinear static pushover load case in SAP2000

The nonlinear pushover analysis is performed using displacement control option. A monitored displacement is defined at the roof level of each analytical model and is used for plotting the pushover curve.

Initially, it is not known how far the building should move, therefore a larger displacement component is selected and the pushover curve is obtained. Afterward, the obtained pushover curve is plotted in the same coordinate with the demand curve in spectral format and then the displacement demand is obtained using the procedure explained in Chapter 4. Finally, the models are pushed again up to the computed displacement demand and the real pushover curves are obtained. In addition, the global and component-based performance levels of the studied buildings are investigated. The inter-story drifts corresponding to the performance point are used for the global performance check and the damage states of the ground columns corresponding to the performance point are used to identify the component-based performance levels.

## **5.5. Analysis Results and Discussions**

In this section, the results of the single-mode pushover analysis of the analytical models are presented. The flexible base condition of the case studies is developed using a simplified soil-structure interaction (SSI) model (Section 5.3.4.) appropriate for pushover analysis. The analysis are carried forward for both flexible based (SSI system) and fixed base conditions, both in x and y directions under the loads defined in the former sections.

Furthermore, the main goal of this study is to evaluate the effects of SSI on the seismic actions of RC frames subjected to the design earthquake motion (DD-2) and analyzed according to TEC-2018 regulations. Moreover, it is aimed to put additional light on the importance of including SSI in numerical analyses of structures. For this purpose, the seismic responses of 2, 4 and 8 story buildings (Section 5.1.) are studied, assuming different geological ground conditions for Adapazari region (Section 5.2.). Seismic results obtained from SSI models are compared with those of fixed base conditions in order to observe the effects of SSI. The analysis results are interpreted comparatively in terms of base shear and roof displacement relationships, building vibration periods, inter-story drifts and damage states of the ground floor columns.

### **5.5.1. Effects of SSI on vibration periods**

Based on the obtained results from the modal analysis of the studied buildings, SSI elongates the vibration periods of the RC structures, comparing to the fixed base condition, especially when it is founded on soft soil, soil type ZD and ZE. This happens due to the reduction in lateral stiffness of the buildings, resulting from the deformable behavior of the underlying soils. The amplification of the vibration period, due to the flexibility of the foundation, changes depending on the ground conditions and building heights. The values of building periods as well as the vibration due to SSI effects, both in x and y-directions, are presented in Table 5.8. and 5.9., respectively.



Table 5.8. Variation in vibration period due to the SSI effects in the x-direction

Models	The vibration period of the buildings in x-direction, $T_1$ (s)					
	Soil types	ZA	ZB	ZC	ZD	ZE
2-Story	Fixed base	0.268	0.268	0.268	0.268	0.268
	SSI	0.269	0.270	0.277	0.303	0.384
	Vriation (%)	0.24	0.83	3.21	13.12	43.09
4-Story	Fixed base	0.557	0.557	0.557	0.557	0.557
	SSI	0.558	0.560	0.568	0.603	0.726
	Vriation (%)	0.15	0.51	1.86	8.18	30.23
8-Story	Fixed base	1.163	1.163	1.163	1.163	1.163
	SSI	1.165	1.168	1.182	1.245	1.485
	Vriation (%)	0.17	0.41	1.60	7.07	21.63

Table 5.9. Variation in vibration period due to the SSI effects in the y-direction

Models	The vibration period of the buildings in y-direction, $T_1$ (s)					
	Soil types	ZA	ZB	ZC	ZD	ZE
2-Story	Fixed base	0.275	0.275	0.275	0.275	0.275
	SSI	0.276	0.277	0.283	0.309	0.387
	Vriation (%)	0.23	0.79	3.06	12.53	40.89
4-Story	Fixed base	0.575	0.575	0.575	0.575	0.575
	SSI	0.576	0.578	0.586	0.619	0.726
	Vriation (%)	0.14	0.47	1.83	7.63	26.24
8-Story	Fixed base	1.200	1.200	1.200	1.200	1.200
	SSI	1.202	1.204	1.216	1.265	1.424
	Vriation (%)	0.16	0.34	1.32	5.47	18.69

### 5.5.2. Effects of SSI on the maximum displacement demand

The maximum displacement demand is computed in view of the TEC-2018 provision. The procedure proposed by this standard is also summarized in Chapter 4, where the modal capacity curves and the demand curves are plotted in the same graph and the performance points (i.e. displacement demand) are then determined as the intersection point of these two curves. To simplify the presentation of the results, the application of this method is explained in detail by selecting the 4-story model, resting on soil type ZD, as an example. Accordingly, the estimation of performance point is carried out by following the three basic steps which include (1) determination of modal capacity curve, (2) identification of the demand curve and (3) obtaining the displacement demand. A similar procedure is employed for other cases, and the results are

summarized in Table 5.11. The application of each of these steps are discussed in the following paragraphs.

The capacity curves of the studied buildings are obtained by transforming the pushover curve, which is determined as a result of single-mode pushover analysis (Section 5.4.), into spectral displacement response acceleration format. Equation (4.7) and (4.8) are used to perform the transformation process. Accordingly, the calculated values for constructing the modal capacity curve for the 4-story model, with the fixed base condition, are presented in Table 5.10.

Table 5.10. Determination of modal capacity curve for the 4-story model in the x-direction

Pushover steps	$\mathbf{u}_{N \times 1}^{(k)}$	$V_{tx1}^{(X, k)}$	$m_{tx1}^{(X, 1)}$	$\Gamma_1^{(X, 1)}$	$\Phi_{N \times 1}^{(1)}$	$d_1^{(X, k)}$	$a_1^{(X, k)}$
(k)	(m)	(m/s)	(kN s <sup>2</sup> /m)	—	—	(m)	(m/s <sup>2</sup> )
0	0.0000	0.00	1628.18	37.29	0.0347	0.0000	0.00
1	0.0167	2288.32	1628.18	37.29	0.0347	0.0129	1.63
2	0.0232	2888.43	1628.18	37.29	0.0347	0.0179	2.06
3	0.0370	3356.54	1628.18	37.29	0.0347	0.0286	2.39
4	0.0498	3567.84	1628.18	37.29	0.0347	0.0385	2.54
5	0.0533	3591.80	1628.18	37.29	0.0347	0.0412	2.56
6	0.0633	3644.02	1628.18	37.29	0.0347	0.0489	2.59
7	0.0736	3683.99	1628.18	37.29	0.0347	0.0569	2.62
8	0.0839	3707.48	1628.18	37.29	0.0347	0.0649	2.64
9	0.0928	3735.83	1628.18	37.29	0.0347	0.0718	2.66
10	0.0954	3736.84	1628.18	37.29	0.0347	0.0738	2.66
11	0.1204	3709.05	1628.18	37.29	0.0347	0.0931	2.64
12	0.1204	3709.18	1628.18	37.29	0.0347	0.0931	2.64
13	0.1704	3684.83	1628.18	37.29	0.0347	0.1318	2.62
14	0.1776	3694.80	1628.18	37.29	0.0347	0.1373	2.63
15	0.1850	3707.44	1628.18	37.29	0.0347	0.1431	2.64
16	0.1850	3707.77	1628.18	37.29	0.0347	0.1431	2.64
17	0.1857	3717.43	1628.18	37.29	0.0347	0.1436	2.65

Based on the values presented in Table 5.10, the pushover curve as well as the modal capacity diagram are constructed for the 4-story model, with the fixed base condition, and is demonstrated in Figure 5.17.

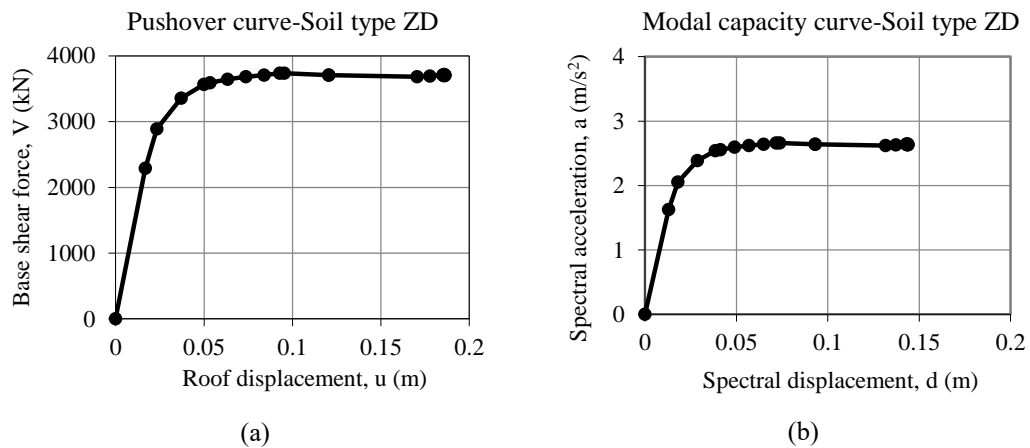


Figure 5.17. Transformation of pushover curve into modal capacity curve for 4-story model with the fixed base condition: (a) pushover curve; (b) capacity curve

The design elastic response acceleration spectrum which represents the design earthquake ground motion level-2 (DD-2) are obtained from Turkish earthquake hazard map in a standard format, by considering 5% damping ratio. The required procedure and formulas to develop this curve are explained in Chapter 2. The necessary parameters for developing the design elastic response spectrum curve for the design earthquake (DD-2) related to different soil types, used in this study, are summarized in Table 5.11.

Table 5.11. Parameters for constructing elastic spectrum for DD-2 and selected site conditions

Soil types	Mapped spectral acceleration coefficients		Local site parameters		Design response acceleration coefficients		Characteristic periods		Coordinates (degree)	
	$S_s$	$S_1$	$F_s$	$F_1$	$S_{DS}$	$S_{D1}$	$T_A$ (s)	$T_B$ (s)	Latitude	Longitude
ZA	1.694	0.464	0.800	0.800	1.247	0.342	0.055	0.275	40.742	30.335
ZB	1.685	0.461	0.900	0.800	1.517	0.369	0.049	0.243	40.748	30.352
ZC	1.672	0.457	1.200	1.500	2.006	0.686	0.068	0.342	40.753	30.352
ZD	1.530	0.420	1.000	1.880	1.530	0.790	0.103	0.516	40.785	30.400
ZE	1.559	0.428	0.800	2.344	1.247	1.003	0.161	0.804	40.779	30.395

The elastic response spectra for the design earthquake (DD-2), considering the soil properties for soil type ZD is illustrated in Figure 5.18. Using Equation (4.9), this diagram is then converted to seismic demand curve which is a plot of spectral acceleration versus spectral displacement that is shown in Figure 5.19.

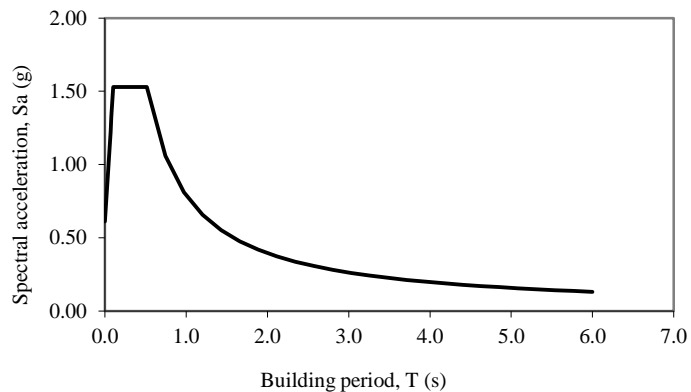


Figure 5.18. Elastic response spectrum diagram representing the design earthquake (DD-2), for soil type ZD

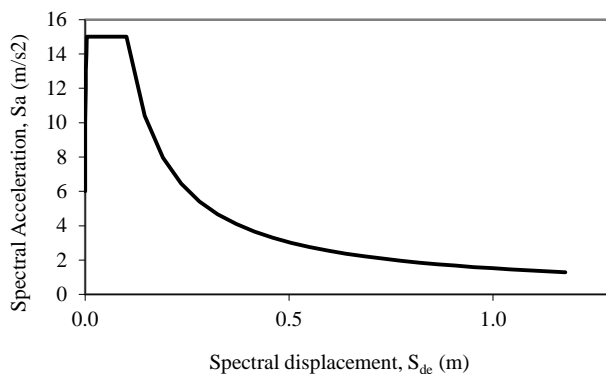


Figure 5.19. Seismic demand diagram for the design earthquake (DD-2), for soil type ZD

Finally, after developing both the capacity and the demand curves, they are plotted in the same coordinates (Figure 5.20.) and the seismic displacement demand is determined in terms of the modal displacement (i.e. inelastic spectral displacement), based on the analytical procedure explained in Chapter 4. The estimation of seismic displacement demand for the 4-story model is graphically presented in Figure 5.20.

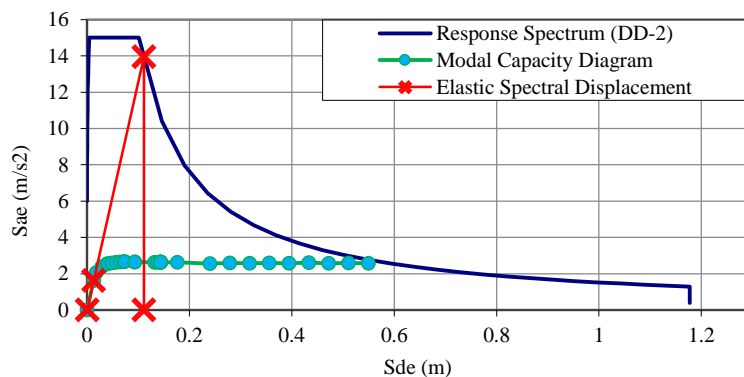


Figure 5.20. Determination of modal displacement demand for 4-story model

From the Figure 5.20., the elastic spectral displacement demand,  $S_{de}(T_1) = 0.1110$  m, is approximated. Afterward the inelastic spectral displacement demand,  $S_{di}(T_1)$ , which simultaneously equals to the maximum modal displacement,  $d_{1,\max}^{(X)}$  is calculated using Equation (4.11). In order to compute the value of  $S_{di}(T_1)$ , first the spectral displacement amplification factor,  $C_R$ , is needed to be determined. As explained in Chapter 4., the value of  $C_R$  can be approximated by comparing the building vibration period,  $T_1$ , with the response spectrum characteristic period,  $T_B$ . In the case of 4-story building with the fixed base condition  $T_1 = 0.557$  sec, which is obtained from Table 5.8. Similarly, for local soil type ZD, the value of  $T_B$  can be estimated from Table 5.11., where  $T_B = 0.516$  sec.

Since  $T_B = 0.516 < T_1 = 0.557$ ,  $C_R = 1$

Accordingly;

$$S_{di}(T_1) = C_R S_{de}(T_1) = 1 \times 0.1104 = 0.1110 \text{ m.}$$

The inelastic spectral displacement,  $S_{di}(T_1)$ , obtained using Equation (4.11) also defines the maximum modal displacement,  $d_{1,\max}^{(X)}$ , of the equivalent SDOF system. The roof (global) displacement of MDOF system is then computed by converting the maximum modal displacement of the SDOF system using Equation (4.15);

$$u_{N \times 1}^{(X)} = d_{1,\max}^{(X)} \Phi_{N \times 1}^{(1)} \Gamma_1^{(X,1)} = 0.1110 \times 0.0347 \times 37.29 = 0.1435 \text{ m}$$

Where the values of  $\Phi_{N \times 1}^{(1)}$  and  $\Gamma_1^{(X,1)}$  are obtained from Table 5.8.

A similar procedure has been carried forward, in order to estimate the maximum displacement demands, for other cases including fixed base and flexible base conditions. Accordingly, the obtained results for the SSI system is compared with

those of the same model when fixed in their bases and are summarized in Table 5.12. and 5.13. for x and y directions, respectively.

Table 5.12. Estimation of seismic displacement demands for the studied buildings in the x-direction

Model	Estimation of seismic displacement demand, $u_{Nx1}$ (m)					
	Soil Types	ZA	ZB	ZC	ZD	ZE
2-Story	Fixed base	0.0308	0.0320	0.0546	0.0547	0.0581
	SSI	0.0310	0.0322	0.0555	0.0613	0.0867
	Variation (%)	0.35	0.56	1.73	12.22	49.11
4-Story	Fixed base	0.0701	0.0681	0.1245	0.1435	0.1693
	SSI	0.0702	0.0684	0.1257	0.1505	0.2243
	Variation (%)	0.12	0.37	0.97	4.87	32.48
8-Story	Fixed base	0.1403	0.1401	0.2602	0.2974	0.3789
	SSI	0.1404	0.1406	0.2640	0.3202	0.4929
	Variation (%)	0.09	0.34	1.47	7.67	30.08

Table 5.13. Estimation of seismic displacement demands for the studied buildings in the y-direction

Model	Estimation of seismic displacement demand, $u_{Ny1}$ (m)					
	Soil Types	ZA	ZB	ZC	ZD	ZE
2-Story	Fixed base	0.0327	0.0330	0.0564	0.0561	0.0592
	SSI	0.0329	0.0331	0.0574	0.0627	0.0873
	Variation (%)	0.41	0.54	1.71	11.71	47.42
4-Story	Fixed base	0.0704	0.0705	0.1274	0.1498	0.1753
	SSI	0.0705	0.0706	0.1291	0.1596	0.2235
	Variation (%)	0.21	0.11	1.29	6.52	27.53
8-Story	Fixed base	0.1445	0.1430	0.2673	0.3072	0.3809
	SSI	0.1447	0.1433	0.2713	0.3236	0.4626
	Variation (%)	0.16	0.19	1.49	5.32	21.47

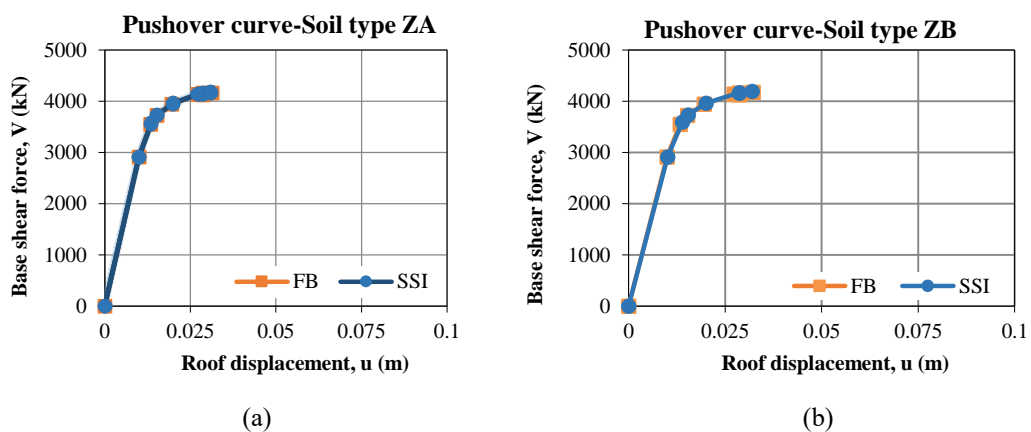
As it is apparent from Tables 5.12. and 5.13., the seismic displacement demands increases due to the inclusion of SSI into the analysis compared to the typical fixed base conditions of the same models. However, the changes are very little or almost negligible when the buildings are founded on stiffer soil profiles such as soil types ZA, ZB, and ZC. Whereas, it increases significantly as the ground conditions soften, which includes soil types ZD and ZE.

### 5.5.3. Effects of SSI on the capacity curves

In order to observe how the SSI will influence the overall behavior of the selected buildings, under the design earthquake (DD-2), they are pushed again up to the computed seismic displacement demands (i.e. performance points) given in Table 5.12 and Table 5.13 for x and y directions, respectively. For this purpose, the pushover curve also known as the capacity curve which is a representative of the global behavior of the buildings against a given seismic loads is constructed for all the models. For better visualization of the outputs, the capacity curves obtained for both compliance base (SSI) and fixed base (FB) states are plotted in the same graphs and are presented in the following subsections for 2, 4 and 8 story models.

#### 5.5.3.1. The SSI effects on the structural capacity in the x-direction

Figures 5.21 to 5.23 shows the changes in the pushover curves of the 2, 4 and 8 story buildings in the x-direction due to the SSI effects for different ground conditions. In all models, ignorable changes are observable for stiffer soil types meaning that the fixed base (FB) and flexible base assumptions provides similar results, while for unfavorable ground conditions (ZD and ZE) the difference between FB and flexible base conditions becomes more considerable, indicating that the buildings behaviors are significantly affected by the properties of the sub-soil. In addition, as the height of the building increases a reduction in the base shear force and an elongation in the roof displacement are visible for both FB and flexible conditions.



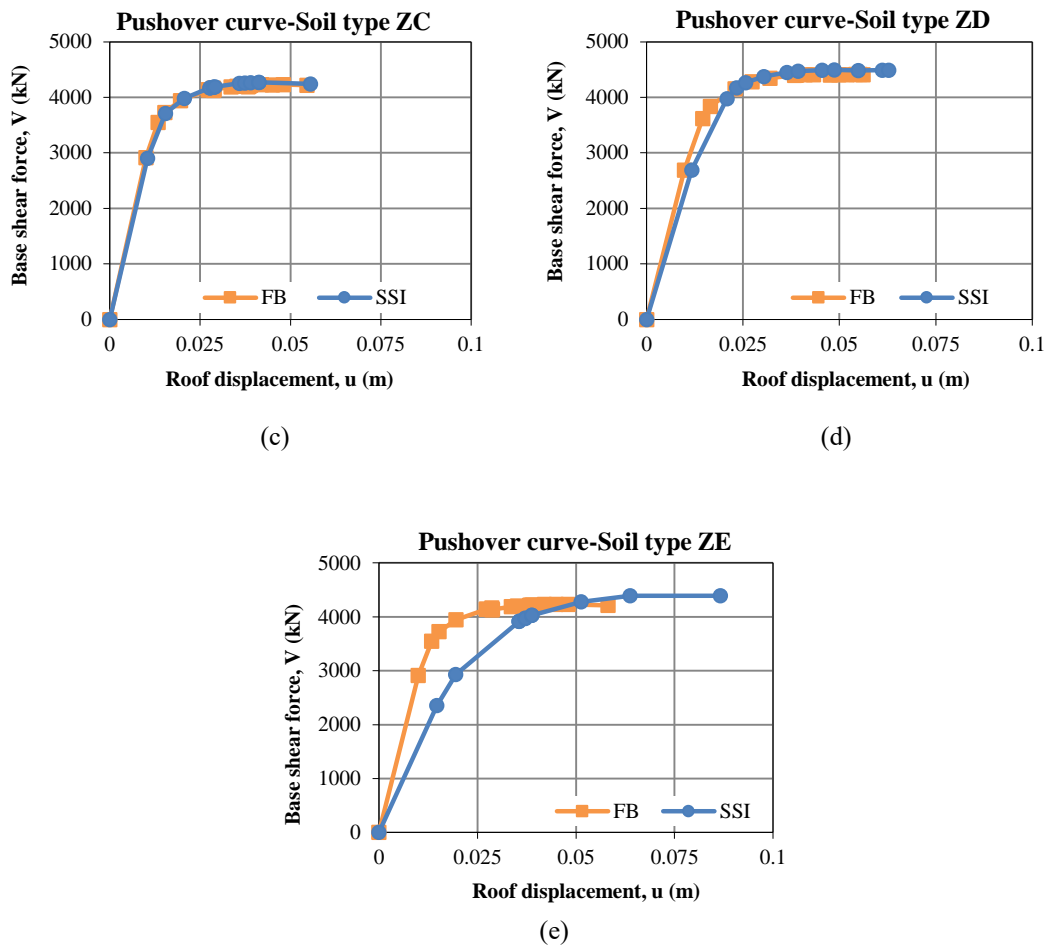
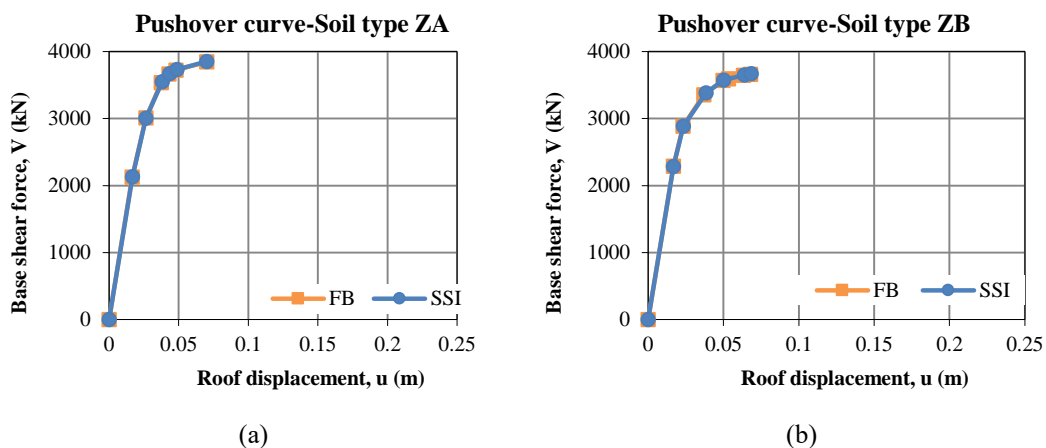


Figure 5.21. Pushover curves of the 2-Story model in the x-direction; comparison between FB and SSI conditions for different soil classes





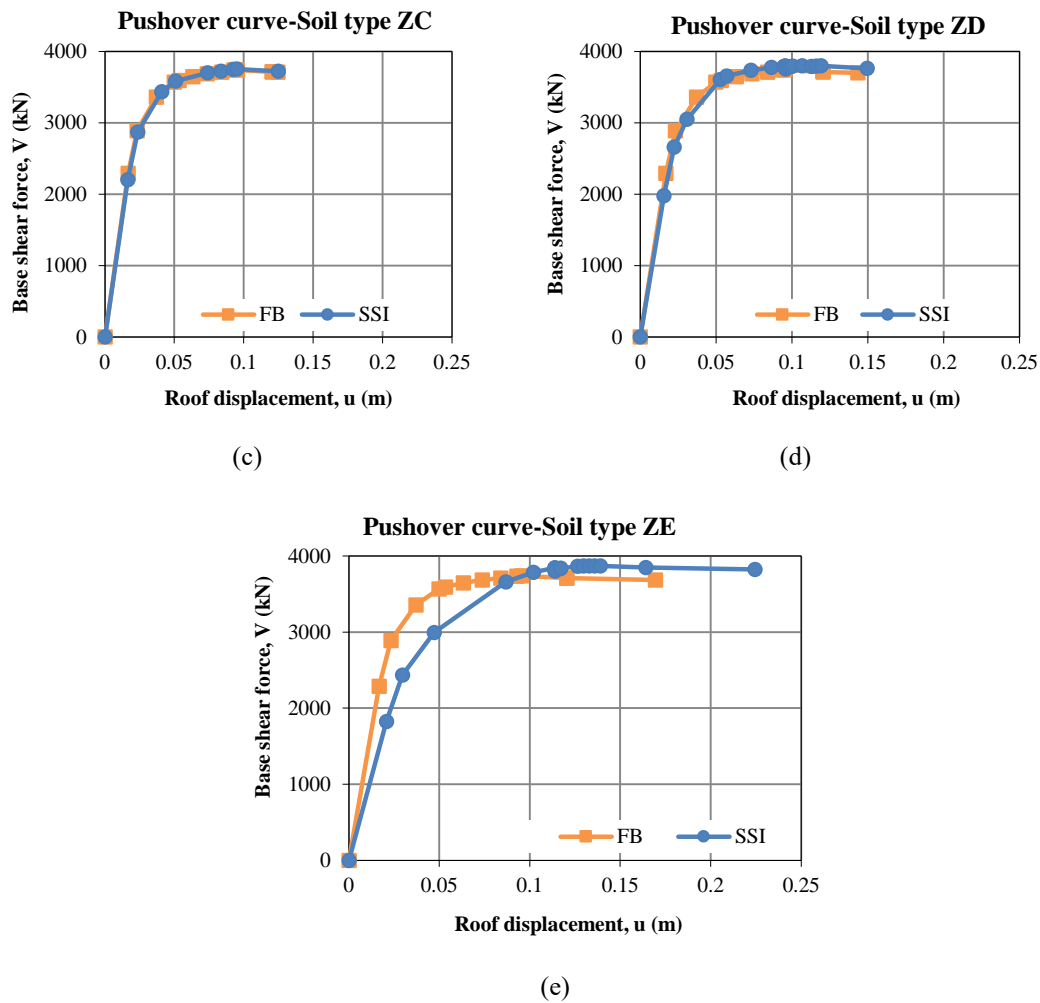
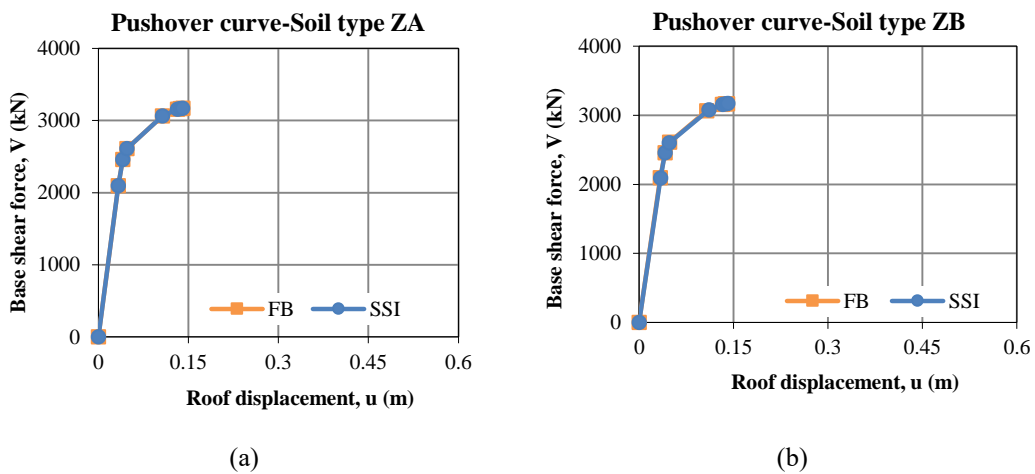


Figure 5.22. Pushover curves of the 4-Story model in the x-direction; comparison between FB and SSI conditions for different soil classes



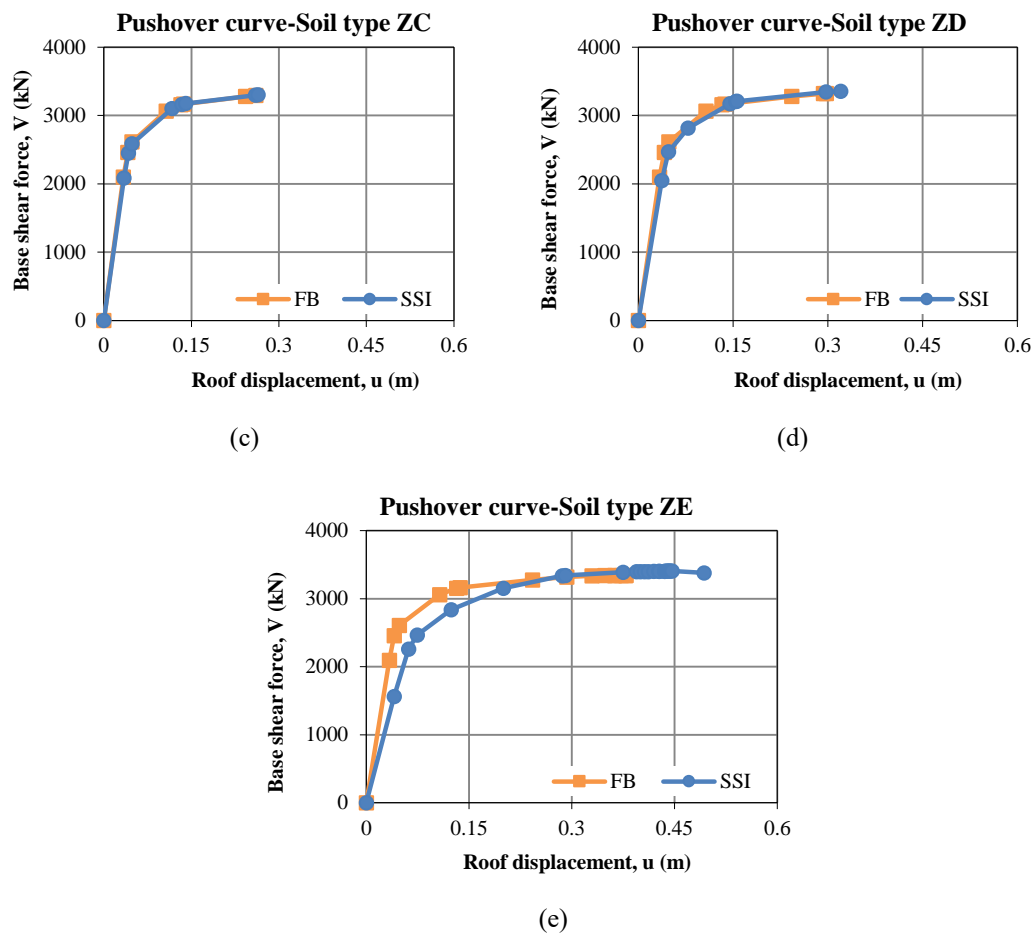


Figure 5.23. Pushover curves of the 8-Story model; comparison between FB and SSI conditions for different soil classes.

### 5.5.3.2. The SSI effects on the structural capacity in the y-direction

Since the studied buildings are symmetric in both x and y directions, similar results in the y-direction are obtained and are demonstrated in the following Figures for the 2, 4 and 8-story models. However, the developed seismic forces at the base of the buildings slightly show an increase when comparing to the results in the x-direction, this might be because the structures are defined stiffer in this direction. In other words, the number of lateral load resisting members in this direction is further.

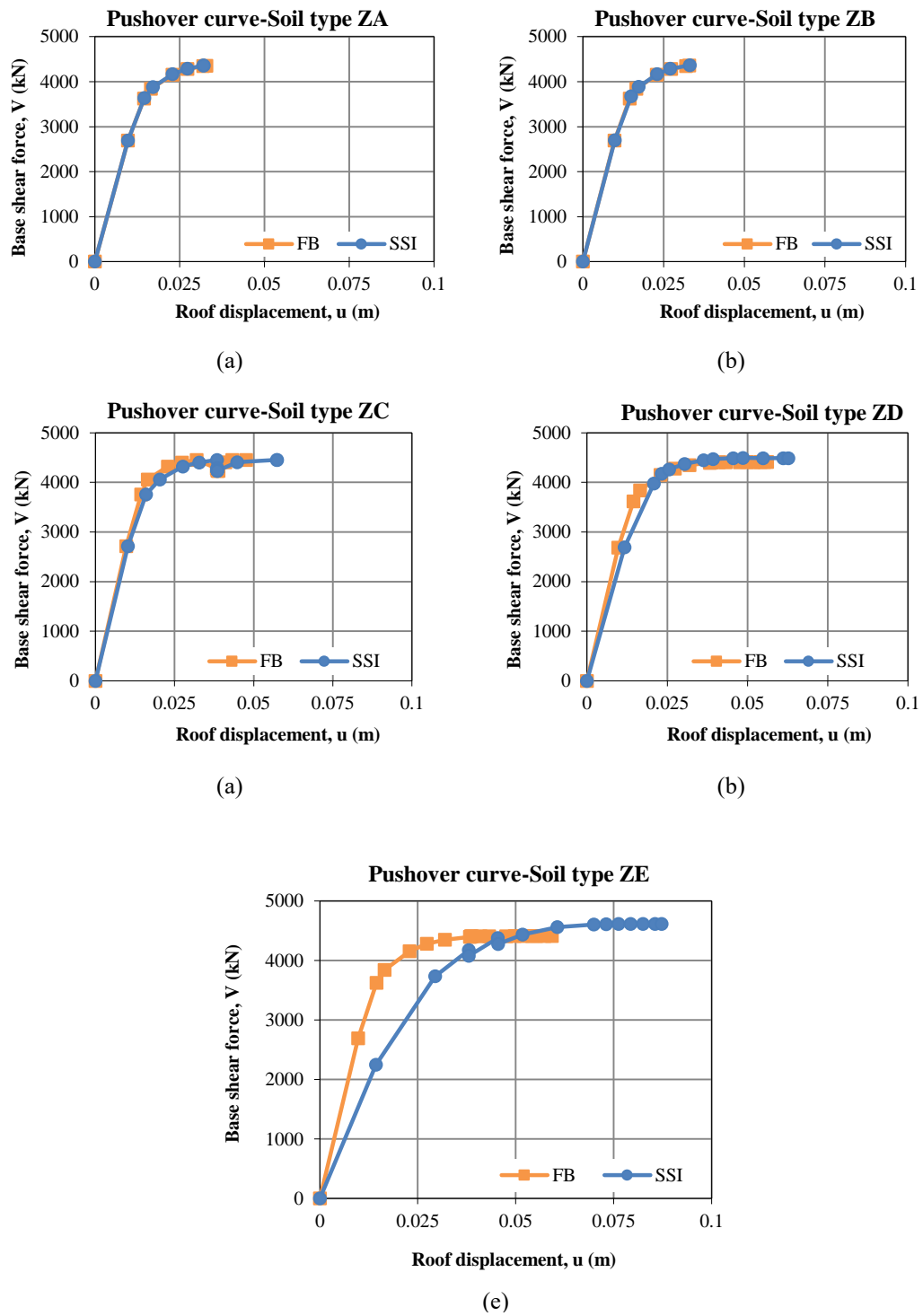


Figure 5.24. Pushover curves of the 2-Story models; comparison between FB and SSI conditions for different soil classes.

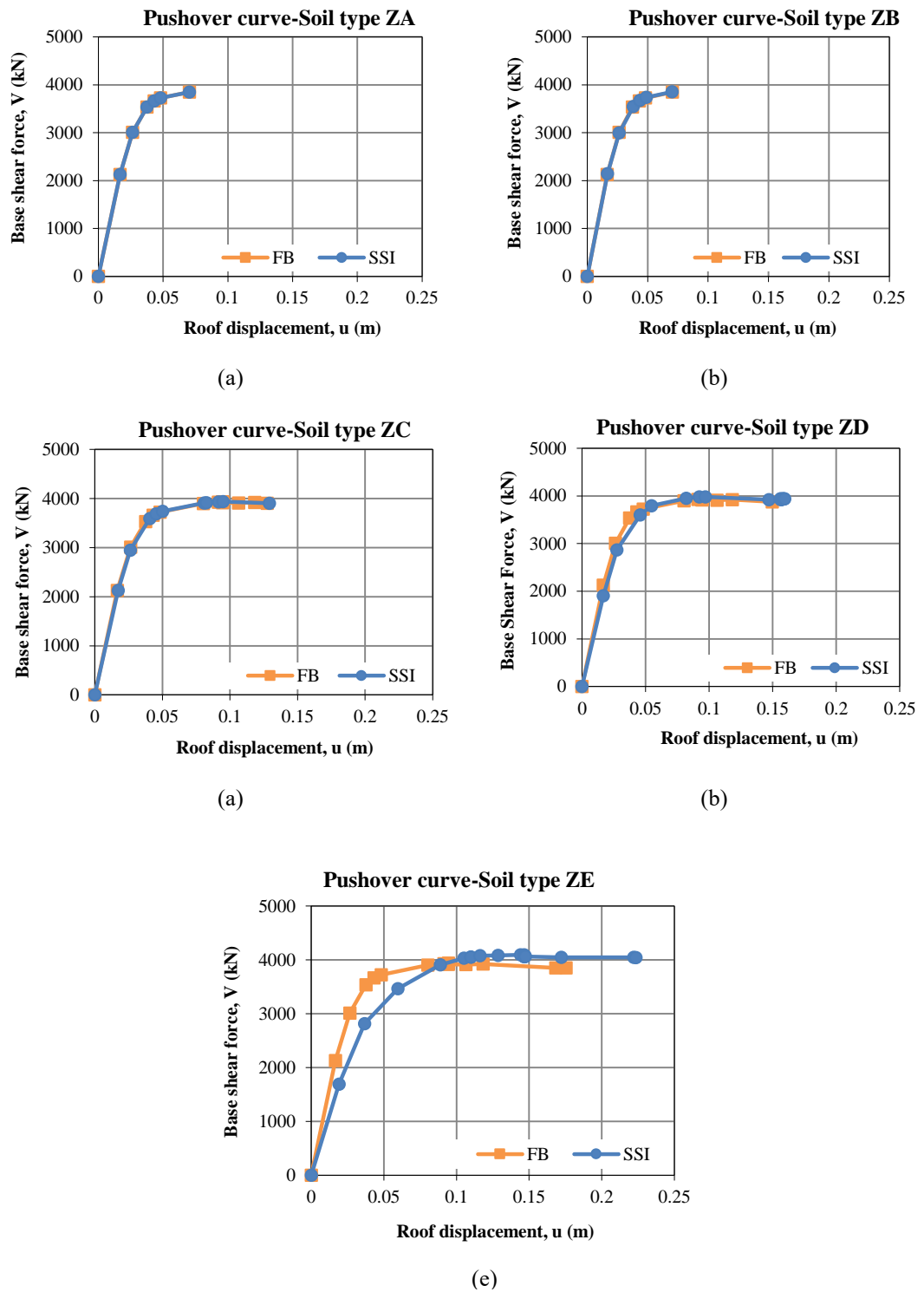


Figure 5.25. Pushover curves of the 2-Story models; comparison between FB and SSI conditions for different soil classes.

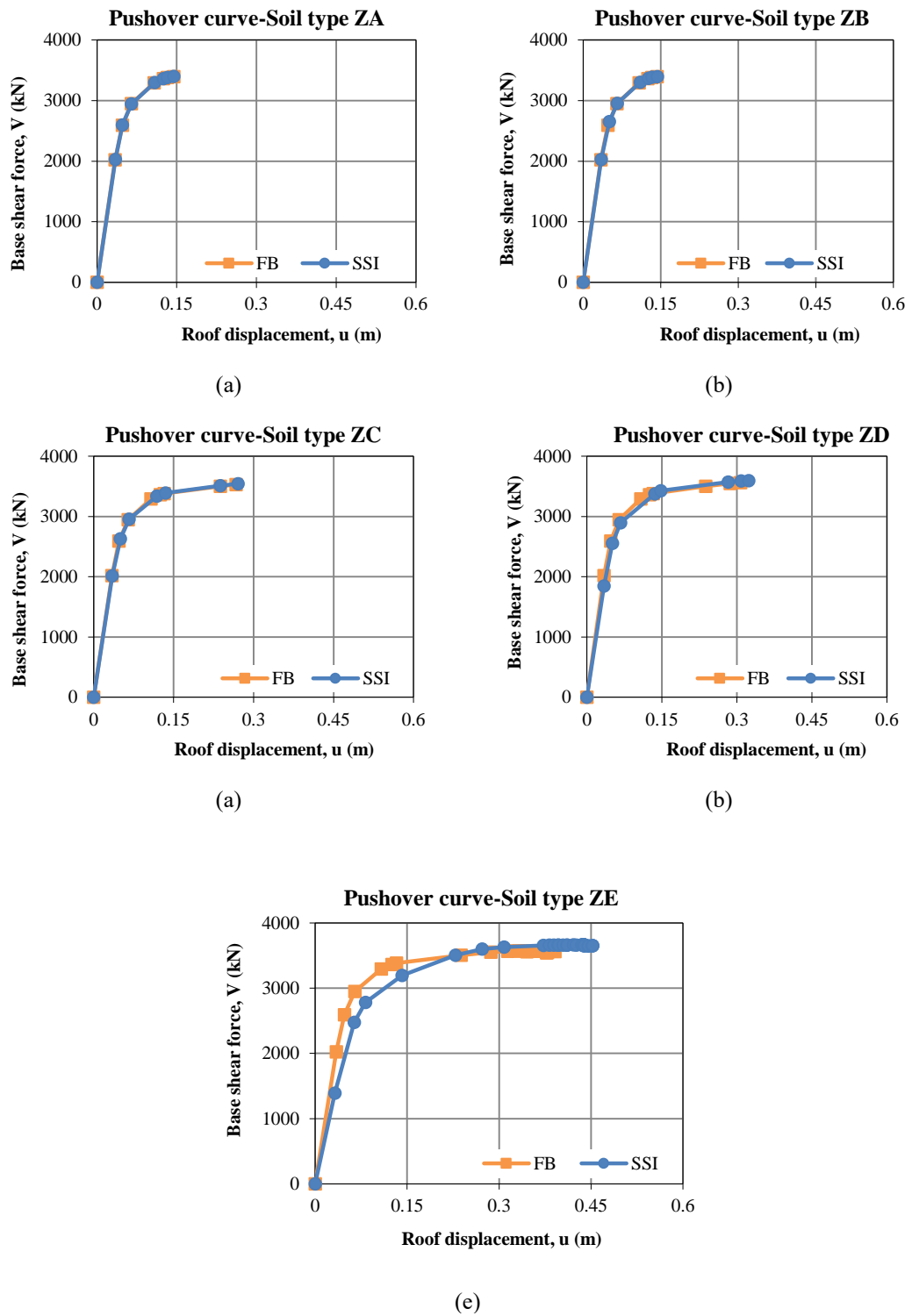


Figure 5.26. Pushover curves of the 8-Story models in the x-direction; comparison between FB and SSI conditions for different soil classes

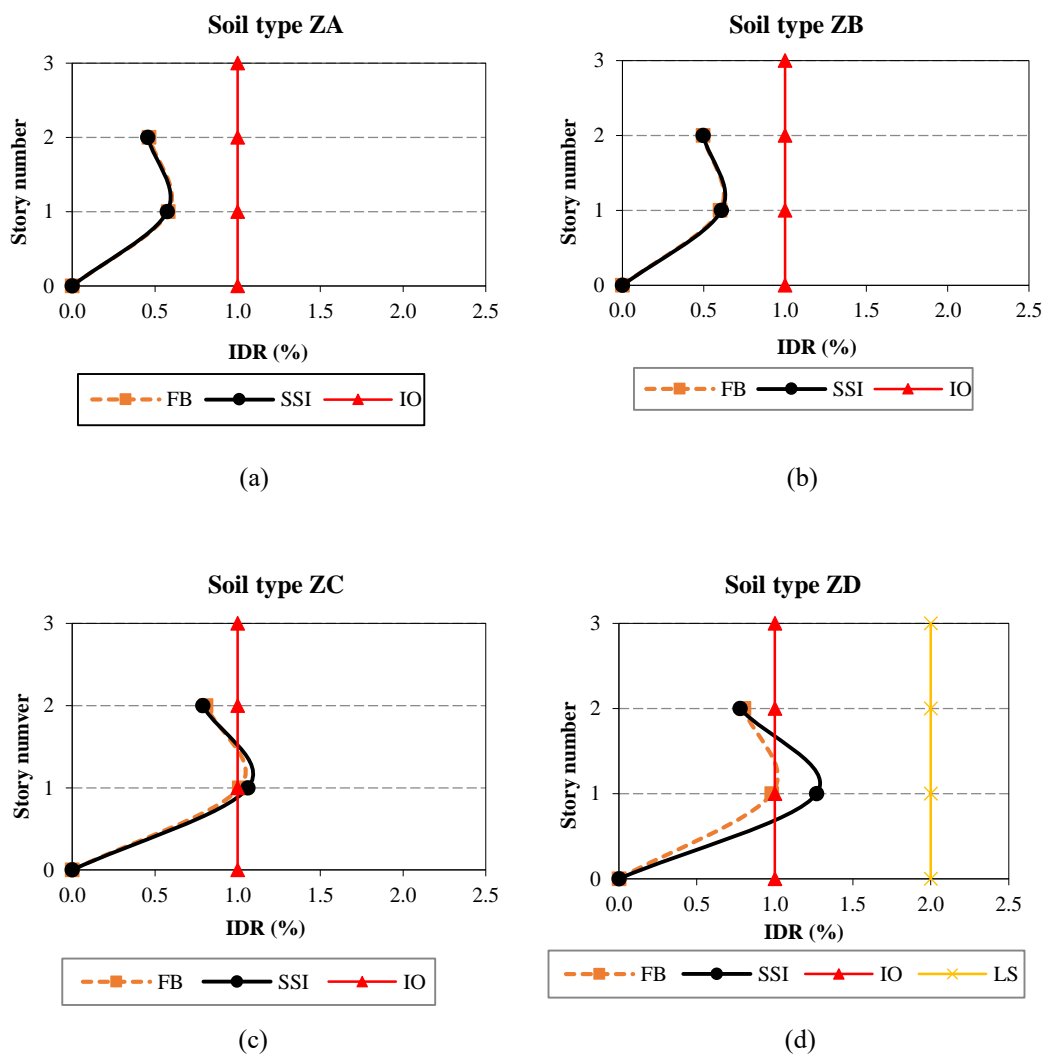
#### 5.5.4. Effects of SSI on the inter-story drift ratios

Inter-story drift ratios (IDR), corresponding to the performance points (Section 5.2), are calculated by dividing the difference in horizontal deflection of the two adjacent floors to the story height. These drift ratios are used to evaluate the global performance levels of the case studies. For this purpose, the computed maximum drift demands (IDR at the performance point) are compared to the drift limits given by FEMA-356 or ATC-40 (Chapter 2). Both standards define similar acceptance criteria for three discrete performance levels including Immediate Occupancy (IO), Live Safety (LS), and Collapse Prevention (CP) for a given type of structure. However, in ATC-40 the CP performance level is termed as Structural stability (SS), which are the same in terms of concepts. These performance levels along with their limit states are discussed in further detail in Chapter 2. In this section, the maximum inter-story drift limits contained in FEMA-356 are used for performance investigation. Based on this standard, the drift ratios corresponding to IO, LS, and CP performance levels, for RC moment-resisting frames, are 1, 2 and 4 percent, respectively.

Furthermore, based on the results of the 3D analysis of the selected RC moment-resisting frames, inter-story drifts of the buildings increases compared to their fixed base conditions when SSI is included in the analyses. However, the effects are observed very little almost ignorable for stiffer soil profiles (soil with shear wave velocities greater than 400 m/s), whereas, as the geotechnical conditions under the foundation changes to softer soil types (ZD and ZE) the SSI effects also getting more serious. For example, for soil type ZE and 2-story building the values of inter-story drifts ratios exceed LS performance limits due to the incorporation of SSI, while it was slightly beyond IO for the fixed base system (Figure 5.27e). In addition, as the height of the buildings (slenderness ratio,  $H/B$ ) increases the inter-story drifts also increase which means that SSI effects is more considerable for high rise buildings (Figures 5.27-5.32). The effects of SSI on IDR of 2, 4 and 8 story buildings are shown comparatively, considering various soil types under the foundation in the following sub-sections.

### 5.5.4.1. The SSI effects on the inter-story drift ratios (IDR) in the x-direction

Figure 5.26 shows the variation in the inter-story drift ratio due to the SSI effects for the two-story model in the x-direction. As it is apparent from the figures, the impacts of SSI becoming more important when the soil properties changes from soil type ZA to soil type ZE. For example, considering the variation in the IDR for soil profiles ZA and ZE. It is clearly shown that there is no difference between the fixed-base assumption and when SSI is included in the analysis for soil type ZA. On the other hand, for soil type ZE significant change can be seen such that the performance level of the building changes from IO to LS when SSI effects are considered.



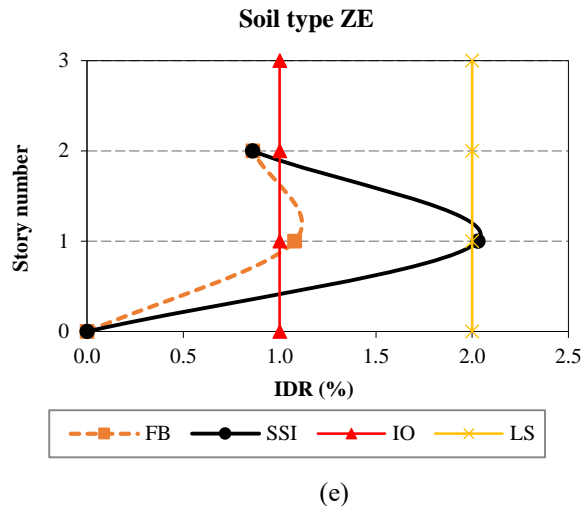
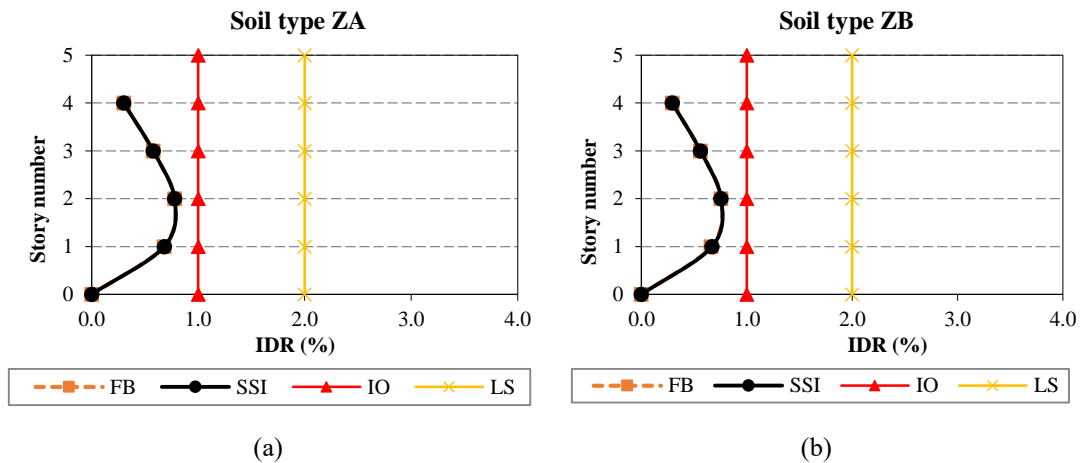


Figure 5.27. Inter-story drift ratios for the 2-Story models; comparison between FB and SSI conditions for different soil classes

The variation in the IDR due to the SSI effects for the 4-story model is presented in Figure 5.28. As can be seen from the figures, the changes are ignorable when stiffer soil profiles (ZA, ZB, and ZC) are considered under the foundation, while it significantly magnifies when the building is founded on less favorable geological conditions, specifically soil type ZE. The IDR intensifies at the first-floor level, where for soil type ZE it exceeds the IO performance limits and extends between LS and CP performance levels. This might be one of the reasons that most of the buildings when struck by strong ground motions, collapse from the failure of their ground floor columns or column-beam connections on the first floor.





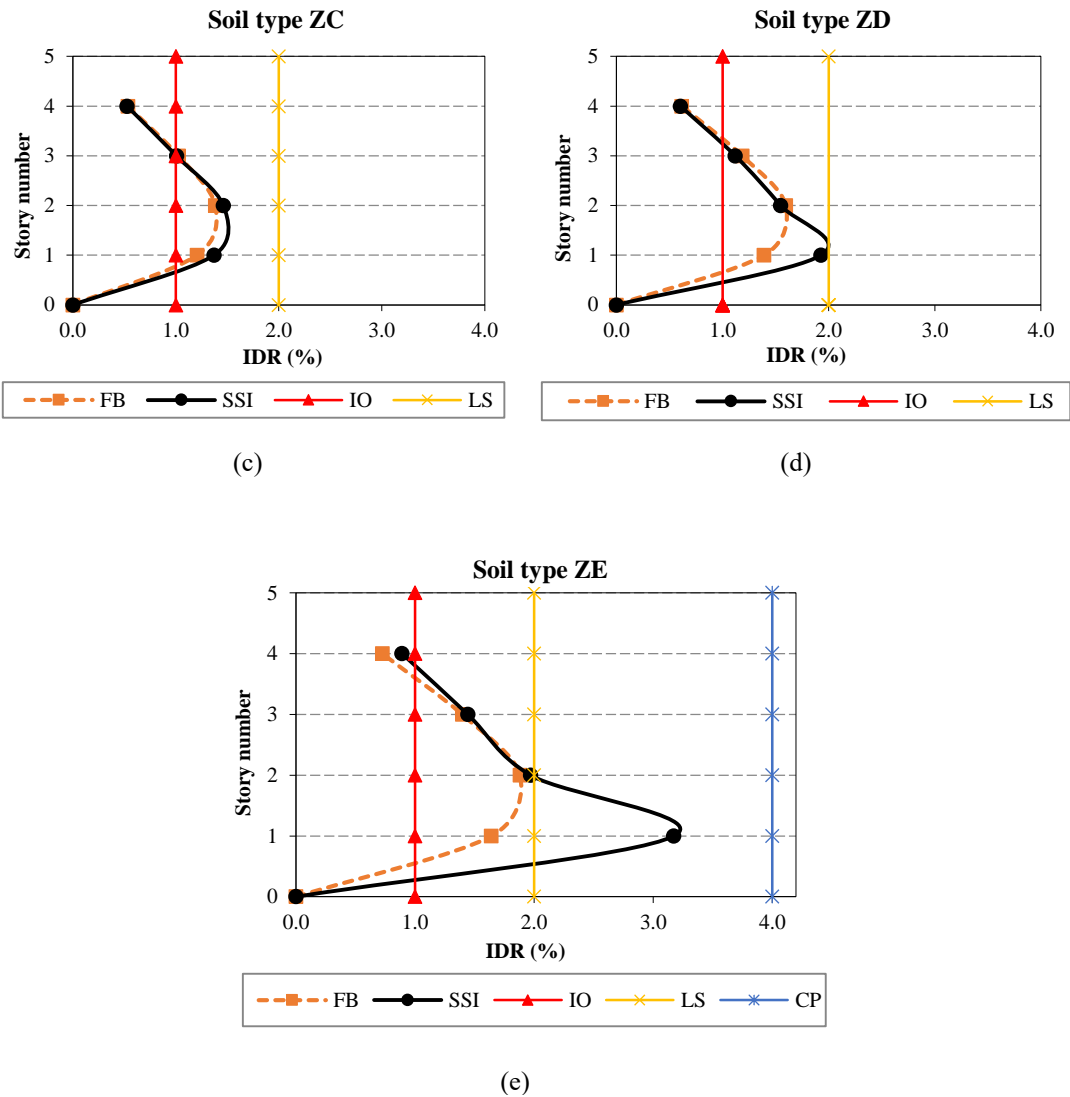


Figure 5.28. Inter-story drift ratios for the 4-Story models; comparison between FB and SSI conditions for different soil classes

Figure 5.29. shows the changes in IDR due to the SSI effects for the 8-story building. In this model like 2 and 4-story models, the SSI does not affect the building performances at all or it is negligible when soil type ZA, ZB and ZC are considered. On the other hand, for soil type ZD the performance level changed from IO to LS (Figure 5.29d) when the SSI effects included in the analysis. Furthermore, for soil type ZE, the IDR exceeds the CP performance limit, while it was just behind the LS

performance level for the fixed base condition. This indicates that the influence of SSI is getting substantial when the building height increases.

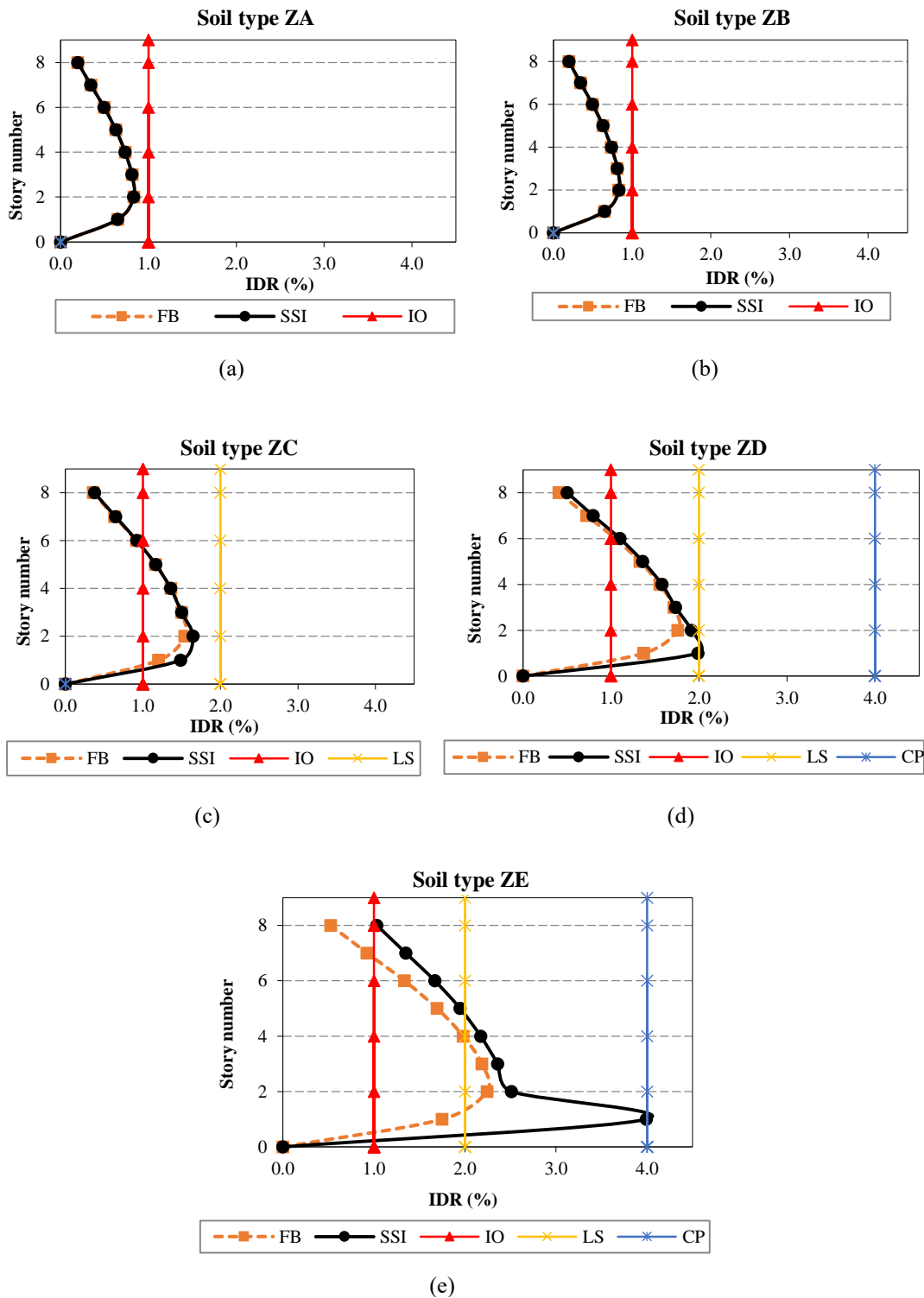
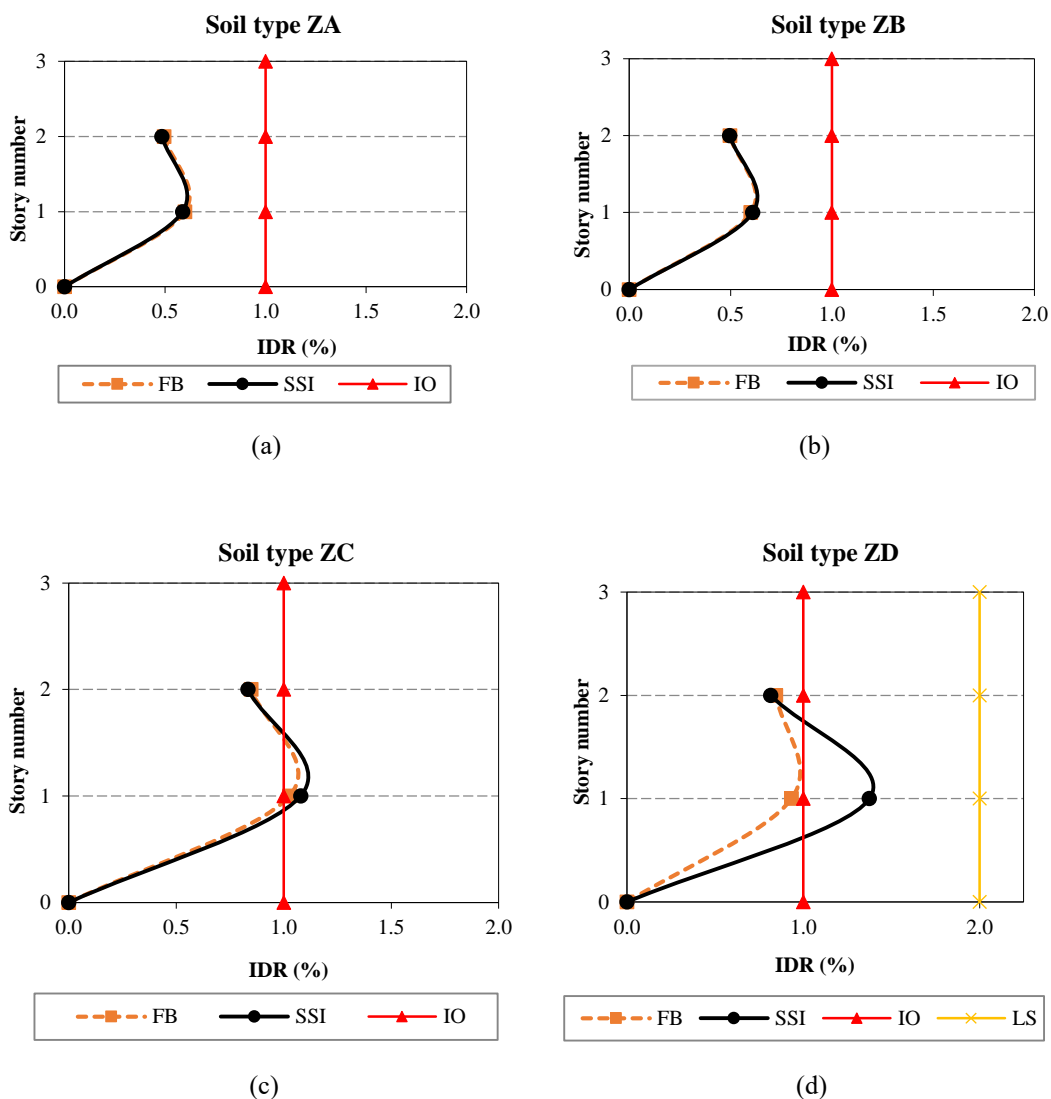


Figure 5.29. Inter-story drift ratios for the 8-Story models; comparison between FB and SSI conditions for different soil classes

5.5.4.2. The SSI effects on the inter-story drift ratios (IDR) in the y-direction

Figure 5.30 shows the variation in IDR for the 2-story model in the y-direction. Since the buildings are symmetric in both x and y directions there are no considerable changes in the results for the two directions. Therefore, the comments and explanations that are given for the x-direction are also can be made in the y-direction.



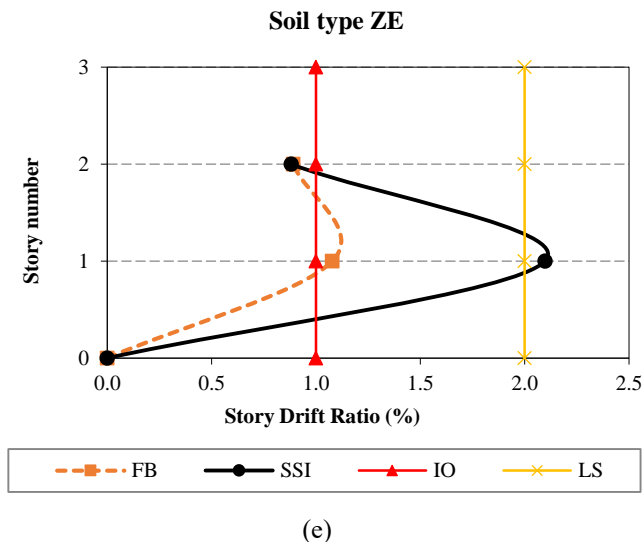
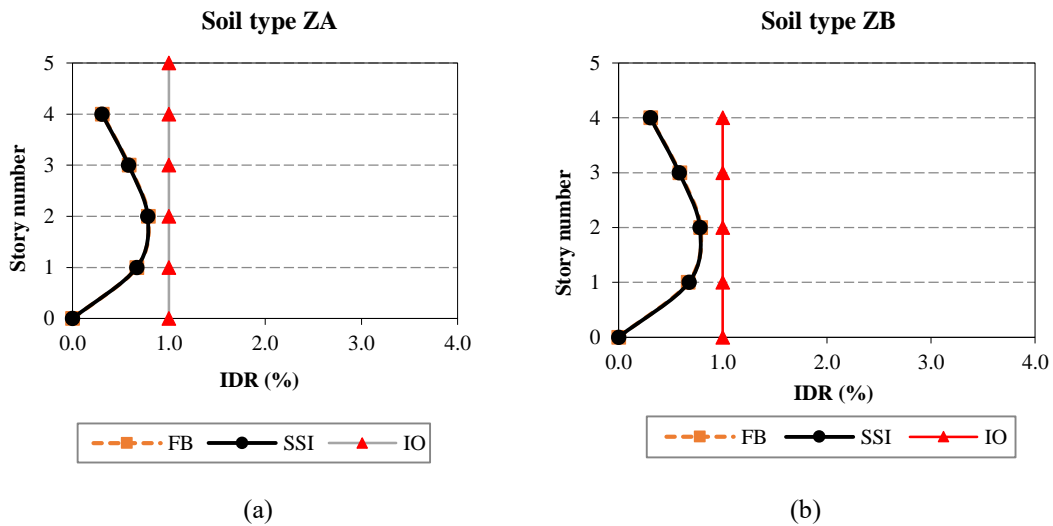


Figure 5.30. Inter-story drift ratios for the 2-Story models; comparison between FB and SSI conditions for different soil classes

The variation in IDR and consequently performance levels resulted from the influence of SSI for the 4-story model is demonstrated in Figure 5.31.



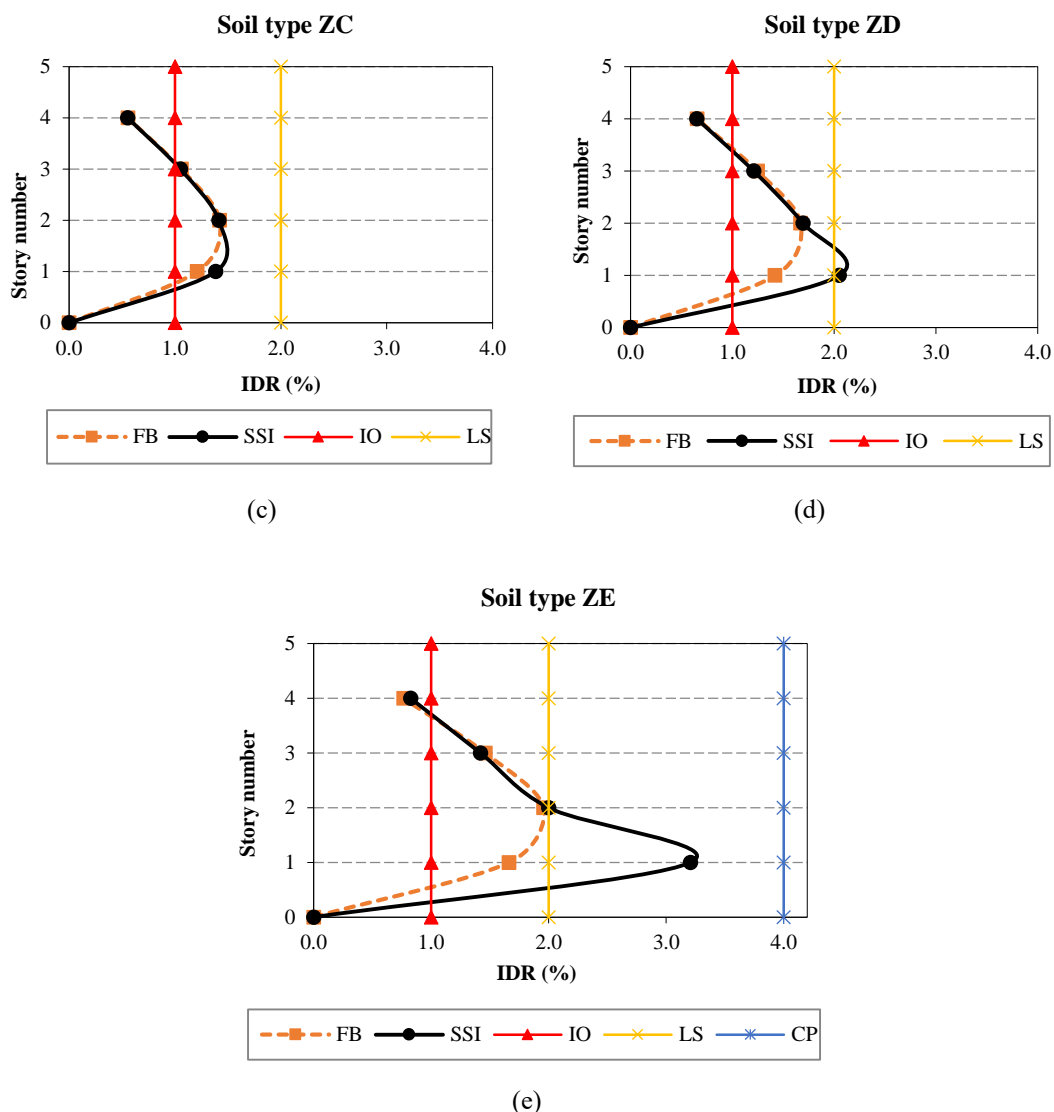


Figure 5.31. Inter-story drift ratios for the 4-Story models; comparison between FB and SSI conditions for different soil classes

Similarly, the changes in performance levels for the 8-story model in the y-direction due to the influence of SSI are illustrated in Figure 5.32. As it is evident from the figures, the changes in IDR when the building is founded on soil types ZD and ZE are considerable, especially intensified on the first-floor level. It causes to change the global performance level of the building from IO to LS for soil type ZD (Figure 5.32d) and from LS to CP for soil type ZE (Figure 5.32e) when compared to the same model when fixed at their basis. For other soil layers the changes are ignorable (Figures 5.32a-5.32c).

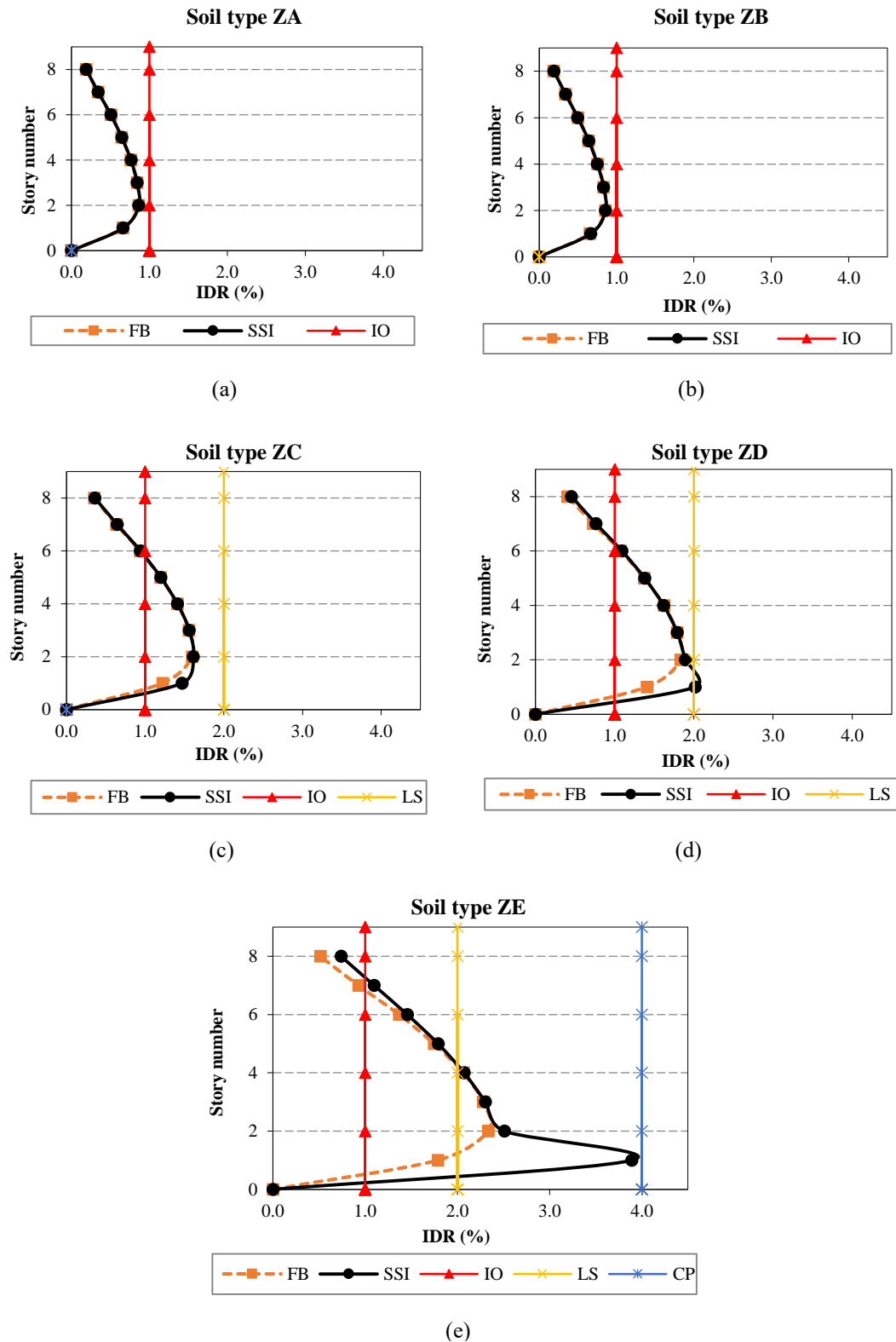


Figure 5.32. Inter-story drift ratios for the 8-Story models; comparison between FB and SSI conditions for different soil classes

### 5.5.5. Effects of SSI on the damage states of structural elements

The demands in plastic rotation at the ground floor columns are designated as a measurement tool to evaluate the SSI effects on the structural components. The rotation demands corresponding to the target displacement (Table 5.10 and 5.11) for all buildings including fixed base and compliance base conditions are determined, for both x and y directions, as a result of single mode pushover analysis. For simplicity, the columns located along the 3-3 axis and A-A axis (Figure 5.33) are selected to represent the results in x and y-directions, respectively.

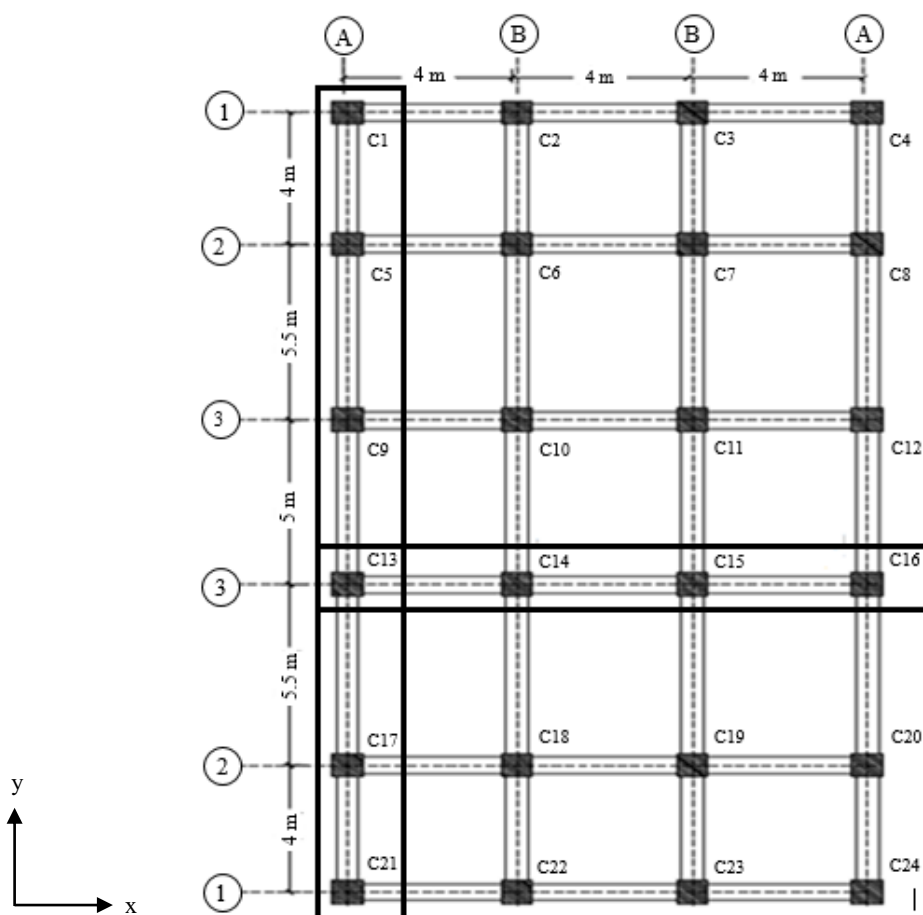


Figure 5.33. Selected columns in the ground floor for performance investigation

Depending on the geotechnical conditions and the height of the structures, the SSI elongates vibration period of all RC frame models founded on different kind of soil profiles with respect to the fixed base conditions. However this increase is more observable for soft soil profiles and for higher structures (Tables 5.8 and 5.9).

Consequently, the seismic displacement demands also increases (Tables 5.10 and 5.11) which may lead to redistribution of internal forces, especially for soft soil profile. The redistribution of internal forces in turn changes the plastic hinge formation in the frame elements which may reduce or increase the plastic rotations and accordingly the performance levels in some particular elements. The variation in plastic rotations of the selected columns in the ground floors due to the SSI effects for 2, 4 and 8 story models are presented in Tables 5.14, 5.15 and 5.16, respectively, for the analyses in the x-direction.

Table 5.14. The changes in plastic rotation demands obtained from SAP2000 for the 2-story model

Soil types	Foundation condition	Plastic rotation corresponding to the performance point, radians			
		C13	C14	C15	C16
ZA	Fixed	0.003364	0.00869	0.004094	0.004073
	Flexible	0.00336	0.00869	0.00409	0.00407
ZB	Fixed	0.003364	0.00869	0.004094	0.004073
	Flexible	0.00336	0.00869	0.00409	0.00407
ZC	Fixed	0.00763	0.00743	0.00896	0.00833
	Flexible	0.00784	0.00979	0.00980	0.00830
ZD	Fixed	0.00776	0.00908	0.00907	0.00756
	Flexible	0.00921	0.00825	0.00815	0.00759
ZE	Fixed	0.00838	0.01053	0.01051	0.00897
	Flexible	0.03801	0.00426	0.00416	0.01098

Table 5.15. The changes in plastic rotation demands obtained from SAP2000 for the 4-story model

Soil types	Foundation condition	Plastic rotation corresponding to the performance point, radians			
		C13	C14	C15	C16
ZA	Fixed	0.00386	0.00294	0.00454	0.00454
	Flexible	0.00397	0.00293	0.00451	0.00451
ZB	Fixed	0.00358	0.00265	0.00425	0.00425
	Flexible	0.00261	0.00357	0.00412	0.00418
ZC	Fixed	0.01060	0.01416	0.01411	0.01261
	Flexible	0.01048	0.01226	0.01222	0.01295
ZD	Fixed	0.01279	0.01578	0.01570	0.01407
	Flexible	0.01293	0.01622	0.01617	0.01471
ZE	Fixed	0.01588	0.02040	0.02035	0.01906
	Flexible	0.01934	0.02364	0.01523	0.01939



Table 5.16. The changes in plastic rotation demands obtained from SAP2000 for the 8-story model

Soil types	Foundation condition	Plastic rotation corresponding to the performance point, radians			
		C13	C14	C15	C16
ZA	Fixed	0.00097	0.00189	0.00186	0.00090
	Flexible	0.00091	0.00177	0.00171	0.00083
ZB	Fixed	0.00096	0.00189	0.00184	0.00088
	Flexible	0.00092	0.00180	0.00170	0.00085
ZC	Fixed	0.01215	0.01305	0.01300	0.01199
	Flexible	0.01230	0.01289	0.01289	0.01215
ZD	Fixed	0.01562	0.01655	0.01646	0.01544
	Flexible	0.01650	0.01590	0.01580	0.01630
ZE	Fixed	0.02260	0.02740	0.02730	0.02660
	Flexible	0.02660	0.02130	0.02080	0.02670

Based on the results presented in the above tables, as the ground condition changes the damage levels of the columns (plastic rotations) also changes. The variation is very little for stiffer soil profiles, soil types ZA, ZB and ZC, whereas it is more serious when the buildings are founded on less favorable ground conditions, soil types ZD and ZE. There is increase in plastic rotations in external columns (C13 and C14) while mostly it decreases in internal columns (C14 and C15) for flexible base models as compared to the same model fixed at their bases. This is because the SSI causes the redistribution of internal forces such as bending moments and axial forces which amplify it for the external columns and reduce it for the internal columns. In addition, when the building height increases the amount of plastic deformation demands also increases.

In order to quantify the damage level of the columns, the calculated plastic rotation demands at each columns are compared to the corresponding rotation capacities, which is defined for different performance levels. For this purpose, the acceptance criteria provided by TEC-2018, summarized in Chapter 2, is used. Accordingly, the damage limits of the reference columns for different performance levels are computed and are presented in Table 5.17.

Table 5.17. Column plastic rotation limits, calculated based on TEC-2018

Columns	hinge length (m)	Shear span (m)	Main bar size (mm)	Curvatures		Plastic rotation limits (radians)		
				$\Phi_y$ (1/m)	$\Phi_u$ (1/m)	GÖ	KH	SH
C13	0.20	1.50	16	0.0105	0.1426	0.0233	0.0175	0.00
C14	0.25	1.50	16	0.0081	0.1078	0.0204	0.0153	0.00
C15	0.25	1.50	16	0.0081	0.1078	0.0204	0.0153	0.00
C16	0.20	1.50	16	0.0105	0.1426	0.0233	0.0175	0.00

Table 5.17. shows the selected columns damage limits, which is calculated based on the cross section dimensions and material properties. First the curvature analysis for every cross section is performed with the help of XTRACT program to compute the ultimate curvature,  $\Phi_u$ , and yield curvature,  $\Phi_y$ . After determining the values of ultimate and yield curvature corresponding to the collapse prevention damage level of the elements, the rotational deformation capacities matching to this damage level is computed using Equation (2.6). Similarly, the limit states for damage control (KH) and limited damage (SH) performance levels are calculated using Equations (2.8) and (2.10), respectively.

The values of plastic rotations for each individual columns (Tables 5.14-5.16) are compared to the corresponding element damage capacities given in Table 5.17. Based on this process, the columns with no plastic rotation falls within the Limited Damage (LD) performance range, if the values of plastic rotations extends between SH and KH limit states, it means that the elements are within the Moderate Damage (MD) region. In the same way, the elements suffers Sever Damage (SD) if the values of plastic rotation falls between KH and GÖ performance levels. Finally, if the amount of plastic rotations in the columns exceeds GÖ limit state, they are categorized to fall in the "collapse damage range", where significant damage has occurred and it may not be reparable. Using this methodology, the damage states of each columns are specified and are demonstrated in Tables 5.18, 5.19 and 5.20 for 2, 4 and 8 story models, respectively.

Table 5.18. Selected columns damage levels for the 2-story model

Soil types	Foundation condition	Column performance levels			
		C13	C14	C15	C16
ZA	Fixed	MD	MD	MD	MD
	Flexible	MD	MD	MD	MD
ZB	Fixed	MD	MD	MD	MD
	Flexible	MD	MD	MD	MD
ZC	Fixed	MD	MD	MD	MD
	Flexible	MD	MD	MD	MD
ZD	Fixed	MD	MD	MD	MD
	Flexible	MD	MD	MD	MD
ZE	Fixed	MD	MD	MD	MD
	Flexible	Collapse	MD	MD	MD

Table 5.19. Selected columns damage levels for the 4-story model

Soil types	Foundation condition	Column performance levels			
		C13	C14	C15	C16
ZA	Fixed	MD	MD	MD	MD
	Flexible	MD	MD	MD	MD
ZB	Fixed	MD	MD	MD	MD
	Flexible	MD	MD	MD	MD
ZC	Fixed	MD	MD	MD	MD
	Flexible	MD	MD	MD	MD
ZD	Fixed	MD	SD	SD	MD
	Flexible	MD	SD	SD	MD
ZE	Fixed	MD	Collapse	SD	SD
	Flexible	SD	Collapse	MD	SD

Table 5.20. Selected columns damage levels for the 8-story model

Soil types	Foundation condition	Column performance levels			
		C13	C14	C15	C16
ZA	Fixed	MD	MD	MD	MD
	Flexible	MD	MD	MD	MD
ZB	Fixed	MD	MD	MD	MD
	Flexible	MD	MD	MD	MD
ZC	Fixed	MD	MD	MD	MD
	Flexible	MD	MD	MD	MD
ZD	Fixed	MD	SD	SD	MD
	Flexible	MD	SD	SD	MD
ZE	Fixed	SD	Collapse	Collapse	Collapse
	Flexible	Collapse	Collapse	Collapse	Collapse

As it is evident from the above tables, the performance levels of the selected columns does not affected by the SSI when the structures are founded on stiffer soil profiles (soil types ZA, ZB and ZC). However, when the geotechnical condition changes to soil types ZD and ZE, the damage levels of the columns also changes from moderate damage to severe damages, and in some cases they falls in the collapse range.

Similar procedure have been performed for the y-direction and the SSI effects are studied by tracking the plastic rotation demands of the ground floor columns located along the axis A-A (Figure 5.33). The obtained results for the 2, 4 and 8 story buildings are presented in Tables 5.21, 5.22 and 5.23, respectively.

Table 5.21. The variation in plastic rotation demands, obtained from SAP2000 for the 2-story model

Soil types	Foundation condition	Plastic rotation corresponding to the performance point, radians					
		C1	C5	C9	C13	C17	C21
ZA	Fixed	0.00448	0.00388	0.00443	0.00445	0.00457	0.00307
	Flexible	0.00450	0.00371	0.00425	0.00427	0.00439	0.00314
ZB	Fixed	0.00450	0.00390	0.00445	0.00447	0.00459	0.00309
	Flexible	0.00451	0.00388	0.00435	0.00438	0.00450	0.00336
ZC	Fixed	0.00856	0.00833	0.00853	0.00845	0.00866	0.00785
	Flexible	0.00861	0.01040	0.01051	0.01036	0.01060	0.00964
ZD	Fixed	0.00856	0.00833	0.00848	0.00841	0.00862	0.00785
	Flexible	0.01354	0.01148	0.01462	0.01471	0.01470	0.00913
ZE	Fixed	0.00915	0.00968	0.00984	0.00975	0.01013	0.00911
	Flexible	0.01042	0.00836	0.00872	0.00854	0.03337	0.00813

Table 5.22. The variation in plastic rotation demands, obtained from SAP2000 for the 4-story model

Soil types	Foundation condition	Plastic rotation corresponding to the performance point, radians					
		C1	C5	C9	C13	C17	C21
ZA	Fixed	0.00476	0.00442	0.00467	0.00467	0.00492	0.00329
	Flexible	0.00460	0.00431	0.00452	0.00453	0.00479	0.00318
ZB	Fixed	0.00477	0.00443	0.00468	0.00468	0.00493	0.00330
	Flexible	0.00459	0.00436	0.00451	0.00452	0.00478	0.00320
ZC	Fixed	0.01212	0.01351	0.02227	0.02215	0.01392	0.01297
	Flexible	0.01210	0.02264	0.022224	0.02321	0.01796	0.01526
ZD	Fixed	0.01472	0.01660	0.02144	0.02144	0.01674	0.01589
	Flexible	0.01514	0.01683	0.03231	0.03203	0.03168	0.01614
ZE	Fixed	0.01775	0.02008	0.02200	0.02190	0.02010	0.01931
	Flexible	0.01945	0.04196	0.04182	0.04165	0.04233	0.03950

Table 5.23. The variation in plastic rotation demands, obtained from SAP2000 for the 8-story model

Soil types	Foundation condition	Plastic rotation corresponding to the performance point, radians					
		C1	C5	C9	C13	C17	C21
ZA	Fixed	0.00274	0.00177	0.00186	0.00171	0.00211	0.00122
	Flexible	0.00283	0.00182	0.00181	0.00176	0.00209	0.00123
ZB	Fixed	0.00284	0.00177	0.00186	0.00177	0.00213	0.00132
	Flexible	0.00280	0.00172	0.00180	0.00175	0.00201	0.00121
ZC	Fixed	0.01497	0.01375	0.013833	0.01375	0.01411	0.01334
	Flexible	0.01501	0.01378	0.01387	0.01381	0.01409	0.01340
ZD	Fixed	0.01765	0.02584	0.02549	0.02552	0.01678	0.02467
	Flexible	0.01884	0.02260	0.02680	0.02670	0.02670	0.02590
ZE	Fixed	0.02586	0.03127	0.03271	0.03233	0.02507	0.03037
	Flexible	0.02603	0.03506	0.03501	0.03510	0.03516	0.03379

The damage levels of the columns in the y-direction are also specified by comparing the values of plastic rotations presented in the above tables with their corresponding damage limits. In this respect, since all of the columns located along the axis A-A have the same cross-section properties as of C13 and C16, in Table 5.17, their performance limits are also equivalent. Therefore, the acceptance criteria for column C13, which is quantified for three different performance levels, are used to identify the performance levels of reference columns in the y-direction. Accordingly, the damage states of each column are specified and are demonstrated in the following tables.

Table 5.24. Damage levels of the reference columns in the y-direction for the 2-story model

Soil types	Foundation condition	Column performance levels					
		C1	C5	C9	C13	C17	C21
ZA	Fixed	MD	MD	MD	MD	MD	MD
	Flexible	MD	MD	MD	MD	MD	MD
ZB	Fixed	MD	MD	MD	MD	MD	MD
	Flexible	MD	MD	MD	MD	MD	MD
ZC	Fixed	MD	MD	MD	MD	MD	MD
	Flexible	MD	MD	MD	MD	MD	MD
ZD	Fixed	MD	MD	MD	MD	MD	MD
	Flexible	MD	MD	MD	MD	MD	MD
ZE	Fixed	MD	MD	MD	MD	MD	MD
	Flexible	MD	MD	MD	MD	Collapse	MD

Table 5.25. Damage levels of the reference columns in the y-direction for the 4-story model

Soil types	Foundation condition	Column performance levels					
		C1	C5	C9	C13	C17	C21
ZA	Fixed	MD	MD	MD	MD	MD	MD
	Flexible	MD	MD	MD	MD	MD	MD
ZB	Fixed	MD	MD	MD	MD	MD	MD
	Flexible	MD	MD	MD	MD	MD	MD
ZC	Fixed	MD	MD	SD	SD	MD	MD
	Flexible	MD	SD	SD	SD	SD	MD
ZD	Fixed	MD	MD	SD	SD	MD	MD
	Flexible	MD	MD	Collapse	Collapse	Collapse	MD
ZE	Fixed	SD	SD	SD	SD	SD	SD
	Flexible	SD	Collapse	Collapse	Collapse	Collapse	Collapse

Table 5.26. Damage levels of the reference columns in the y-direction for the 8-story model

Soil types	Foundation condition	Column performance levels					
		C1	C5	C9	C13	C17	C21
ZA	Fixed	MD	MD	MD	MD	MD	MD
	Flexible	MD	MD	MD	MD	MD	MD
ZB	Fixed	MD	MD	MD	MD	MD	MD
	Flexible	MD	MD	MD	MD	MD	MD
ZC	Fixed	MD	MD	MD	MD	MD	MD
	Flexible	MD	MD	MD	MD	MD	MD
ZD	Fixed	SD	Collapse	Collapse	Collapse	MD	Collapse
	Flexible	SD	SD	Collapse	Collapse	Collapse	Collapse
ZE	Fixed	Collapse	Collapse	Collapse	Collapse	Collapse	Collapse
	Flexible	Collapse	Collapse	Collapse	Collapse	Collapse	Collapse

Tables 5.24 to 5.26 shows the variation in performance levels of the reference columns in the y-direction. It can be seen from the result that the SSI effects are more significant for the buildings which are constructed on the softer soil profiles (soil types ZD and ZE). Similar to the results in the x-direction no changes have been occurred when the buildings are founded on the stiffer soil-medium (ZA and ZB).

In addition, based on the analysis results in both x and y-directions, the damage levels of some particular component may increase or decrease due to the SSI effects. However, when studying the damage states of more elements it can be clearly understood that the plastic rotations in most of them increases and accordingly the

overall damages occurred in the system increases, compared to the fixed base condition.

Furthermore, as also mentioned earlier the incorporation of the SSI into the analysis results in the redistribution of the internal forces which in turn changes the plastic hinge formation in the buildings. As an example, the plastic hinge formation corresponding to the last step of pushover analysis, for the axis 3-3 with considering soil type ZE, is illustrated in Figure 5.34.

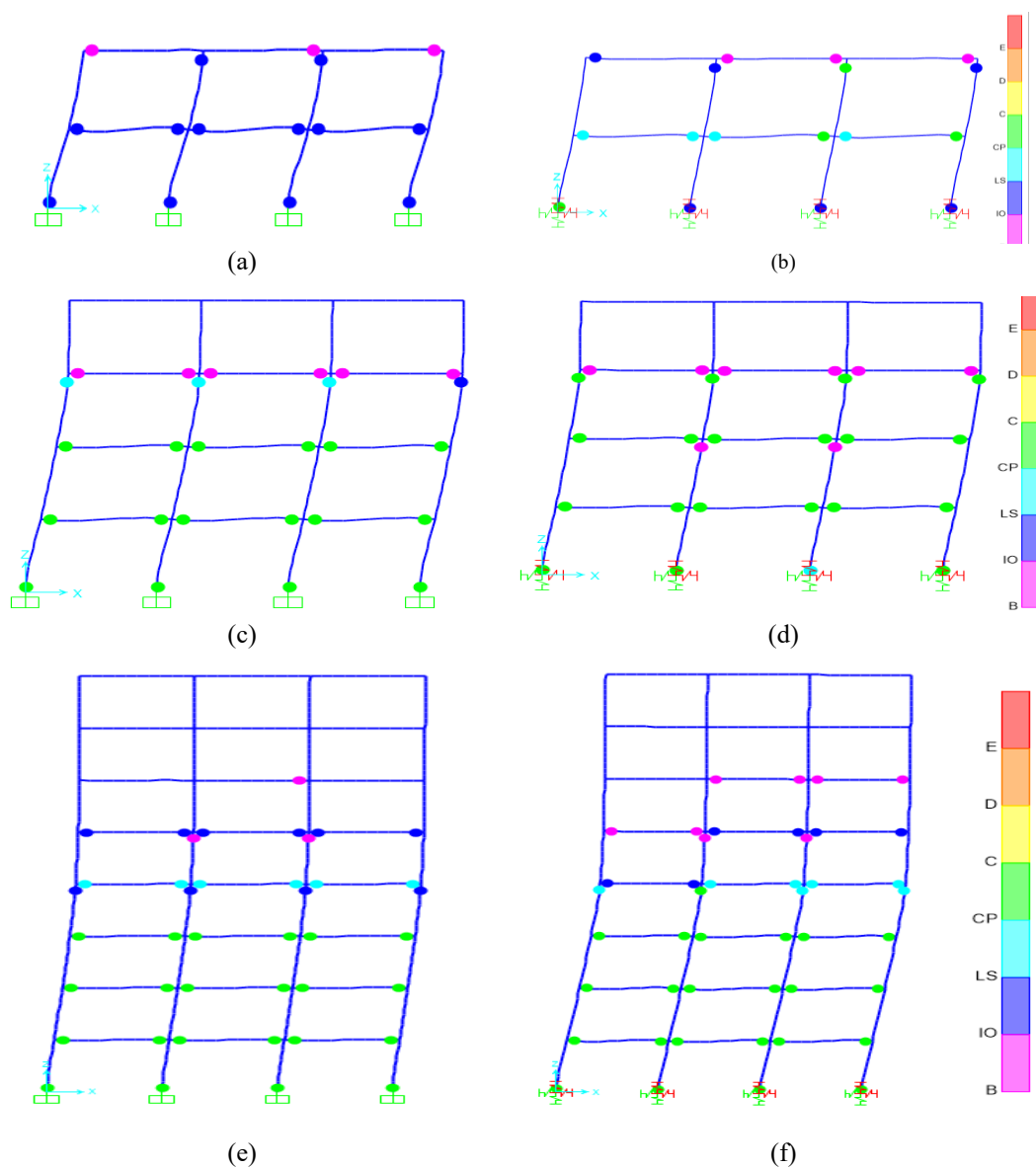


Figure 5.34. Comparison of plastic hinge formations for 2, 4 and 8 story models in the x-direction; (a), (c), (e) shows fixed base and (b), (d), (f) represent flexible base condition

Similarly, the plastic hinge formations corresponding to the last step of pushover analysis in the direction of y-axis, for the axis A-A with considering soil type ZE, is demonstrated in Figure 5.35.

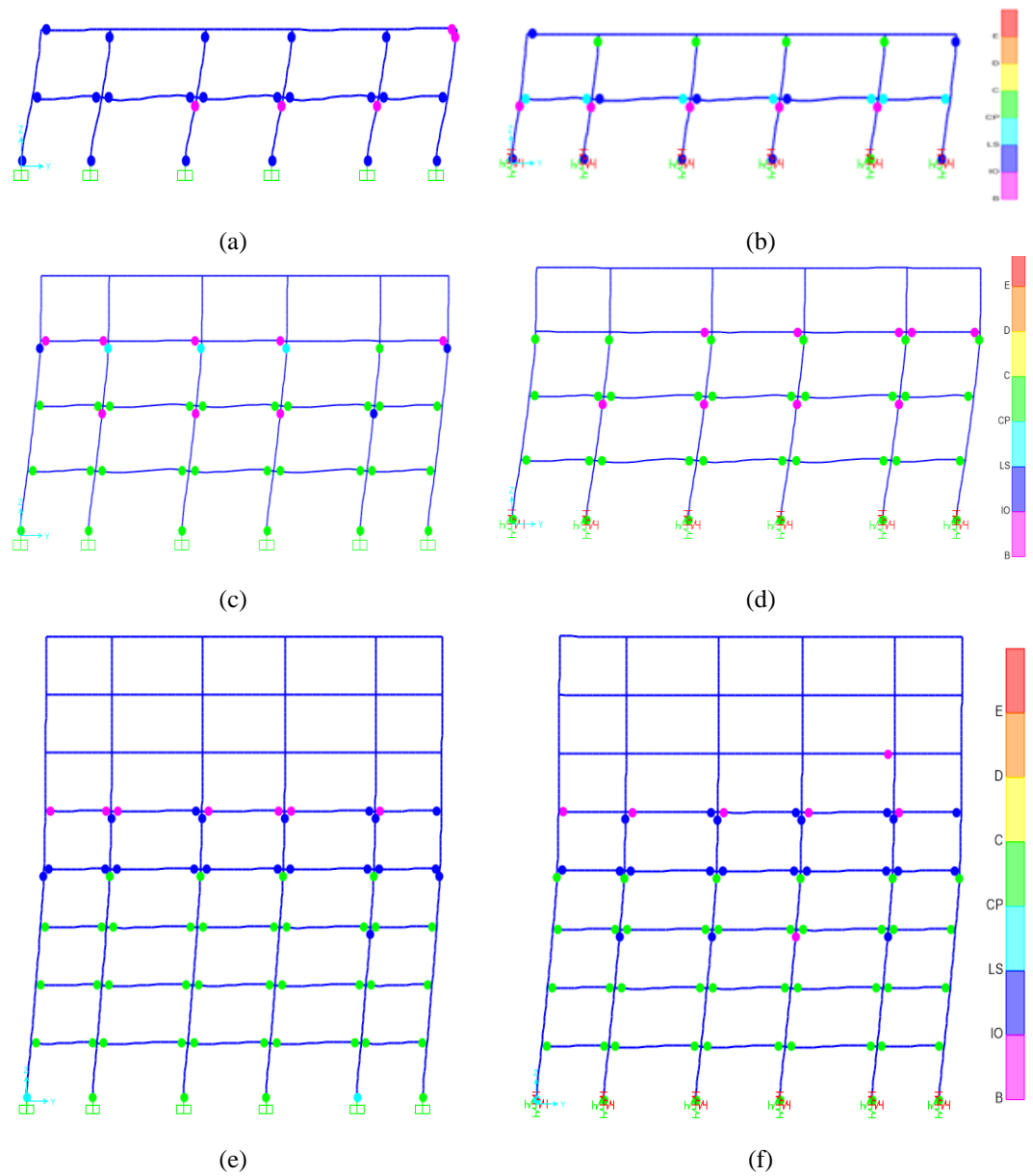


Figure 5.35. Comparison of plastic hinge formations for 2, 4 and 8 story models in the y-direction; (a), (c), (e) shows flexible base and (b), (d), (f) represent fixed base conditions



## **CHAPTER 6. CONCLUSIONS AND RECOMMENDATIONS**

### **6.1. Conclusion**

In this research, three different RC moment-resisting frame models employing SAP2000 were developed to perform nonlinear static analyses on the soil-foundation-structure system. Single-mode pushover analyses, based on the TEC-2018 standard, were performed by subjecting the buildings to the design earthquake level (DD-2) taking into account both material and geometric (P-  $\Delta$  effects) nonlinearities. In order to observe how the seismic responses of the compliant and fixed base models differ from each other, a simplified SSI model (Chapter 4) suitable for pushover analysis has been used. For what concern the soil layer under the foundation different soil properties for Adapazari regions have been considered and the effects of soil-foundation interaction was modeled by means of equivalent springs. Accordingly the spring stiffness was computed using the impedance functions developed by G. Gazetas, for the foundation located at the surface of the ground, which is also recommended by seismic codes such as ATC-40 and FEMA-356. The analysis were carried forward for both flexible based (SSI system) and fixed base conditions, both in x and y directions. The seismic responses such as building vibration periods, pushover curves (base shear force vs. roof displacement relationship), inter-story drift ratios, maximum seismic displacement demand and damage levels of ground columns have been investigated. Based on the results obtained in this study, the following conclusions can be made:

- a) Incorporating the SSI effects into the analysis results in lengthening of the vibration periods of the RC structures, comparing to the fixed base condition. However, the amplification is negligible for stiffer soil layers (soil types ZA, ZB

and ZC) and are significant when it is founded on weak ground conditions, soil type ZD and ZE. This happens due to the reduction in lateral stiffness of the buildings, resulting from the deformable behavior of the underlying soils. Depending on the height of the structures, the SSI increases the vibration period up to 43% for soil type ZE and around 0.2% for soil Type ZA.

- b) The seismic displacement demands increases due to the inclusion of SSI to the analysis compared to the typical fixed base conditions of the same models. However, the changes are very little or almost negligible (0.12% -1.73%) when the buildings are founded on stiffer soil profiles such as soil types ZA, ZB, and ZC. Whereas, it increases significantly (8% - 50%) as the ground conditions soften, which includes soil types ZD and ZE.
- c) Considering the soil-structure interaction in numerical analysis, results in a reduction in the values of maximum base shear force for all 2, 4 and 8-story models, compared to the conventional fixed-base conditions. On the other hand, an increase in the maximum base shear force is observed as the number of stories decreases for both fixed base and flexible base cases.
- d) Compared to the fixed base conditions, as the ground properties soften (soil type ZD and ZE), a significant increase in the maximum inter-story drift ratios has been observed due to the SSI effects, whereas negligible variations was witnessed for stiffer soil profiles. Specifically, it was intensified at the first floor levels for all the models. The maximum drift ratios have been used to measure the global performance levels of the buildings and were compared with the acceptance criteria purposed by FEMA-356. Accordingly, depending on the height of the buildings and the properties of the soil layer under their foundation, the performance levels was changed from IO to LS and then to CP. In addition, the amplification in inter-story drift ratios due to the SSI effects becomes more obvious as the building height increases. Considering the soil type ZE, for the 8-story model, the performance levels changed from

LS to CP, while for the 4 and 2-story model it was amplified from IO to LS compared to the fixed base condition.

- e) An increase in vibration period results in an increase in roof displacement demand which lead to redistribution of internal forces such as bending moments and axial forces. Accordingly, the redistribution of internal forces in turn changes the plastic hinge formation in the frame elements which may reduce or increase the values of plastic rotations and consequently changes the performance levels in some particular elements. Particularly, these changes in performance levels have been more noticeable for soil types with shear wave velocity less than 200 m/sec, as well as for higher buildings.
- f) The SSI changes the damage levels of RC frame element in a significant amount, especially when the buildings are founded on less favorable geotechnical conditions, soil types ZD and ZE. The values of plastic rotations in external columns increases while mostly it decreases in internal columns for flexible base models as compared to the same model fixed at their bases. Based on the obtained results, the damage level of columns changed from limited damage (LD) to moderate damage (MD) and then to sever damage (SD) and in some cases it collapsed. Specifically, for soil type ZD and ZE as well as higher buildings, the damage level of external columns suffers the most when SSI is included in the model, such that the performance levels change from MD to SD or even falls within the Collapse performance range.

In summary, it is clearly shown that the changes in soil properties change the seismic performance of the structures. However, an increase in soil shear wave velocity,  $V_s$ , and soil shear modulus,  $G_0$ , causes a less variation in seismic structural responses, indicating that the behavior of SSI systems are more similar to the fixed base condition of the same model. On the other hand, as these parameters decrease as well as when the building heights increase, the variation in seismic responses gets more significant which means that SSI is more important for softer soil profile (ZD and ZE). In addition, the SSI effects can be ignored for stiffer soil types (ZA, ZB, and ZC), whereas it should

be included in the numerical analysis and performance evaluation when the buildings are founded on soft or very soft soil layers (ZD and ZE).

## **6.2. Recommendation for the Future Studies**

The framework presented and parametric investigation carried out in this study only covered simplified nonlinear static analysis (i.e. single mode pushover analysis), where the first mode of vibration is assumed to be predominant. Thus, for obtaining more accurate results, it is suggested to perform a non-linear time history analysis as well as it would be insightful to account for the effects of higher modes. Using this method the SSI effects should be considered and accordingly the variation in seismic responses for each mode of vibration should be studied. In addition, it should be noted that the effects of ground motion is represented by smoothed code based response spectra, but many major earthquakes that occur are often different from the spectra. For this reason, performing such an investigation for each local soil types, considering a real earthquake record happened in that region, will provide more realistic results about the seismic behavior of structures.

Furthermore, this study only covered the inertial-interaction of the SSI system by means of simplified methods. Therefore, it is recommended to replicate the methodology presented in this study and investigate all the components of soil-structure interaction including kinematic interaction and inertial interaction. In addition, the non-linear behavior of the soil medium are also ignored. Therefore, in order to account for the non-linear behavior of the soil layers, in addition to the simplified (equivalent elastic spring model) method which is based on the elastic behavior of the soil, sub-structure finite element model or the direct methods can be used.

## REFERENCES

- [1] D. Abdullah, "Assessment of nonlinear static (pushover) analysis procedures using field experience.pdf," PHD Thesis, Middle East Technical University, Ankara, Turkey, 2013.
- [2] M. Moghaddasi, "Probabilistic Quantification of the Effects of Soil-Shallow Foundation-Structure Interaction on Seismic Structural Response," PHD Thesis, University of Canterbury, Christchurch, New Zealand, 2012.
- [3] "Recommended Seismic Provisions for New Buildings and Other Structures. FEMA P-750," National Earthquake Hazards Reduction Program (NEHRP), Washington, D.C., 2009.
- [4] S. H. R. Tabatabaiefar, "Determining seismic response of mid-rise building frames considering dynamic soil-structure interaction," PHD Thesis, University of Technology Sydney, Sydney Australia, 2012.
- [5] ATC-40, "Seismic evaluation and retrofit of existing concrete buildings," Applied Technology Council, Redwood City (CA), SSC 96-01, 1996.
- [6] K. Golghate, V. Baradiya, and A. Sharma, "Pushover Analysis of 4 Storey's Reinforced Concrete Building," *International Journal of Latest Trends in Engineering and Technology*, vol. 2, no. 3, pp. 80–84, 2013
- [7] R. A. Hakim, M. S. Alama, and S. A. Ashour, "Application of Pushover Analysis for Evaluating Seismic Performance of RC Building," *International Journal of Engineering Research*, vol. 3, no. 1, pp. 157–1662, 2014.
- [8] P. Panyakapo, "Cyclic Pushover Analysis procedure to estimate seismic demands for buildings," *Engineering Structures*, vol. 66, pp. 10–23, May 2014, doi: 10.1016/j.engstruct.2014.02.001.
- [9] A. Çollaku, "Pushover Analysis of Reinforced Concrete Frames Designed as per Albanian Codes of Practice," Master Thesis, Epoka University, Albania, 2015.
- [10] İ. B. Karaşın and E. Işık, "Farklı yapı davranış katsayıları için zemin koşullarının yapı performansına etkisi," *DÜMF Mühendislik Dergisi*, vol. 8, no. 4, pp. 661–673, 2017.

- [11] I. Kraus and D. Džakić, "Soil-structure interaction effects on seismic behaviour of reinforced concrete frames," In 50 years Skopje Earthquake-50 years European Earthquake Engineering., 2013.
- [12] A. Demir, O. Kirtel, and E. Çelebi, "Pushover Analyses of RC Buildings with Soil-Structure Interaction for Adapazari Region under Linear and Nonlinear Soil Conditions," presented at the International Civil Engineering and Architecture Symposium for Academicians, Antalya, Turkey, 2014, pp. 226–223.
- [13] G. Gazetas, "Formulas and Charts for Impedances of Surface and Embedded Foundations," *Journal of geotechnical engineering*, vol. 117, no. 9, pp. 1363–1381, 1991.
- [14] O. Kirtel, "Doğrusal Olmayan Zemin Ortamında Rijit Şerit Temeller İçin Dinamik Empedans Fonksiyonları," PHD Thesis, Sakarya University, Turkey, 2013.
- [15] L. B. Storie and M. J. Pender, "SFSI in shallow foundation earthquake response," presented at the New Zealand Society for Earthquake Engineering (NZSEE) Conference, New Zealand, 2013, vol. 2628, pp. 1–8.
- [16] M. G. Kalyanshetti, S. A. Halkude, and Y. C. Mhamane, "Seismic response of R.C. building frames with strap footing considering soil structure interaction," *International Journal of Research in Engineering and Technology*, vol. 04, no. 25, pp. 7–14, Dec. 2015, doi: 10.15623/ijret.2015.0425002.
- [17] M Roopa, H. G. Naikar, and D. S. Prakash, "Soil Structure Interaction Analysis on a RC Building with Raft foundation under Clayey Soil Condition," *International Journal of Engineering Research and Technology (IJERT)*, vol. V4, no. 12, pp. 319–323, Dec. 2015, doi: 10.17577/IJERTV4IS120402.
- [18] F. Behnamfar and M. Banizadeh, "Effects of soil–structure interaction on distribution of seismic vulnerability in RC structures," *Soil Dynamics and Earthquake Engineering*, vol. 80, pp. 73–86, Jan. 2016, doi: 10.1016/j.soildyn.2015.10.007.
- [19] R. Tomeo, A. Bilotta, D. Pitilakis, and E. Nigro, "Soil-structure interaction effects on the seismic performances of reinforced concrete moment resisting frames," *Procedia Engineering*, vol. 199, pp. 230–235, 2017, doi: 10.1016/j.proeng.2017.09.006.
- [20] M. Ghandil and F. Behnamfar, "Ductility demands of MRF structures on soft soils considering soil-structure interaction," *Soil Dynamics and Earthquake Engineering*, vol. 92, pp. 203–214, Jan. 2017, doi: 10.1016/j.soildyn.2016.09.051.

- [21] A. Anvarsamarin, F. R. Rofooei, and M. Nekooei, "Soil-Structure Interaction Effect on Fragility Curve of 3D Models of Concrete Moment-Resisting Buildings," *Shock and Vibration*, vol. 2018, pp. 1–13, 2018, doi: 10.1155/2018/7270137.
- [22] Applied Technology Council (ATC), "Guidelines for Performance-Based Seismic Design of Buildings," Redwood City, California, USA, FEMA P-58-6, 2018.
- [23] M. J. N. Priestley, "Performance Based Seismic Design," *Bulletin of the New Zealand society for earthquake engineering*, pp. 325–346, 2000.
- [24] "TEC-2018: Turkish Building Earthquake Code," Disaster and Emergency Management Authority, Ankara, Turkey, Official Gazette 30364, Mar. 2018.
- [25] Applied Technology Council (ATC), "Improvement of Nonlinear Static Seismic Analysis Procedures," Redwood City, California, FEMA-440, ATC-55 Project, 2005.
- [26] J. P. Stewart, R. B. Seed, and G. L. Fenves, *Empirical evaluation of inertial soil-structure interaction effects*. Univ. of California, Berkeley, CA: Pacific Earthquake Engineering Research Center, 1998.
- [27] J. P. Stewart, C. B. Crouse, T. Hutchinson, B. Lizundia, F. Naeim, and F. Ostadan, "Soil-structure interaction for building structures," NISTGCR-12-917-21, 2012.
- [28] J. P. Wolf, "Classification of Analysis Methods for Dynamic Soil-Structure Interaction," presented at the International Conferences on Recent Advances in Geotechnical Earthquake Engineering and Soil Dynamics, 1991.
- [29] A. S. Veletsos, S. Anestis, and B. Verbič, "Vibration of viscoelastic foundations," *Earthquake Engineering & Structural Dynamics*, vol. 2, no. 1, pp. 87–102, 1973.
- [30] A. Pais and E. Kausel, "Approximate formulas for dynamic stiffnesses of rigid foundations," *Soil Dynamics and Earthquake Engineering*, vol. 7, no. 4, pp. 213–227, 1988.
- [31] G. Mylonakis, S. Nikolaou, and G. Gazetas, "Footings under seismic loading: Analysis and design issues with emphasis on bridge foundations," *Soil Dynamics and Earthquake Engineering*, vol. 26, no. 9, pp. 824–853, Sep. 2006, doi: 10.1016/j.soildyn.2005.12.005.
- [32] S. H. R. Tabatabaiefar, "Determining seismic response of mid-rise building frames considering dynamic soil-structure interaction," PHD: thesis, University of Technology Sydney, Sydney Australia, 2012.

- [33] G. Mylonakis and G. Gazetas, "Seismic soil-structure interaction: beneficial or detrimental?," *Journal of Earthquake Engineering*, vol. 4, no. 3, pp. 277–301, Jul. 2000, doi: 10.1080/13632460009350372.
- [34] Federal Emergency Management Agency (FEMA), "Prestandard And Commentary For The Seismic Rehabilitation Of Buildings," American Society of Civil Engineers (ASCE), 2000.
- [35] X.-K. Zou and C.-M. Chan, "Optimal seismic performance-based design of reinforced concrete buildings using nonlinear pushover analysis," *Engineering Structures*, vol. 27, no. 8, pp. 1289–1302, Jul. 2005, doi: 10.1016/j.engstruct.2005.04.001.
- [36] S. OĞUZ, "Evaluation of Pushover Analysis Procedures for Frame Structures," Master Thesis, Middle East Technical University, Turkey, 2005.
- [37] S. Manohar and S. Madhekar, *Seismic Design of RC Buildings*. New Delhi: Springer India, 2015.
- [38] H. Krawinkler and G. D. P. K. Seneviratna, "Pros and cons of a pushover analysis of seismic performance evaluation," *Engineering Structures*, vol. 20, no. 4–6, pp. 452–464, Apr. 1998, doi: 10.1016/S0141-0296(97)00092-8.
- [39] J. D. Bray et al., "CPT Liquefaction Investigations," p. 10.
- [40] Computer and Structure, INC, *SAP2000 CSI Analysis Reference Manual*. Berkeley, California, USA, 2016.
- [41] XTRACT Manuals, *Cross Section Analysis Of Structural Components*. California, USA: Imbsen and Associates Inc., 2007.
- [42] "Requirements for Design and Construction of Reinforced Concrete Structures," Turkish Standard Institute, Ankara, Turkey, Technical Report 19054, 2000.



## **RESUME**

Mukhtar AHMADI was born on 7 July 1991 in Daykundi, the central province of Afghanistan. He completed his primary and secondary education in his home province; In 2009, he graduated from Charkh Bargar High School. Afterward, he started higher education at Kabul Polytechnic University, department of civil engineering, at the same time he was awarded a scholarship by the Afghanistan government to pursue his education in Turkey. Accordingly, after studying the Turkish language for one year he started school in 2012 at Gazi University, department of civil engineering and graduated in 2016. In January of 2017, he was accepted to Sakarya University Structural Engineering graduate programs. After completing the master courses, he continued working on his master thesis and during this period, the author has published two conference papers (ISESH 2019, Karabük and IESKO 2019, Kocaeli) presented at international scientific meetings and published in the proceeding books and still continues his academic studies.